KNOCKDOWN OF DELTA-5 DESATURASE TO ELICIT ANTI-CANCER EFFECT OF DIHOMO-γ-LINOLENIC ACID: DEVELOPMENT OF AN ω-6 FATTY ACID-BASED THERAPEUTIC STRATEGY FOR PANCREATIC CANCER

A Dissertation
Submitted to the Graduate Faculty
of the
North Dakota State University
of Agriculture and Applied Science

By

Xiaoyu Yang

In Partial Fulfillment of the Requirements
for the Degree of
DOCTOR OF PHILOSOPHY

Major Department:
Pharmaceutical Sciences

August 2017

Fargo, North Dakota

North Dakota State University
Graduate School

Title

KNOCKDOWN OF DELTA-5 DESATURASE TO ELICIT ANTI-CANCER EFFECT OF DIHOMO-γ-LINOLENIC ACID: DEVELOPMENT OF AN ω-6 FATTY ACID-BASED THERAPEUTIC STRATEGY FOR PANCREATIC CANCER

By

Xiaoyu Yang

The Supervisory Committee certifies that this ***disquisition*** complies with North Dakota State University's regulations and meets the accepted standards for the degree of

DOCTOR OF PHILOSOPHY

SUPERVISORY COMMITTEE:

Dr. Steven Qian
Chair

Dr. Sanku Mallik

Dr. Amanda Brooks

Dr. Changhui Yan

Approved:

10/09/2017
Date

Dr. Jagdish Singh
Department Chair

ABSTRACT

Pancreatic cancer is one of the most common causes of cancer death in the United States. Unlike ω-3 fatty acids, which have been commonly used as complementary therapy to treat pancreatic cancer, ω-6s (more abundant fatty acids in the human diet) have received much less attention in cancer treatment due to generation of deleterious metabolites from cyclooxygenase (COX)-catalyzed peroxidation of arachidonic acid, a downstream ω-6. However, dihomo-γ-linolenic acid (DGLA), the immediate precursor of arachidonic acid, has been recently reported to be associated with some anti-cancer effects on various types of cancer cells. Recent studies from Dr. Qian's lab have shown that the exclusive free radical byproduct 8-hydroxyoctanoic acid (8-HOA) formed from DGLA peroxidation catalyzed by COX-2 may actually account for DGLA's anti-cancer activities. However, the generation of 8-HOA can be readily limited by the conversion from DGLA to arachidonic acid mediated by delta-5 desaturase (D5D).

Here, we hypothesized that the high COX-2 expression in cancer cells and tumors can be exploited to promote formation of 8-HOA from COX-catalyzed DGLA peroxidation, and knockdown of D5D can reserve more DGLA to form 8-HOA which thus inhibits pancreatic cancer cell growth and migration. Clonogenic assay, apoptosis assay, transwell assay, immunofluorescence, and western blot were used to assess cancer cell and tumor viability, apoptosis, migration, invasion, and the associated molecular mechanisms. Our study showed that 8-HOA can inhibit pancreatic cancer cell growth and migration by acting as a histone deacetylase inhibitor to alter the expression of proteins involved in cancer growth and metastasis. We observed that knockdown of D5D (*via* siRNA/shRNA transfection) can promote formation of 8-HOA from COX-catalyzed DGLA peroxidation to a threshold level, leading to inhibition of pancreatic cancer cell growth and migration as well as subcutaneous tumor xenografts.

Knockdown of D5D and DGLA treatment improved the efficacy of many chemotherapy drugs. We demonstrated that we could take advantage of the commonly overexpressed COX-2 level in cancers to control pancreatic cancer cell and tumor growth and metastasis. With this shifting paradigm of COX-2 biology in cancer treatment, the research outcome may provide us a ω-6s-based diet care strategy to supplement current chemotherapy.

ACKNOWLEDGEMENTS

Firstly, I would like to express my sincere gratitude to my advisor Dr. Steven Qian for the continuous support of my Ph.D. study and related research. Since I joined his lab, Dr. Steven Qian has taught me numbers of skills, techniques and massive knowledge. During my Ph.D. study, Dr. Steven Qian encouraged me to pursue the best of myself. His guidance and encouragement helped me in all the time of research and writing of this thesis. I could not have achieved what I achieved without him. Dr. Steven Qian not only made me a better researcher, but also made me a better person.

In addition, I would like to thank the rest of my committee members: Dr. Sanku Mallik, Dr. Amanda Brooks, and Dr. Changhui Yan, for their insightful comments and encouragement during my Ph.D. work, but also for the inspiring questions which incented me to widen my research from various perspectives.

I thank Dr. Jagdish Singh for providing me with the opportunity to work in the wonderful department. I am grateful to the secretaries, Janet Krom, Jean Trautmann, and Diana Kowalski in the pharmaceutical science department, for assisting me in many different ways.

I am indebted to the whole department of pharmaceutical sciences for providing a stimulating and fun environment in which to learn and grow. I am especially grateful to my lab mates and people who helped me with my experiments, Yi Xu, Lizhi Pang, and Dr. Jin Qi.

I would also like to thank my friends for their support, encouragement, entertainment, and caring. Last but not the least, I would like to thank my family for supporting me throughout my life.

TABLE OF CONTENTS

LIST OF TABLES

LIST OF FIGURES

LIST OF SCHEMES

LIST OF ABBREVIATIONS

AA.....arachidonic acid.

ACN.....acetonitrile.

ALA.....α-linolenic acid.

COX.....cyclooxygenase.

DGLA.....dihomo-γ-linolenic acid.

DHA.....docosahexaenoic acid.

D5D.....delta-5-desaturase.

D5D-*KD*.....delta-5-desaturase knockdown.

EMT.....epithelial mesenchymal transition.

EPA.....eicosapentaenoic acid.

ESR.....electron spin resonance.

FBS.....fetal bovine serum.

GC.....gas chromatography.

GLA.....γ-linolenic acid.

HAc.....glacial acetic acid.

HCl.....hydrogen chloride.

HDAC.....histone deacetylase.

HDACi.....histone deacetylase inhibitor.

HPLC.....high performance liquid chromatography.

LA.....linoleic acid.

LC.....liquid chromatography. lipoxygenases (LOX)

LOX.....lipoxygenases.

MMP.....matrix metalloproteinase.

MS.....mass spectrometry.

MTS .....3-(4,5-dimethylthiazol-2-yl)-5-(3-carboxymethoxyphenyl)-2-(4-sulfophenyl)-2H-tetrazolium.

NaCl .....sodium chloride.

NC-si .....negative control siRNA transfected.

PBS .....phosphate buffered saline.

PFB .....pentafluorobenzyl.

PG .....prostaglandin.

PGE1 .....prostaglandin E1.

PGE2 .....prostaglandin E2.

PI .....propidium iodide.

PUFAs.....polyunsaturated fatty acids.

SD .....standard deviation.

SDS .....sodium dodecyl sulfate.

SPE.....solid phase extraction.

TBS .....Tris buffered saline.

8-HOA.....8-hydroxyoctanoic acid.

1. INTRODUCTION

1.1. Polyunsaturated fatty acids ω-3 and ω-6

Polyunsaturated fatty acids (PUFAs), fatty acids that contain more than one C=C double bonds in their backbone, are important cellular components and are indispensable to maintain cellular functions [1-6]. We mainly take in PUFAs from our daily diet as the human body cannot synthesize PUFAs *de novo* due to mammals lacking the enzyme to convert C-C single bond to C=C double bond beyond carbons 9 and 10 from the carboxyl end in fatty acids [7-9].

There are two important classes of PUFAs, namely ω-3s and ω-6s. The ω-3 fatty acids are normally found in fish and marine food chain elements, such as plankton and algae, and the primary source of ω-3 fatty acids in the human diet is fish oil [10-11]. ω-3s, including α-linolenic acid (ALA), eicosapentaenoic acid (EPA) and docosahexaenoic acid (DHA), etc., are PUFAs with a double bond at the third carbon atom from the end of the carbon chain (**Scheme 1**). Upon consumption into the human body, ALA, the precursor of ω-3s, can be metabolized *via* elongase, delta-6-desaturase (D6D) and delta-5-desaturase (D5D) to produce various downstream PUFAs, including EPA and DHA which are enriched in fish oil [12-15].

The ω-3s can lead to many beneficial effects in human health, including decreasing depression and stress, preventing cardiovascular disease, ameliorating the symptoms of chronic inflammation and improving cognitive ability [16-21]. ω-3 fatty acids have also been used as an adjuvant therapy for treatment of many cancers, including pancreatic cancer [22-25]. DHA and EPA showed some growth inhibitory effects on several pancreatic cancer cell lines [26-32], and were also able to sensitize pancreatic cancer cells to a variety of chemo-drugs, including front-line chemotherapy drug, gemcitabine [33-35]. *In vivo* studies demonstrated that ω-3 fatty acids can significantly suppress tumor progression in pancreatic cancer mice model [36-37].

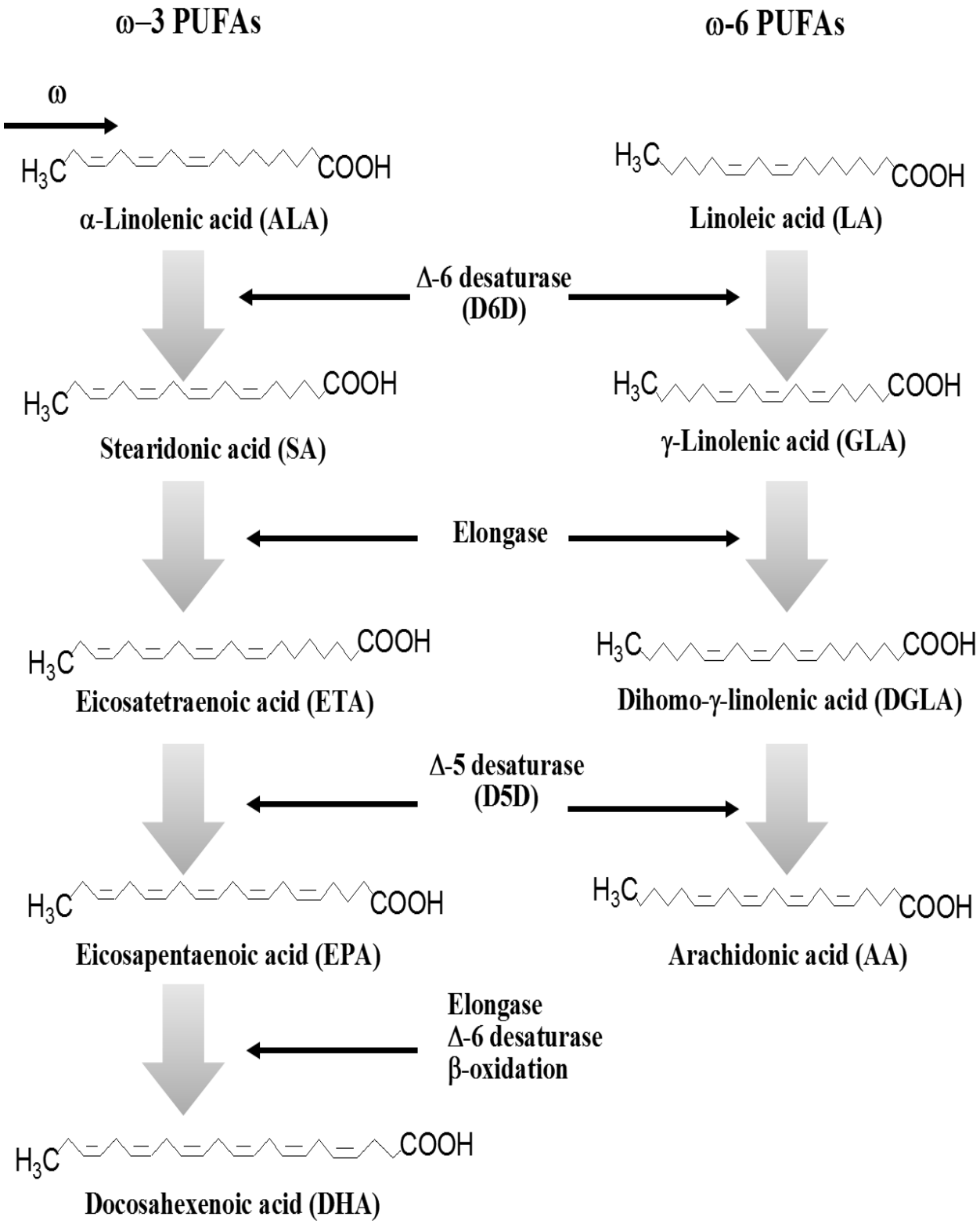

Scheme 1. ω-3 and ω-6 PUFAs in the human body.
Once consumed into the human body, ALA (upstream ω-3) and LA (upstream ω-6) will be converted to their corresponding downstream fatty acids under the catalysis of a series of enzymes, including D6D, elongase, and D5D.

ω-6 fatty acids, including linoleic acid (LA, main ω-6 fatty acid in the human diet), gamma-linolenic acid (GLA), dihomo-gamma-linolenic acid (DGLA) and arachidonic acid (AA), are PUFAs with a double bond at the sixth carbon from the end of the carbon chain (Scheme 1). Upon being taken into the human body, LA, the precursor of ω-6s, will be converted to GLA by D6D which changes a C-C single bond to C=C double bond. GLA will then be converted into DGLA by elongase which adds two additional carbon atoms. DGLA is further metabolized to AA by D5D which converts another C-C single bond to C=C double bond.

The ω-6 fatty acids are normally found in vegetable oils, including sunflower, safflower, corn and soybean oil as well as cereals [38-39], which makes them much more abundant in our daily diet compared to ω-3. The typical western diet is considered to be a high fat, high energy diet but with low fiber intake. As a consequence of the increased intake of LA-enriched vegetable oils in the western diet, the ratio of ω-6 fatty acids *vs.* ω-3 fatty acids in traditional western diets is between ~ 10:1 and 30:1 [40]. However, a variety of studies have suggested that the recommended ratio of ω-6s *vs.* ω-3s for keeping human healthy should be ~1:1 and 4:1 [41-43]. Over the last few decades, studies have shown that the increased ratio of ω-6s *vs.* ω-3s can lead to an overall increase in the incidence of diseases involving inflammatory processes such as cardiovascular disease, obesity, inflammatory bowel disease, rheumatoid arthritis, and cancer [44-49]. The health implications of high dietary ω-6 fatty acids are majorly derived from their bioactive metabolites.

After being directly consumed from food or released from membrane phospholipids, ω-6 fatty acids can undergo enzymatic or non-enzymatic lipid peroxidation to produce various important lipid-derived signaling molecules with diverse bioactivities [50-53]. For example, AA can go through non-enzymatic lipid peroxidation to form isoprostanes (e.g. 5-F_2-isoprostane,

Scheme 2) [55-57]. AA can also go through enzymatic lipid peroxidation to form prostaglandins (e.g. prostaglandin G2) by cyclooxygenase (COX), hydroperoxyeicosatetraenoic acids (e.g. 5-hydroperoxyeicosatetraenoic acid, 5-HPETE) by lipoxygenase (LOX), and hydroxyeicosatetraenoic acids (e.g. 20- hydroxyeicosatetraenoic acid, 20-HETE) by cytochrome P450 (CYP450, Scheme 2) [54].

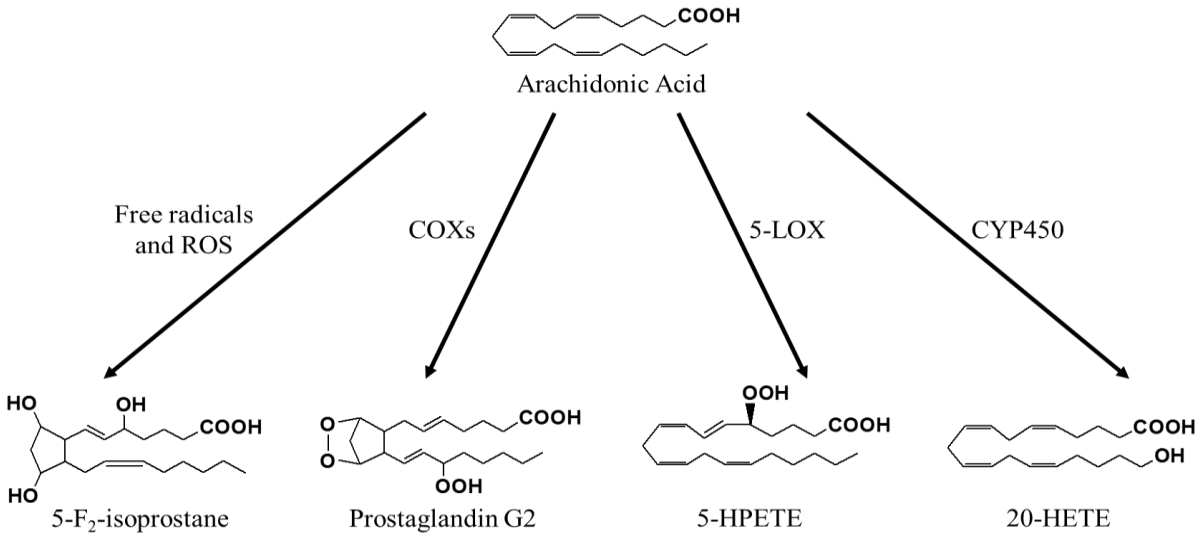

Scheme 2. Examples of metabolites formed from non-enzymatic or enzymatic lipid peroxidation of AA.
AA can go through non-enzymatic lipid peroxidation to form isoprostanes (e.g. 5-F_2-isoprostane) as well as enzymatic lipid peroxidation to form prostaglandins (e.g. prostaglandin G2) by COX, hydroperoxyeicosatetraenoic acids (e.g. 5-HPETE) by LOX, and hydroxyeicosatetraenoic acids (e.g. 20-HETE) by CYP450.

DGLA and AA, the two ω-6 fatty acids we focused in our study, can both be metabolized by a bi-functional enzyme, COX, to form 1-series and 2-series prostaglandins. The cyclooxygenase activity of COX incorporates two oxygen molecules into DGLA and AA to generate prostaglandin G1 (PGG1) and prostaglandin G2 (PGG2), while the peroxidase activity of COX, which generally coupled with a reducing agent, reduces PGG1 and PGG2 to form prostaglandin H1 (PGH1) and prostaglandin H2 (PGH2), respectively. PGH1 and PGH2 can be further converted to a second series of prostaglandins e.g. prostaglandin E1 (PGE1) and prostaglandin E2 (PGE2, **Scheme 3**).

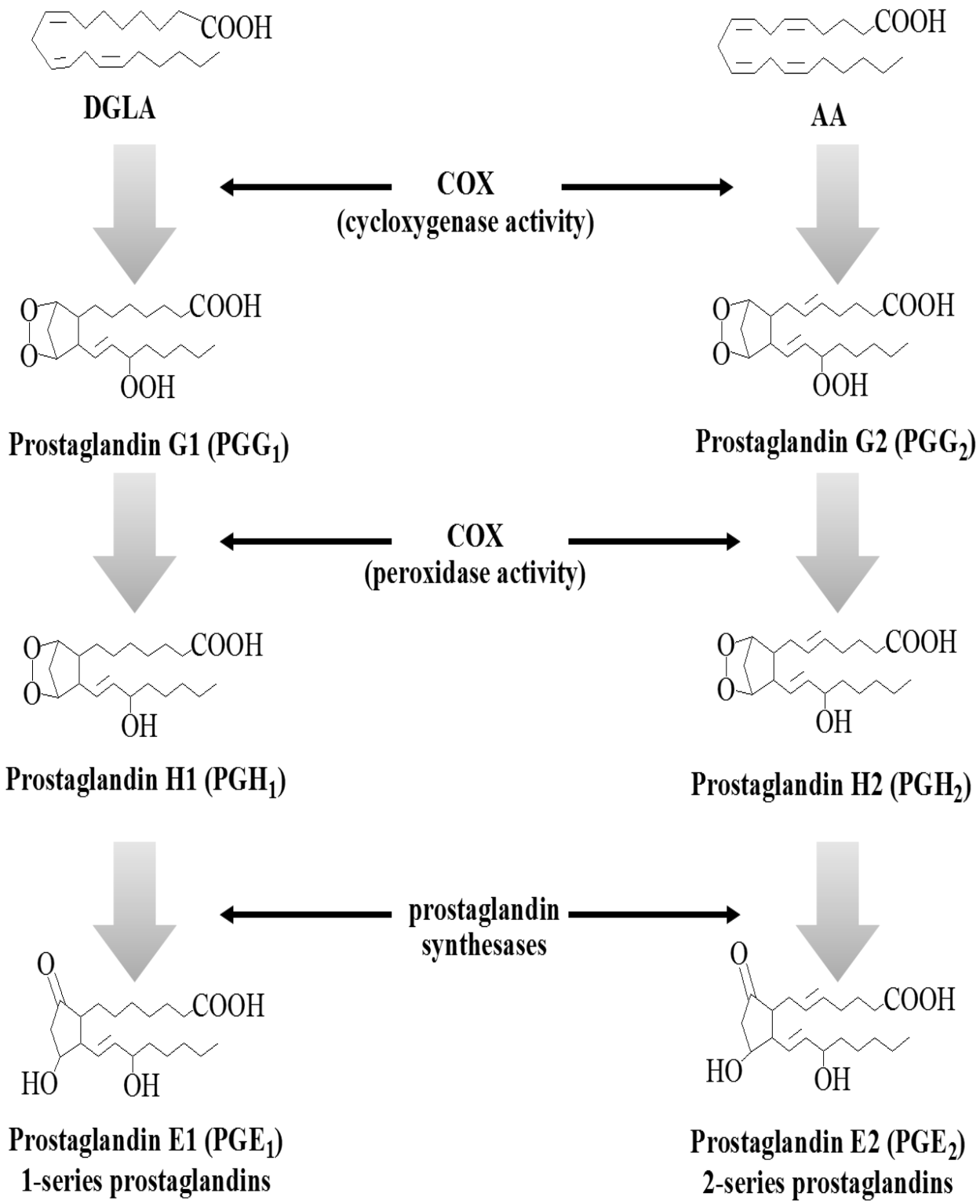

Scheme 3. COX-catalyzed DGLA and AA peroxidation.
DGLA and AA (two ω-6 fatty acids), can be metabolized to 1-series prostaglandins (e.g. PGE1) and 2-series prostaglandins (e.g. PGE2), respectively. 1-series and 2-series prostaglandins have been found to play an important role in inflammation and cancer.

1.2. COX-catalyzed fatty acid peroxidation and pancreatic cancer

COX, also named prostaglandin endoperoxide synthase, is a lipid peroxidizing enzyme that catalyzes prostaglandin biosynthesis. COX is a bi-functional enzyme containing a cyclooxygenase site and a peroxidase site; thus, it converts fatty acids to prostaglandins in two reactions, e.g. its cyclooxygenase activity incorporates two oxygen molecules into fatty acids, and its peroxidase activity reduces the relative metabolites to corresponding alcohol [58]. There are two isoforms of COX: COX-1 and COX-2. COX-1 has been generally considered the constitutive form, expressed in most tissues under basal conditions, while the inducible form COX-2 is undetectable in most normal tissues, but can be readily induced by cellular stresses, growth factors, cancer promoters, and pro-inflammatory signals in diseases such as inflammation and cancer [59-62].

High COX-2 expression has been commonly found in a variety of cancers, including colon, breast, and pancreas. Over 70% of pancreatic cancer patients have been reported to possess overexpressed COX-2 [63]. COX-2-catalyzed peroxidation of AA has been shown to play an important role in pancreatic cancer development and progress [64-70]. Studies have shown that there is an increase in levels of PGE2 as well as PGE2 receptors in pancreatic cancer cells [64-66]. Elevated levels of PGE2 can facilitate pancreatic cancer invasiveness by upregulating the expressions of MMP-2 and MMP-9, thus promoting cancer cell migration and invasion [67-68]. PGE2 has also been shown to induce angiogenesis in pancreatic cancer early stages by increasing levels of vascular endothelial growth factor and basic fibroblast growth factor inducing endothelial cells' growth, migration and survival [69-70]. Besides cancer cells, PGE2 also enhances the proliferative activity of pancreatic stellate cells, which contributes to pancreatic cancer desmoplasia, an important factor in regulating pancreatic carcinogenesis [71-

72]. In addition, PGE2, acting as a proinflammatory factor, plays an important role in chronic inflammation, which can initiate cancer [73-75]. For example, increased levels of PGE2 were found in patients with chronic pancreatitis, which could progress to pancreatic cancer [76-77].

As COX-2 catalyzed AA peroxidation is closely associated with pancreatic carcinogenesis, COX-2 has been studied extensively as a drug target in pancreatic cancer treatments. A variety of COX-2 inhibitors such as celecoxib, apricoxib, rofecoxib, *etc.*, aiming to limit PGE2 formation from COX-2-catalyzed AA peroxidation, have been tested as a complementary strategy to enhance the efficacy of front-line chemotherapeutic drugs for pancreatic cancer treatment [78-86]. However, over the past decades, COX-2 inhibitors have never achieved the desirable anti-cancer effects in clinical trials. COX-2 inhibitors not only failed to increase the survival indices of cancer patients, but also suffer from some safety issues in patients, e.g., increased risks of cardiovascular disease and gastrointestinal tract injury [87-90]. Alternative strategies for exploiting commonly high COX-2 levels in cancer to improve chemotherapy efficacy were not yet considered and developed.

1.3. Anti-cancer activities of exclusive free radical byproducts formed from COX-2 catalyzed DGLA peroxidation

1.3.1. DGLA, an exceptional ω-6 that may be associated with anti-cancer activities

Although ω-6s have not received much attention in cancer research due to deleterious metabolites generated from AA, DGLA, the immediate precursor of AA, may represent an exceptional ω-6 due to some reported anti-inflammation effects. For example, treatment with DGLA as well as its upstream GLA (presumably metabolized to DGLA) can prevent atherosclerosis and treat atopic dermatitis [91]. Dietary supplementation of DGLA prevented atherosclerosis in ApoE-deficient mice which develop extensive atherosclerotic lesions, but

naproxen, a COX inhibitor, reduced the anti-atherosclerotic effect from DGLA [92]. Oral supplementation of DGLA also can prevent development of atopic dermatitis by storing the serum level of DGLA in NC/Nga mice (spontaneously develop human atopic dermatitis like skin lesions). However, discontinuation of DGLA can lead to recurrence of atopic dermatitis [93-94]. In addition, it has been demonstrated that an increase in the level of DGLA generated from GLA can ameliorate of atopic eczema in rats, showing that the dietary effect of DGLA is more dominant than GLA on treating skin inflammation [95].

Research studies have shown that DGLA potentially owns some anti-cancer effects. In rats with 7,12-dimethylbenz(α) anthracene-induced mammary tumors, the percentage of rats bearing tumors was much lower after 12 weeks of DGLA administration (by oral intubation, 0.15 g, twice a week) compared to groups treated with GLA and corn oil (which contains mainly LA) [96]. When mouse myeloma cells and human cervical carcinoma cells (HeLa) were treated with ω-6 fatty acids, including LA, GLA, DGLA and AA, both GLA and DGLA inhibited cell proliferation in a dose-dependent manner in two cancer cell lines [97-98]. These evidence suggested that DGLA is associated with anti-cancer activities, however, the molecular mechanism was not elucidated.

1.3.2. Free radical byproducts generated from COX-catalyzed peroxidation

COX-catalyzed fatty acid peroxidation is a well-known free radical chain reaction during which a variety of free radical intermediates are produced [99]. In the process of lipid peroxidation, weakest carbon-hydrogen bonds, at the bis-allylic methylene position of PUFAs, are typically vulnerable to oxidation as they have a much lower dissociation energy than that of a typical alkyl C-H bond, which leads to formation of a lipid radical [100-101]. The lipid radical then reacts with oxygen to form a peroxyl radical, which can further attack another lipid

molecule. Peroxyl radical can also be converted to other types of free radicals *via* Fe^{2+} mediated Fenton-type reactions, β-scission and β'-scission (**Scheme 4**) [102].

As the most reactive byproducts in fatty acid peroxidation, these free radical intermediates formed from COX-catalyzed lipid peroxidation were unable to characterize for a long period of time due to their extremely short half-life. Recently, Dr. Qian's lab has developed a high-performance liquid chromatography (HPLC)/electron spin resonance (ESR)/mass spectrometry (MS) in combination with spin trapping technique (α- [4-pyridyl 1-oxide]-N-tert-butyl nitrone, POBN as the trapping agent) to characterize the individual PUFA-derived free radicals. In this system, spin-trapped free radicals can be separated based on their distinct chromatographic behavior by the HPLC column, monitored by ESR, and detected by MS for structure identification. HPLC/ESR/MS and spin trapping technique were used to successfully identify and characterize both same and unique free radicals generated from COX-catalyzed DGLA and AA peroxidation [103-105].

Previous studies from our lab have shown that DGLA and AA can go through different pathways during COX-catalyzed lipid peroxidation [103-105]. Due to the common structural moiety (C-8 to C-20) in DGLA and AA, COX can catalyze their free radical peroxidation *via* C-15 oxygenation, to form the same free radical byproducts, e.g. pentane and 1-hexanol (HEX) (**Scheme 5**) [103-104]. The different structural moiety (C-1 to C-7) in DGLA leads to formation of exclusive free radical byproducts including heptanoic acid (HTA) and 8-hydroxyoctanoic acid (8-HOA) from its unique C-8 oxygenation (**Scheme 6**) [104-105]. HTA and 8-HOA are called exclusive free radical byproducts as they can only be generated from COX-catalyzed DGLA peroxidation (different from pentane and HEX which can be formed from both COX-catalyzed DGLA and AA peroxidation).

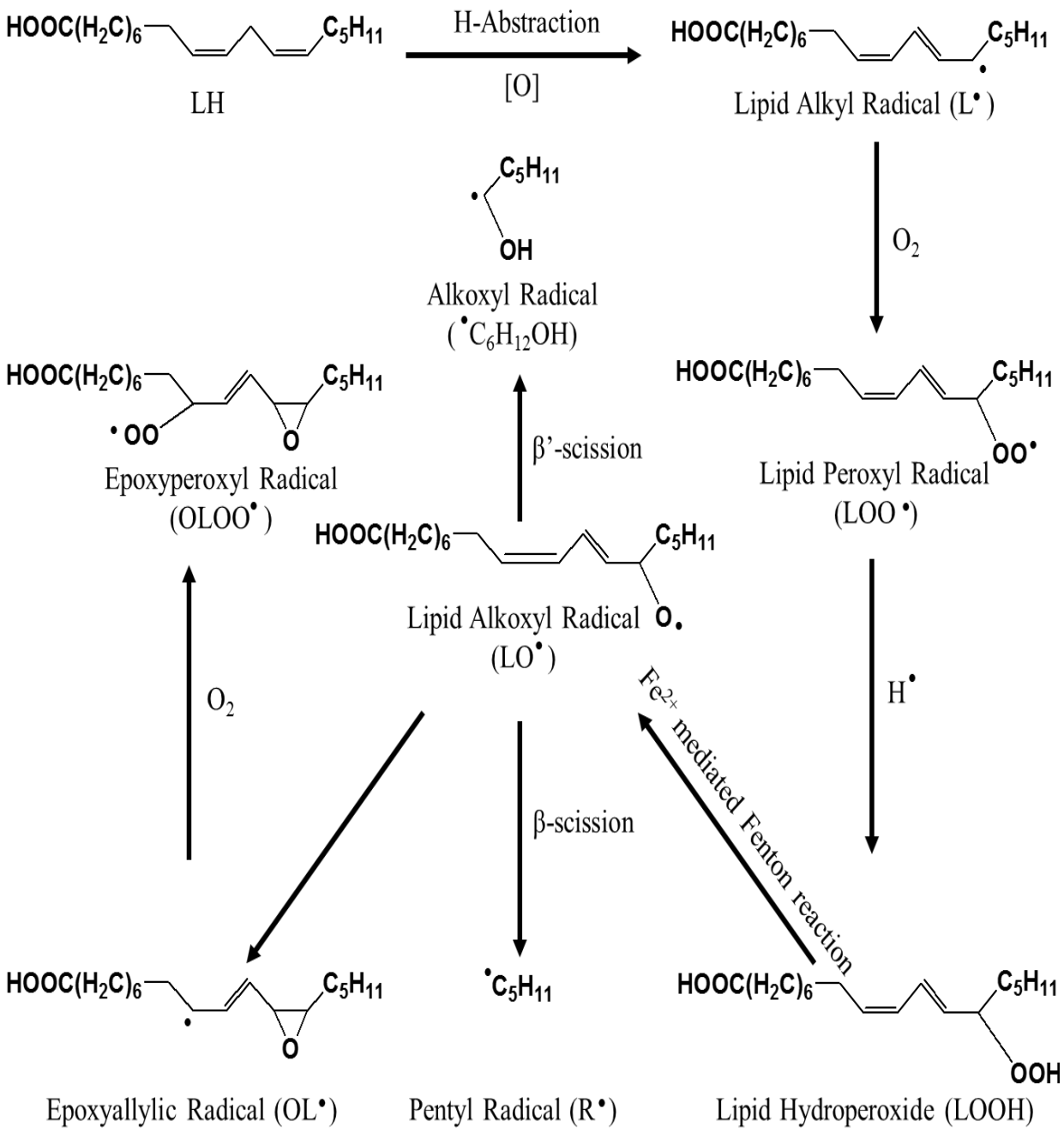

Scheme 4. An overview of the formation of lipid-derived radicals produced from lipid peroxidation (adapted from Qian et al. [102]).

This scheme shows some of the radical species formed in the peroxidation of linoleic acid. During the process of lipid peroxidation, the lipid molecule was vulnerable to oxidation as it loses a hydrogen become a carbon-centered lipid alkyl radical (L•). The lipid radical can either react with oxygen to form a peroxyl radical (LOO•) to attack other lipid molecules or be converted to other types of free radicals *via* Fe^{2+} mediated Fenton-type reactions, β-scission and β'-scission.

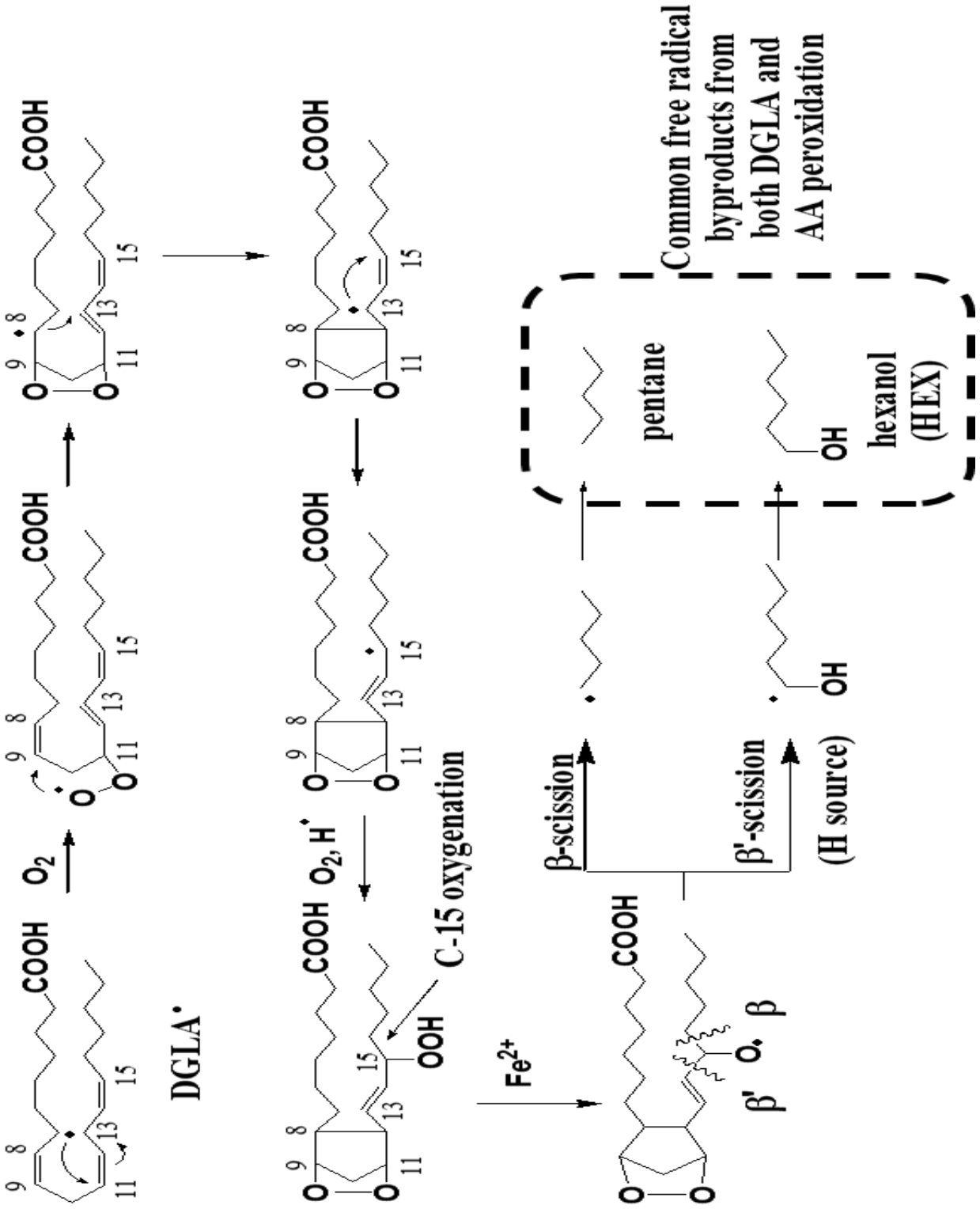

Scheme 5. Pathways of COX-2-catalyzed DGLA peroxidation and generation of DGLA derived free radical byproducts from C-15 oxygenation.

Due to the common structural moiety (C-8 to C-20) in DGLA and AA, COX can catalyze their free radical peroxidation by the same pathway, i.e., C-15 oxygenation, to form the same free radical byproducts e.g. pentane and hexanol (HEX).

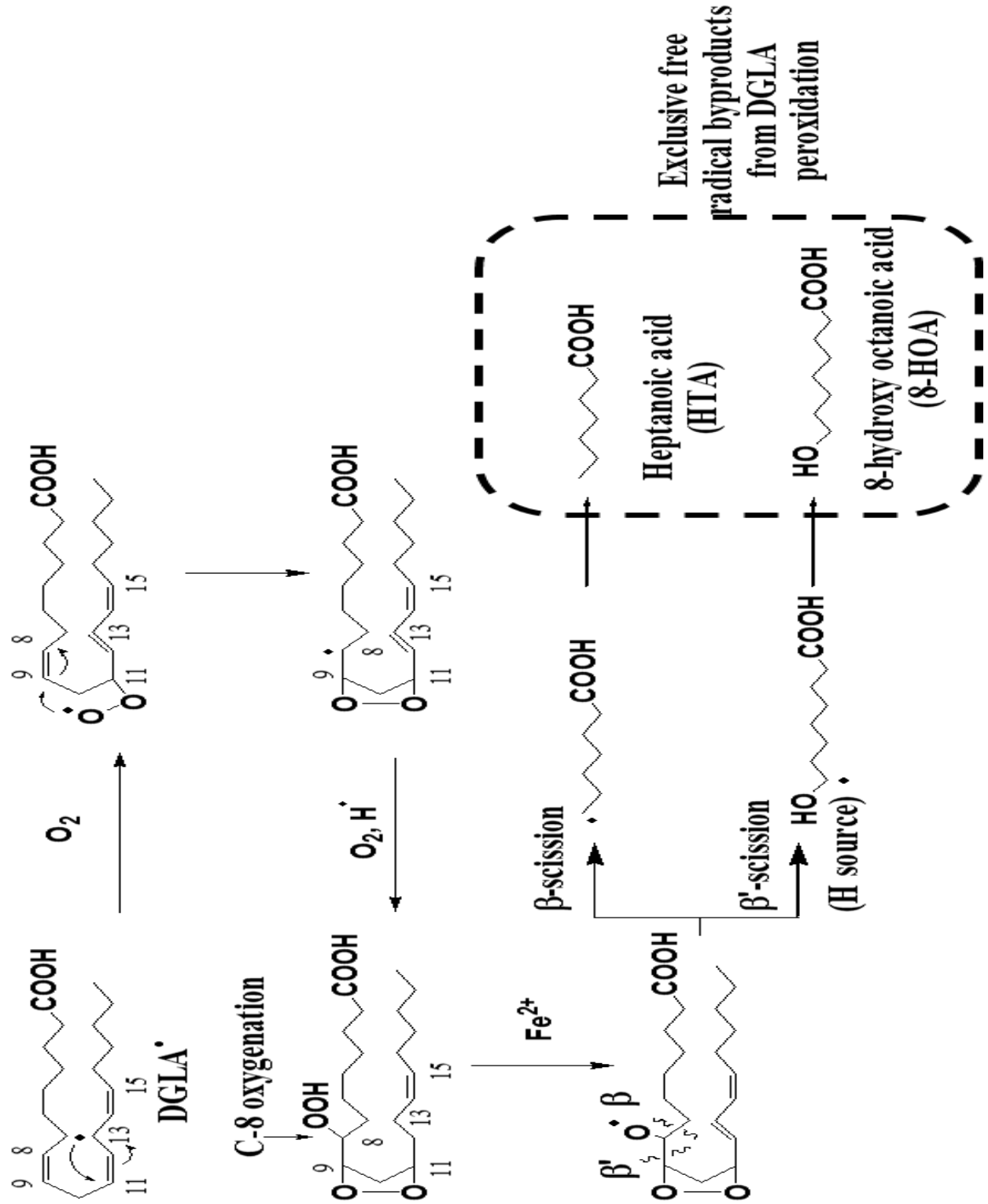

Scheme 6. Pathways of COX-2-catalyzed DGLA peroxidation and generation of DGLA derived free radical byproducts from C-8 oxygenation.

The different structural moiety (C-1 to C-7) in DGLA leads to formation of distinctive free radical byproducts including heptanoic acid (HTA) and 8-hydroxyoctanoic acid (8-HOA) from its unique C-8 oxygenation.

In light of these findings, we proposed that the exclusive free radical byproducts may be responsible for DGLA's anti-cancer activities. Thus, in this study, we investigated the potential anti-cancer effects and the possible molecular mechanism of DGLA's free radical byproducts on pancreatic cancer cells. It was found that DGLA's exclusive free radical byproduct 8-HOA (Scheme 6) can suppress pancreatic cancer cell growth and migration. As many short chain fatty acids have shown effects on inhibiting histones deacetylases (HDACs), we further proposed that, 8-HOA, with a structure similar to these HDAC inhibitors, may exert its anti-cancer activities by serving as a HDAC inhibitors to cause DNA damage and induce cancer cell apoptosis, resulting in inhibiting growth of pancreatic cancer cells [106].

More recently, we also found that 8-HOA can downregulate expressions of matrix metalloproteinase-2 (MMP-2) and MMP-9 (proteins involved in degradation of extracellular matrix) to inhibit pancreatic cancer cell and tumor migration and invasion [107].

These novel findings have led to a paradigm shifting concept that, instead to inhibit high level of COX-2, overexpressed COX-2 in cancers can be exploited to promote formation of 8-HOA from COX-2-catalyzed DGLA peroxidation for controlling cancer cell growth and migration. In the present study, we took advantage of the high COX-2 expression in pancreatic cancer to work against cancer cells, which not only provided an innovative ω-6s-based strategy to treat cancer, but also established a new dogma for COX-2 biology in cancer therapy.

1.4. Delta-5 desaturase knockdown (D5D-*KD*) as a novel strategy in cancer therapy

Although DGLA can generate the free radical byproduct 8-HOA, which possesses anti-cancer effects, from COX-2-catalyzed lipid peroxidation, the formation of 8-HOA can be limited by delta-5-desaturase (D5D). D5D is the rate limiting enzyme to convert DGLA to AA by forming double bond at the delta-5 position in DGLA. D5D, expressed in most organs, especially

in the liver, has two membrane spanning domains, three histidine-rich regions, and a cytochrome b5 domain [108]. D5D is encoded by FADS1 genes belonging to FADS family which is located on chromosome 11 as a cluster [108]. D5D plays an important role in regulating the composition of ω-6 fatty acids and has been studied in various diseases, including obesity, insulin resistance and coronary heart disease [109-110].

There are no man-made or natural compounds that have been characterized as effective D5D inhibitors. A variety of synthetic such as CP-24879 (p-(Isopentyloxy)-aniline) and natural compounds such as sesamin have been used to inhibit D5D to manipulate the metabolism of DGLA to AA [111-114]. For example, CP-24879, a dual D5D and D6D inhibitor, was characterized as a potential anti-inflammatory agent as it can decrease the levels of AA and its metabolites PGE2 and increase levels of DGLA and its metabolite PGE1 [111-112]. In addition, sesamin also exerted an inhibitory effect on the activity of D5D, resulting in decreased production of PGE2 and interleukin-6 in mice supplemented with safflower oil diets [113-114]. Gene trapping was also used to create FADS1-deficient mice which had suppressed colon tumor cell development attributed to increased levels of DGLA and PGE1 and decreased levels of AA and PGE2 [115-117].

Although D5D has been studied extensively in metabolic syndrome, it has not received much attention as a target in cancer treatment. In our study, we used siRNA or shRNA transfection to knock down D5D in pancreatic cancer cells. Knockdown of D5D can limit the generation of deleterious metabolites such as PGE2 from COX-catalyzed AA peroxidation, achieving similar effects of COX-2 inhibitors. Meantime, formation of 8-HOA (cancer inhibitor) can be promoted from COX-2-catalyzed DGLA peroxidation as more DGLA is reserved by downregulation of D5D, providing an innovative strategy for treating pancreatic cancer.

A variety of chemotherapeutic drugs have been developed to treat pancreatic cancer such as gemcitabine, oxaliplatin and erlotinib [118-127]. Gemcitabine is the most common chemotherapeutic drug for inhibiting pancreatic cancer growth and metastasis. Gemcitabine acts as a nucleoside analog to replace one of the building parts of nucleic acids in the process of DNA replication [128]. However, pancreatic cancer cells can develop a high tolerance toward gemcitabine. The resistance to gemcitabine is associated with a variety of different cellular pathways, transcriptional factors and nucleotide metabolism enzymes [129-133]. For example, pancreatic cancer cells have shown resistance to gemcitabine due to decreased expression of hENT1 (human equilibrative nucleoside transporter 1, e.g., gemcitabine transporter) [129]. Many complementary strategies have been investigated in order to achieve the improvement of efficacy and safety of chemotherapy [34-35, 75-80].

It has also been reported that COX-2 inhibitors (e.g. apricoxib and celecoxib) and ω-3 fatty acids (e.g. EPA and DHA) can sensitize chemoresistant pancreatic cancer cells to gemcitabine [34-35, 75-80]. However, ω-6 fatty acids have received much less attention as a complementary strategy to improve the efficacies of chemotherapy drugs due to the deleterious metabolites (e.g. PGE2) generated from COX-2 catalyzed AA peroxidation.

In this study, direct treatment of 8-HOA as well as endogenous formation of 8-HOA from D5D knockdown and DGLA treatment can both promote the efficacies of many chemotherapy drugs (e.g. gemcitabine, erlotinib, and oxaliplatin) on pancreatic cancer cells or tumors by further inducing apoptosis. The efficacy of chemotherapy drugs was enhanced on suppressing pancreatic cancer cell migration and invasion potential as our strategy can alter expression of proteins involved cancer metastasis.

1.5. Summary of research aims

Considering abundant and inevitable source of ω-6s in daily diet and DGLA's association with anti-cancer bioactivities, DGLA supplementation and D5D inhibition may represent a novel strategy for pancreatic cancer treatment. However, the molecular mechanism of DGLA's anti-cancer activities have not been elucidated. DGLA can be readily converted to AA by D5D which results in limited availability and activity of DGLA. Here we hypothesize that the 8-HOA formed from COX-catalyzed DGLA peroxidation is responsible for DGLA's anti-cancer activities, and downregulation of D5D can promote formation of 8-HOA which can serve as an HDAC inhibitor to inhibit cancer cell growth and migration.

We tested our hypotheses by pursuing the following aims: (1) to assess the effects and molecular mechanism of 8-HOA in pancreatic cancer cells; (2) genetically knocking down D5D to elicit DGLA's anti-cancer effects, and enhance efficacies of chemotherapy drugs; (3) to test the effect of D5D-*KD* and DGLA supplementation on pancreatic tumors in a xenograft mouse model (**Scheme 7**). In our study, instead of COX-2 inhibition, we aim to establish a new dogma for COX-2 biology in cancer by taking advantage of the fact that cancer cells and tumor commonly overexpress COX-2. We expect that the outcome of this research will provide guidance for developing a novel ω-6-based strategy for pancreatic cancer therapy.

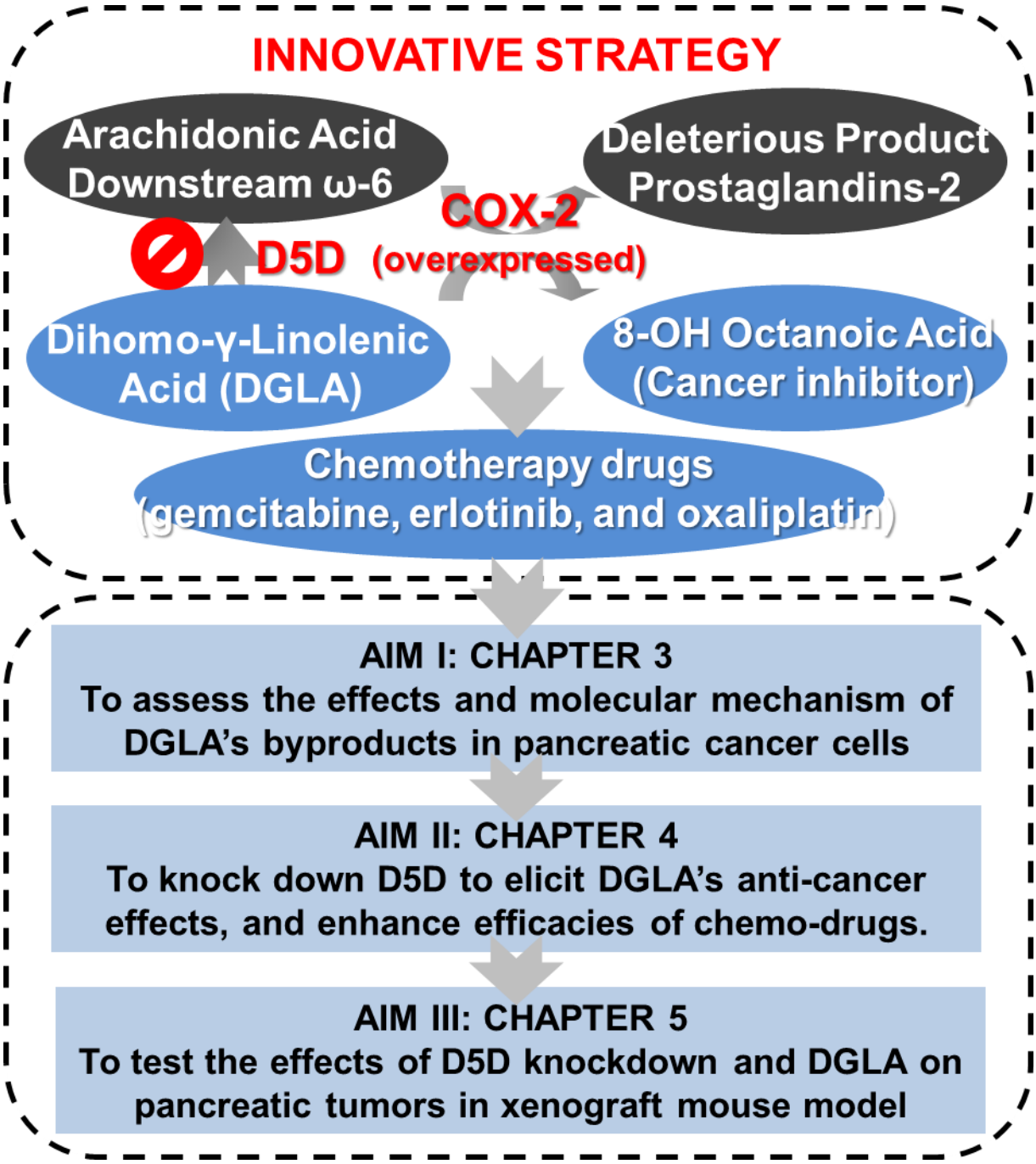

Scheme 7. Research outline.

We hypothesized that the potential anti-cancer activities were derived from free radical byproducts formed from COX-catalyzed DGLA peroxidation. Thus, in this study, we aimed to (1) assess the effects and molecular mechanism of DGLA's byproducts in pancreatic cancer cells; (2) knock down D5D to elicit DGLA's anti-cancer effects, and enhance efficacies of chemotherapy drugs; and (3) test the effects of D5D-*KD* and DGLA on pancreatic tumors in xenograft mouse model.

2. METHODS AND MATERIALS

2.1. Chemicals and reagents

Pure DGLA for *in vitro* cell treatment was obtained from Nu-Chek-Prep (MN, USA). Analytic standard solution of DGLA, AA, PGE1, PGE2, DGLA-d_6, AA-d_8, PGE1-d_4, PGE2-d_9, and chemotherapeutic drugs (e.g. gemcitabine and oxaliplatin) were purchased from Cayman Chemicals (MI, USA). CelLytic™ lysis reagent, D5D primary antibody (from rabbit), 8-HOA was obtained from Sigma-Aldrich (MO, USA). Erlotinib was acquired from Adooq Biosciences (CA, USA). CellTiter® 96 Aqueous One Solution Reagent was acquired from Promega (Madison, WI, USA). Annexin V Apoptosis Detection Kit I was acquired from BD Pharmingen™ (NJ, USA). Acetonitrile (ACN, HPLC grade), water (H_2O, HPLC grade), methanol and ethyl alcohol pure were bought from EMD Chemicals (Gibbstown, NJ, USA).

D5D siRNA (catalog # 4390824, sense strand: ACAUCAUCCACUCACUAAATT, anti-sense strand: UUUAGUGAGUGGAUCG), and negative control siRNA (catalog # 4390843, NC-si, sense strand: UAAGGCUAUGAAGAGAUAC, anti-sense strand: AGCUUGUAAAGA-UCUGUUUUU), Lipofectamine™ RNAiMAX transfection reagent, and GlutaMAX™ Opti-MEM reduced serum medium was obtained from Thermo Fisher Scientific (MA, USA). X-ray film was purchased from Phoenix Research Products. (NC, USA).

TRIS base was obtained from J.T. Baker (Phillipsburg, NJ, USA). Hydrogen chloride (HCl, 12.1 N) was bought from EMD Chemicals (Gibbstown, NJ, USA). Sodium chloride (NaCl) was procured from VWR International (West Chester, PA, USA). cOmplete Protease Inhibitor Cocktail Tablets were obtained from Roche Applied Science (Indianapolis, IN, USA).

Bovine serum albumin solution (2.0 mg/mL) was purchased from Thermo Scientific (Rockford, IL, USA). The *DC*™ BCA protein assay, glycine, Sodium dodecyl sulfate (SDS), and

Precision Plus Protein™ Kaleidoscope Standards were obtained from Bio-Rad Laboratories (Hercules, CA, USA). Acrylamide/bis-acrylamide (30 % solution), 2-mercaptoethanol and CAPS were acquired from Sigma-Aldrich (St. Louis, MO, USA). Ammonium persulfate (APS) was purchased from AMRESCO (Solon, OH, USA). TEMED was bought from Research Organics (Cleveland, OH, USA). Tween® 20 was obtained from G-Bioscience (St. Louis, MO, USA).

Polyclonal anti-COX-2 antibody produced in rabbits was obtained from Abcam (Cambridge, MA, USA). Polyclonal anti-D5D antibody produced in rabbits and monoclonal β-actin antibody produced in mice were obtained from Sigma-Aldrich (St. Louis, MO, USA). γ-H2AX primary antibody was procured from Bethyl Laboratories (TX, USA). All other primary antibodies and horseradish peroxidase-conjugated goat anti-rabbit IgG and horseradish peroxidase-conjugated goat anti-mouse IgG were obtained from Cell Signaling (MA, USA). Pierce ECL Western Blotting Substrate was acquired from Thermo Scientific (Logan, UT, USA).

2.2. Cell culture

The human pancreatic cancer cell line BxPC-3 (ATCC, Manassas, VA) was grown in RPMI-1640 medium (Thermo Fisher Scientific, MA, USA) supplemented with 10% FBS (Thermo Fisher Scientific, MA, USA). The human pancreatic cancer cell line PANC-1 (ATCC, Manassas, VA) was grown in Dulbecco's Modified Eagle's Medium (Thermo Fisher Scientific, UT, USA) supplemented with 10% FBS (Thermo Fisher Scientific, UT, USA). Cells were cultured in an incubator containing a 95% humidified atmosphere with 5% CO_2 at 37°C. Cells were sub-cultured at a ratio of 1:5 after they had reached ~90% confluency.

2.3. MTS assay

Cell viability upon different treatment was assessed *via* MTS assay using CellTiter 96® AQueous One Solution Cell Proliferation Assay, which is a colorimetric method for determining

the number of viable cells. The CellTiter 96® AQueous One Solution Reagent contains a tetrazolium compound [3-(4,5-dimethylthiazol-2-yl)-5-(3-carboxymethoxyphenyl)-2-(4-sulfophenyl)-2H-tetrazolium inner salt MTS] and an electron coupling reagent (phenazine ethosulfate, PES). PES has enhanced chemical stability as it combines with MTS to form a stable solution. In metabolically active cells, the MTS tetrazolium compound can be bioreduced by NADPH or NADH (produced by dehydrogenase enzymes) into a soluble colored formazan product. The quantity of formazan product measured by the absorbance at 490 nm is directly proportional to the number of living cells in culture.

The MTS assay was performed according to the manufacturer's instructions. Briefly, cells were seeded at 8,000 cells (in 100 μL medium) per well into 96-well plates, incubated overnight and exposed to various treatment. Then 20 μL of CellTiter® 96 Aqueous One Solution Reagent was added into each well. After 4 h incubation at 37°C, the quantity of formazan product was measured by recording the absorbance at 490 nm with a 96-well plate reader (SpectraMax M5; Molecular Devices). Cell viability was calculated as a percentage of the control group (normalized to 100%).

2.4. Colony formation assay

2.4.1. Cell culture and experimental setup

Cell survival upon various treatment was assessed by colony formation assay, which is a method based on the ability of a single cell to grow into a colony [134]. Cells are washed with PBS and incubated with 2 mL trypsin for 10 min to prepare the single cell suspensions. When most of the cells start to detach from the surface of cell culture flask, 6 mL of medium containing 10% FBS is added to neutralize the trypsin. The detached cells are pipetted up and down about 20 times. Cells are counted using a hemocytometer.

2.4.2. Cells plating and treatment

The number of cells is counted carefully using a hemocytometer and 2,000 cells per well are seeded into 6-well plates. The cells were incubated overnight for cells to attach to the surface of the plate and exposed to different treatments (e.g. fatty acids or/and chemo-drugs) for 48 h. Then the cells were washed with PBS and incubated with fresh complete medium for 10-14 days.

2.4.3. Fixing and staining colonies

After 10-14 days' incubation, the media from each plate was gently removed by aspiration and the cells in each well were washed with 1.0 mL PBS. The colonies were fixed with 2.0 mL of 10% neutral buffered formalin solution for 30 min and stained with 2.0 mL of 0.5% (w/v) crystal violet solution for 30 min.

2.4.4. Colony counting

Cell colonies with at least 50 cells/colony in each well were then counted. Plate efficiency and survival fraction were calculated as:

$$Plate\ Efficiency = \frac{number\ of\ colonies\ counted}{number\ of\ cells\ plated}$$

$$Survival\ Fraction = \frac{plate\ efficiency\ in\ treatment\ group}{plate\ efficiency\ in\ control\ group}$$

2.5. Cell apoptosis analysis

Cell apoptosis upon different treatments (e.g. ω-6s and/or chemo-drugs) was analyzed using Annexin V Apoptosis Detection Kit I (BD Pharmingen™, NJ, USA). Annexin V is a Ca^{2+} dependent phospholipid-binding protein that has a high affinity for phosphatidylserine. During early stage of apoptosis, the membrane phosphatidylserine is translocated from the inner to the outer leaflet of the plasma membrane, thereby can be bound with Annexin V. Conjugated with a fluorochrome FITC, Annexin V is commonly used as a sensitive probe for flow cytometric

analysis of cells that are undergoing apoptosis. Staining with FITC Annexin V is typically used in conjunction with a vital dye such as propidium iodide (PI) to allow the investigator to distinguish between early apoptotic cells vs. dead or damaged cells. This is because viable cells with intact membranes exclude PI, whereas the membranes of dead and damaged cells are permeable to PI. Therefore, cells that are both FITC Annexin V and PI negative are considered viable; cells that are FITC Annexin V positive and PI negative are considered in early apoptosis; and cells that are both FITC Annexin V and PI positive are considered in late apoptosis or already dead.

Cell apoptosis analysis was performed according to the manufacturer's instruction. Briefly, 3.0×10^5 cells were seeded overnight in each well of 6-well plates followed by different treatment. After exposure to treatment for certain time, the cells were harvested by trypsinization, washed with PBS and re-suspended in 1 × binding buffer (supplied in the kit) at a concentration of 1.0×10^6 cells/ml. Then 100 μl/sample of such cell suspension was treated with 5.0 μL of FITC Annexin V and 5.0 μL of PI solution (supplied in the kit), and incubated for 15 min at 25°C in the dark. After mixed with 400 μL of 1 × binding buffer, the samples were subject to apoptosis analysis using a Accuri C6 flow cytometer, 10,000 cells were counted for each sample. Unstained cells, cells stained with FITC Annexin V only and PI only was used to set up compensation and quadrants. Data were analyzed by FlowJo (TreeStar, Ashland, OR, USA).

2.6. HDAC activity assay

HDAC activity in pancreatic cancer cells upon assay different treatments was measured using HDAC activity colorimetric assay kit (BioVision, Pal Alto, USA) according to manufacturer's instructions. After BxPC-3 cells treated with 8-HOA or DGLA for 48 h, nuclear

proteins were extracted with NE-PER™ nuclear and cytoplasmic extraction reagents (Thermo Fisher Scientific, UT, USA). Nuclear extracts were diluted to 85 µL using H_2O and 10 × HDAC assay buffer was added to each well. 5 µL of the HDAC colorimetric substrate was added to each well and mixed thoroughly. The plates containing samples were incubated at 37°C for 1 h. 10 µL of lysine developer was added to each well to stop the reaction and incubated for 30 min at 37°C. The chromophore produced from the reaction of lysine developer and deacetylated substrate was analyzed using a microplate reader at 405 nm and used as an index for HDAC activity. The HDAC activity in BxPC-3 cells was calculated as a percentage of the control group without 8-HOA or DGLA treatment (normalized to 100%).

2.7. Western blot

Expression of D5D, COX-2 and cell signaling proteins involved in cancer cell growth and migration, including acetyl histone H3, γH2AX, Bcl-2, procaspase-9, procaspase-3, MMP-9, MMP-2, E-cadherin, vimentin and Snail were assessed by western blot as described below.

2.7.1. Preparation of buffers and reagents

Protein standard solutions: for protein concentration assay, bovine serum albumin solution (2 mg/mL) was diluted with deionized water to prepare a series of concentration at 0.25, 0.5, 0.75, 1.0 and 1.5 mg/mL. 1.0 ml aliquots of the standard solutions were stored at -20°C.

Protein assay reagent A: 1.0 mL of protein assay reagent A and 20 µL of protein assay reagent S supplied in DCTM BCA protein assay were mixed immediately before use.

SDS (10%) was prepared by dissolving 1.0 g of SDS in 10 mL deionized water.

APS (10%) was freshly prepared by dissolving 0.1 g of APS in 1 mL deionized water.

Tris buffer (1.5 M, pH 8.8) was prepared by transferring 18.2 g of Tris base into a 100 mL reagent bottle. 90 mL of deionized water was added and stirred to dissolve completely. The

pH was adjusted to 8.8 ± 0.05 with HCl (10 N). The volume was made up to 100 mL with deionized water.

Tris buffer (1.0 M, pH 6.8) was prepared by transferring 12.1 g of Tris base into a 100 mL reagent bottle. 90 mL of deionized water was added and stirred to dissolve completely. The pH was adjusted to 6.8 ± 0.05 with concentrated HCl (10 N). The volume was made up to 100 mL with deionized water.

Running buffer 10 × stock solution was prepared by transferring 30.3 g of Tris base, 144.0 g glycine and 10.0 g SDS into a 1000 mL reagent bottle. Then 900 mL of deionized water were added and stirred to dissolve completely. The volume was made up to 1000 mL with deionized water and stored at 4°C.

Running buffer 1 × working solution was prepared by transferring 100 mL of 10 × running buffer into a 1000 mL reagent bottle. The volume was made up to 1000 mL with deionized water and stored at 4°C.

Transfer buffer 10 × stock solution was prepared by transferring 22.1 g of CAPS into a 1000 mL reagent bottle. 900 mL of deionized water was added and stirred to dissolve completely. The pH was adjusted to 11.0 ± 0.05 with NaOH (10 N). The volume was made up to 1000 mL with deionized water and stored at 4°C.

Transfer buffer 1 × working solution was prepared by transferring 100 ml of 10 × transfer buffer to a 1000 mL reagent bottle. 200 mL methanol was added. The volume was made up to 1000 ml with deionized water and stored at 4°C.

Tris buffered saline (TBS) 10 × stock solution was prepared by transferring approximately 12.1 g of Tris base to a 1000 mL reagent bottle. 87.7 g of NaCl and 900 mL of

deionized water was added and stirred to dissolve, and the pH adjusted with HCl (10 N) to 7.6.±.0.05. The volume was made up to 1000 mL with deionized water and stored at 4°C.

Tris buffered saline-Tween (TBS-T, 1 × working solution) was prepared by transferring 100 mL of 10 × TBS in a 1000 mL reagent bottle. Then 1 mL Tween-20 was added and the volume was made up 1000 mL with deionized water and stored at 4°C.

Blocking Solution (5% non-fat dry milk) was prepared by transferring approximately 5 g of non-fat dry milk in a 100 mL reagent bottle. 90 mL of 1× TBS-T (Tween concentration, 0.1%, v/v) was added and stirred to dissolve, the volume was made up to 100 mL with 1× TBS-T.

SDS-PAGE gel: The resolving gel (10%) and stacking gel (4%) were prepared using 1.5 mm plates according to **Table 1**.

Table 1. Volume of components required to cast gels.

	Resolving Gel (10%)	Stacking Gel (4%)
H_2O	7.8 mL	7.25 mL
Tris buffer	2 mL (1.5 M, pH 8.8)	1.25 mL (1.0 M, pH 6.8)
acrylamide/bis-acrylamide (30 % solution)	5 mL	1.3 mL
10% SDS	150 µL	100 µL
10 % APS	150 µL	100 µL
TEMED	15 µL	10 µL
Total	~15 mL	~10 mL

2.7.2. Procedure

The cells were seeded in 6-well plates and exposed to different treatment. At experimental point, the culture medium was discarded and the cells were washed with PBS. Then ~100 µL of CelLytic™ lysis reagent was added into each well, the plates were allowed to sit on

ice for 10-15 min. The cell lysates were then collected by scraping them off from the plates. After centrifugation at 12,000 rpm for 10 min, the supernatant was collected.

The protein concentration in the cell lysates were measured using DC™ protein assay kit according to the manufacturer's instructions. Briefly, 5.0 μL of diluted cell lysate samples, 25 μL of reagent A and 200 μl reagent B were added in each well of a 96-well plate and mixed well. After 15 min incubation at room temperature in the dark, the absorbance was read at 750 nm using a microplate reader (SpectraMax M5, Molecular Devices). For every measurement, a series of protein standards was also included to construct a standard curve for quantification.

Each protein sample was normalized to the same concentration by diluting with certain amount of lysis buffer. The samples were mixed with 4 × loading buffer (sample: loading buffer = 3:1) and denatured at 95°C for 5 min. Then 40-60 μg protein in each sample was loaded onto a well of 10% SDS-PAGE gel, a protein weight marker (5 μL) was included for each gel.

The gel was run at constant voltage of 90 V, and switched to 120 V after samples passed the stacking gel. The power was switched off just before the blue line reached the bottom of gel.

Membranes, sponges and filter paper were soaked in transferring buffer for 15 min prior to transferring. Then the proteins on the gel were transferred electrophoretically to the membrane at constant voltage of 80 V for 2 h on ice.

After transferring, the membranes were incubated in 6 mL of blocking solution (5% non-fat dry milk) with continuous rock for 15 min to prevent non-specific binding, then incubated with primary antibody (e.g. COX-2, D5D, acetyl histone H3, γH2AX, Bcl-2, procaspase-9, procaspase-3, MMP-9, MMP-2, E-cadherin, vimentin and Snail, diluted in blocking solution) for overnight at 4°C in dark with continuous rocking, respectively. The next day, membranes were washed 3 times for 5 min each in 1 × TBS-T, and incubated with secondary antibody (anti-rabbit

IgG and anti-mouse IgG, diluted in blocking solution) for 1 h at room temperature with continuous rocking, respectively. Then the membranes were washed 3 times for 5 min each in 1× TBS-T again, incubated in ECL western blot substrates (Pierce, Thermo Fisher Scientific, UT, USA) for 2 min, and exposed to X-ray film (Phoenix Research Products, NC, USA). Luminescent signals were captured on a Mini-Medical Automatic Film Processor (Imageworks). Image of the film was captured and analyzed using NIH ImageJ software.

2.8. siRNA transfection

2.8.1. Preparation of siRNA transfection mixture

For transfection in each well of 96 well plates, 0.15 µL D5D targeted siRNA (100 µM stock, catalog number: 4390825, sense strand: ACAUCAUCCACUCACUAAATT, anti-sense strand: UUUAGUGAGUGGAUCG) and 0.6 µL of Lipofectamine™ RNAiMAX transfection reagent were diluted into 50 µL GlutaMAX™ Opti-MEM reduced serum medium, respectively. Then the two dilutions were mixed together and incubated for 5 min prior to adding into each well.

For transfection in each well of 6 well plates, 1.5 µL D5D targeted siRNA (100 µM stock) and 6.0 µL of Lipofectamine™ RNAiMAX transfection reagent were diluted into 500 µL GlutaMAX™ Opti-MEM reduced serum medium, respectively. Then the two dilutions were mixed together and incubated for 5 min prior to adding into each well.

2.8.2. Procedure

Cells were seeded at 3.0×10^5 cells per well in a 6-well plate or 8,000 cells per well in a 96-well plate for different experiments. After overnight incubation, cell culture medium was removed and the cells were washed by PBS. Then 1.0 mL (for 6-well plate) or 100 µL (for 96-well plate) of abovementioned siRNA transfection mixture was prepared and added into each

well of the plates. After 6 h transfection, the reduced serum medium (5% FBS) was replaced by fresh complete cell culture medium supplemented with 10% FBS. After 48 h, the transfected cells were ready for further treatments (e.g. fatty acids and chemotherapy drugs or their combinations) and other assessments, e.g. western blot, MTS assay, colony formation assay, LC/MS analysis, GC/MS analysis, and apoptosis analysis, etc. Cells transfected with a non-target control siRNA were used as controls.

2.9. Stable D5D knockdown *via* shRNA transfection

2.9.1. Design of D5D-targeted DNA oligonucleotides

D5D-targeted DNA oligonucleotides design: Using BLOCK-iT™ RNAi Designer (www.invitrogen.com/rnai), two strands of DNA oligonucleotides encoding D5D-targeted shRNA were designed and purchased (Integrated DNA Technol. IA). The sequences are as follows: target strand, TGCTGTAATCATCCAGGCCAAGTCCAGTTTTGGCCACTGACTG-ACTGGACTTGCTGGATGATTA; complementary strand, CCTGTAATCATCCAGCAAGTC-CAGTCAGTCAGTGGCCAAAACTGGACTTGGCCTGGATGATTAC.

2.9.2. Annealing reaction

The reaction system was set up in a 0.5 ml sterile centrifuge tube at room temperature according to **Table 2**:

Table 2. Annealing reaction reagents and amount.

Reagent	Amount
Target strand DNA oligo (200 μM)	5.0 μL
Complementary strand DNA oligo (200 μM)	5.0 μL
10× Oligo Annealing Buffer	2.0 μL
DNase/RNase-Free Water	8.0 μL
Total	20 μL

The mixture was incubated at 95°C for 4 minutes and allowed to cool down to room temperature for 5-10 minutes during which time the single-stranded oligos anneal to form a double-stranded oligo (at final concentration of 50 μM). The tube was centrifuged briefly (~5 seconds), gently mixed and stored at -20°C (stable for at least a year).

2.9.3. Diluting the double-stranded oligo

Prior to cloning the double-stranded oligo into pcDNA™6.2-GW/± EmGFP-miR vector, the 50 μM stock solution was diluted to a final concentration of 10 nM working solution (i.e. 5,000-fold dilution) by two steps: first, 1.0 μL of 50 μM ds oligo stock was mixed with 99 μL of DNase/RNase-free water to obtain a final concentration of 500 nM; second, 1.0 μL of 500 nM ds oligo was mixed with 5.0 μL of 10× Oligo Annealing Buffer and 44 μL of DNase/RNase-free water to obtain a final concentration of 10 nM.

2.9.4. Ligation reaction

The reaction was set up at room temperature according to **Table 3**.

Table 3. Ligation reaction reagents and amount.

Reagent	Amount
5× Ligation Buffer	4.0 μL
pcDNA™6.2-GW/miR, linearized (5 ng/μl)	2.0 μL
ds oligo (10 nM)	4.0 μL
DNase/RNase-Free Water	9.0 μL
T4 DNA Ligase (1 U/μl)	1.0 μL
Total	20 μL

The reaction system was mixed well by pipetting (do not vortex) and incubated for 5 minutes at room temperature. The mixture was put on ice for transforming into *E. coli* immediately or stored at -20°C overnight.

2.9.5. Transformation

2.0 µl of the ligation reaction was added into a vial of One Shot® TOP10 chemically competent *E. coli* and mixed gently (do not mix by pipetting). The mixture was incubated on ice 30 minutes. The cells were then heat-shocked for 30 seconds at 42°C without shaking. The tube was immediately transferred to ice and added with 250 µl of room temperature low salt LB medium. The tube was then shaken horizontally at 200 rpm, 37°C for 1 h. Then 50-200 µl from each transformation was spread on a pre-warmed low salt LB agar plate containing 100 µg/ml blasticidin, followed by overnight incubation at 37°C.

2.9.6. Extraction of plasmid DNA

5-10 blasticidin-resistant colonies were collected and incubated overnight in LB medium containing 100 µg/ml blasticidin. Then the plasmid DNA was isolated using PureLink™ HQ Mini Plasmid Purification Kit according to manufacturer's instruction. The concentration of plasmid DNA in each sample was determined using a Nanodrop spectrophotometer.

2.9.7. Transfecting cells

In 6-well plates, cells were seeded at 3×10^5 cells/well and incubated overnight. The cell culture medium was removed and cells were washed with PBS. For transfection in one well, 20 ng plasmid DNA and 15 µl transfection reagent was diluted into 500 µl of medium, respectively, then mixed together for 30 min at room temperature and added into each well. pcDNA™6.2-GW/± EmGFP-miR-neg control plasmid was also transfected into cells as a negative control. After 6 h transfection, the reduced serum medium was replaced with fresh complete medium with 10% FBS and the cells was incubated overnight. Then the cells in each well of the 6-well plates were trypsinized and re-plated into a 10 cm tissue culture plate in fresh complete medium containing 10 µg/ml of blasticidin. The blasticidin-containing medium was refreshed every 3-4

days until blasticidin-resistant colonies were identified (~10-14 days). 20 blasticidin-resistant colonies were collected and expanded, followed by western blot analysis to evaluate the knockdown effect in order to obtain a stable D5D knockdown cell line.

2.10. Wound healing assay

Wound healing assay was used to assess cell migration of D5D-*KD* and negative control BxPC-3 cells upon treatments (e.g. 8-HOA and DGLA). BxPC-3 cells were trypsinized, counted, and seeded 1×10^6 cells per well into 6-well plate. After the cells reached 90% confluence, a sterile 200 µL pipette tip was used to scratch on the bottom of a cell culture plate to create a vertical wound down through the cell monolayer. Excessive force against the plate was avoided so as not to damage the cell culture surface. The wells were washed using phosphate buffered saline subsequently to eliminate the impaired cells. The cell culture medium was changed to one with 1% FBS to avoid interference of cell growth. The cells were subjected to different treatments (e.g. 8-HOA, DGLA, and chemotherapy drugs) for 48 h. Images of cells in each well were captured by a bright field microscope immediately after wound creation as well as at different experimental time points. The wound area in each image was analyzed using Image-J software (NIH, Bethesda, MD, USA). The wound area percentage was calculated as the wound area from 24 h or 48 h *vs.* the wound area from 0 h in each group.

2.11. Transwell assay

Transwell migration assays were performed to assess cancer cell migration upon treatments with DGLA and chemo-drugs in transwell chamber with the non-coated membrane (24-well insert, pore size: 8 mm, Corning, Life Sciences). After treated with DGLA or chemo-drugs for 48 h, D5D-*KD* and negative control BxPC-3 cells were trypsinized, counted, and seeded 5×10^4 cells per 200 µL into each upper chamber. 600 µL medium with 10% FBS was

added into the lower chamber. After 48 h incubation, the medium in the upper and lower chambers was removed. The inserts were moved to clean wells and washed with PBS. The cells in the inserts were fixed with 10% formalin by adding formalin to the upper and lower chamber. After 30 min, formalin was removed and cells were stained with 0.05% crystal violet solution for another 30 min. After staining, cells on the upper sides of the inserts were removed with a Q tip and the cells on the lower side were taken picture using a phase contrast microscope (40 magnification).

For transwell invasion assay, the inserts were coated with Matrigel to mimic the extracellular matrix. The Matrigel was thawed at 4°C and diluted with medium containing no FBS (ratio: 1:8, total 100 µg). About 35-40 µL of diluted Matrigel was added to each insert and the Matrigel was solidified by putting the inserts into incubator for 2 h. The following experiments procedures for transwell invasion assay is the same as transwell migration assay.

2.12. HPLC/MS analysis of FAs and PGs

The free ω-6s and PGs from cells treated with/without DGLA were quantified *via* LC/MS analysis. Briefly, cells were seeded at 3.0×10^5 cells per well in 6-well plates and incubated overnight followed by siRNA transfection and fatty acids treatment. At different time points, the cells (scraped off from well) with 1 mL of culture medium were collected and mixed with 0.45 mL of methanol and 1.55 mL of water to make a total of 3 mL of 15% methanol solution. After adding internal standards (AA-d_8, DGLA-d_6, PGE1-d_4 and PGE2-d_9, 5.0 µL each), the mixture was vortexed for 1 min and set on ice for 30 min. Then sample solutions were centrifuged for 15 min at 3,000 rpm, the supernatant was collected and adjusted to pH 3.0 using 1.0 N HCl, followed by solid phase extraction (SPE) using a reverse phase SPE cartridge (SampliQ Silica C18 ODS, Agilent, CA, USA). For SPE, the cartridge was pre-conditioned with 2.0 mL water

and 2.0 mL methanol, then 3.0 mL sample solution was loaded into each cartridge. After washing with 1.0 mL of water, the free fatty acids and PGs were eluted with 2.0 mL ethyl acetate from cartridge, the elution containing analytes was vacuumed to dryness and reconstituted with 100 μL ethanol for LC/MS analysis.

The LC/MS system consisting of Agilent 1200 series HPLC system and Agilent 6300 LC/MSD SL ion trap mass was used to quantify the free ω-6s and PGs in reconstituted sample solution described in 2.8. LC separations were performed on a C18 column (Zorbax Eclipse-XDB, 4.6×75 mm, 3.5 μm) with 5.0 μL sample injection at a flow rate of 0.8 mL/min. The gradient of mobile phases (A: H_2O-0.01% HOAc and B: ACN-0.01% HOAc) is as follows: 0-12 min (isocratic), 68% A and 32% B; 12-14 min, 68 to 44% A and 32 to 56% B; 14-28 min (isocratic), 44% A and 56% B; 28-30 min, 44 to 14% A and 56 to 86% B; 30-38 min, 14 to 4% A and 86 to 95% B; and 38-44 min (isocratic), 5% A and 95% B. MS settings are as follows: electrospray ionization in negative mode; total ion current chromatograms in full mass scan mode (m/z 50 to m/z 600) were performed; nebulizer press, 15 psi; dry gas flow rate, 5.0 L/min; dry temperature, 325°C; compound stability, 20%; number of scans, 50.

For quantification, an internal standard curve was constructed from a series of mixtures consisting of PGE2, PGE1, AA, DGLA at various concentrations, and internal standards PGE1-d_4, PGE2-d_9, AA-d_8 and DGLA-d_6 at a constant concentration. Extracted ion current with m/z 353, 357, 351, 360, 305, 303, 311 were used to monitor the peak area PGE1, PGE1-d_4, PGE2, PGE2-d_9, DGLA, AA, AA-d_8 (m/z 311) and DGLA-d_6 (m/z 311), respectively. The concentrations of fatty acids and PGs in the samples were calculated using the internal standard curve by comparing the ratios of the peak areas of the analytes to the peak areas of their corresponding internal standards.

2.13. GC/MS analysis of 8-HOA

8-HOA produced from cells treated with/without DGLA were quantified *via* GC/MS analysis as a derivative of pentafluorobenzyl bromide (PFB-Br, **Scheme 8**) [135]. Briefly, 3.0 × 10^5 cells were seeded overnight in each well of a 6-well plate followed by various treatments. At experimental time points, the cells (scraped off from plate) and ~1.0 mL medium were collected and mixed with 500 μL of methanol containing internal standard (hexanoic acid), 50 μL of 1.0 N HCl, as well as 3.0 mL of dichloromethane. The mixture was vortexed for 30 s, centrifuged at 3,000 rpm for 4 min and the organic layer was collected. The same extraction was repeated once, and the dichloromethane layers were combined and evaporated to dryness using a vacuum evaporator. The sample was then reconstituted in 50 μL of 1.0% diisopropylethylamine in acetonitrile (v/v) and derivatized with 50 μL of 1% PFB-bromide in acetonitrile (w/v) at 37°C for 30 min. After the acetonitrile was removed using a vacuum evaporator, the residue was reconstituted in 100 μL of dichloromethane and ready for GC/MS analysis.

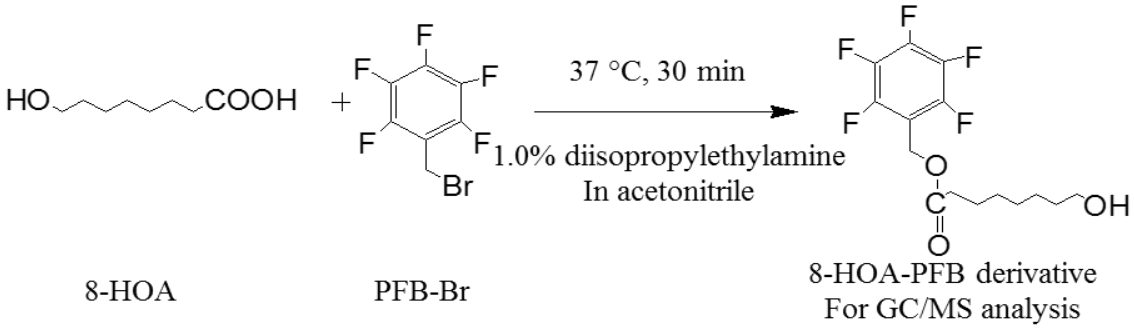

Scheme 8. Reaction of 8-HOA and PFB-Br to form PFB derivative for GC/MS analysis.

Sample solution (1.0 μL) was injected into an Agilent 7890A gas chromatograph. The GC oven temperature is programmed from 60 to 300°C at 25°C /min. The injector and transfer line are kept at 280°C. Quantitative analysis was performed using a mass selective detector with a source temperature of 230°C. For quantification, an internal standard curve was constructed from a series of mixtures consisting of 8-HOA at various concentrations, and internal standard

hexanoic at a constant concentration. Extracted ion current with m/z 181 (base peak for both 8-HOA-PFB and hexanoic acid-PFB derivatives) was used to monitor the peak area of 8-HOA and hexanoic acid derivatives. The concentrations of 8-HOA in the samples were calculated using the internal standard curve by comparing the ratios of the base peak at m/z 181 to the peak area of internal standard (hexanoic acid).

2.14. Tumor xenografts in nude mouse

Animal experiments were approved by the Institutional Animal Care and Use Committee at North Dakota State University (protocol A16039 and A16040). A total of 48 four-weeks old female nude mice (J:Nu, stock number 007850) were purchased from The Jackson Laboratory (Bar Harbor, ME). The mice were housed five per cage in the pathogen-free Innovive IVC system with water and food ad libitum. After allowing the mice to acclimate for one week, tumor xenografts were established by subcutaneously injecting 2×10^6 wild-type or D5D knockdown BxPC-3 cells (suspended in 200 µL DMEM medium without FBS) into both of the flanks of mice. The mice were fed with standard diet for another two weeks to allow tumors to reach ~10 mm^3, then divided into four different treatments groups (e.g., control, DGLA supplementation, gemcitabine, or combination of DGLA and gemcitabine) for four weeks. Tumor growth was monitored twice a week by measuring two axes of the tumor (L, longest axis; W, shortest axis) with a digital caliper during the treatment. Tumor volume was calculated as: $V = L \times W^2/2$ [136]. Mice body weight were also measured twice a week. At the endpoint, the mice were euthanized with an overdose of pentobarbital (200 mg/kg, i.p.) and the tumor tissues were collected for further analysis.

2.15. DGLA and gemcitabine treatments for mice

Mice injected with D5D-*KD* BxPC-3 cells or wild-type BxPC-3 cells were divided into four sub-groups (6 mice per group) and subjected the following treatment groups: (1) untreated control (standard diet); (2) DGLA alone; (3) gemcitabine alone; and (4) DGLA and gemcitabine. DGLA ethyl ester (8.0 mg/mouse, oral gavage, twice a week) were used to treat the mice for up to 4 weeks. Gemcitabine (intraperitoneal, ~30 mg/kg [137]) was administered to mice twice a week for up to 4 weeks.

2.16. Quantification of PGs and FAs from tumor tissues

After 4-week treatment, tumor tissues (tumor weight range: 0.05 g – 0.2 g) were excised from the mice and frozen in liquid nitrogen and smashed to powder, then mixed with 2.55 mL of water and 0.45 mL of methanol. After adding internal standards (AA-d_8, DGLA-d_6, PGE1-d_4 and PGE2-d_9, 5.0 µL each), the mixture was vortexed for 1 min and set on ice for 30 min. followed by centrifugation for 15 min at 3,000 rpm. The supernatant was collected and adjusted to pH 3.0 using 1.0 N HCl, followed by solid phase extraction using SampliQ Silica C18 ODS cartridge. The free fatty acids and PGs eluted with 2.0 mL ethyl acetate from cartridge were vacuumed to dryness and reconstituted with 100 µL ethanol for LC/MS analysis as described previously.

2.17. Quantification of 8-HOA from tumor tissues

After 4-week treatment, tumor tissues (tumor weight range: 0.05 g – 0.2 g) were taken from the mice and put in liquid nitrogen. The frozen tumors were smashed to powder and suspended in 1.0 mL water. The suspension was mixed with 500 µL of methanol containing internal standard (hexanoic acid), 50 µL of 1.0 N HCl, as well as 3.0 mL of dichloromethane. The mixture was then vortexed for 30s, centrifuged at 3,000 rpm for 4 min and the organic layer was collected. The same extraction was repeated once, and the dichloromethane layers were

combined and evaporated to dryness using a vacuum evaporator. The sample was then reconstituted in 50 μL of 1.0% diisopropylethylamine in acetonitrile (v/v) and derivatized with 50 μL of 1% PFB-bromide in acetonitrile (w/v) at 37°C for 30 min. After the acetonitrile was removed using a vacuum evaporator, the residue was reconstituted in 100 μL of dichloromethane and ready for GC/MS analysis as described previously.

2.18. Western blot for tumor tissue

After 4-week treatment, tumor tissues (tumor weight range: 0.05 g – 0.2 g) were taken from the mice. The protein in tumor tissue was extracted using CelLytic™ lysis. Briefly, the tissue samples were weighted and mixed with CelLytic™ lysis (the ratio of tissue weight and CelLytic™ lysis: 1:20, g/mL). The sample was homogenized on ice and centrifuged at 12,000 rpm for 10 min to pellet the tissue debris. The supernatant was then collected and transferred to a pre-chilled test tube. The expressions of acetyl histone H3, γH2AX, Bcl-2, procaspase-9, and procaspase-3 in tumor tissues were assessed by western blot using primary antibody (e.g. acetyl histone H3, γH2AX, Bcl-2, procaspase-9, and procaspase-3) and secondary antibody (anti-rabbit IgG and anti-mouse IgG) as described in section 2.7.

2.19. Immunofluorescence

Expressions of COX-2, D5D, cleaved PARP, Ki-67, MMP-2 and E-cadherin in tumor tissues were assessed by immunofluorescence. The immunofluorescence staining of COX-2, D5D, cleaved PARP, Ki-67, MMP-2 and E-cadherin was done by the staff in the advanced imaging and microscopy laboratory at North Dakota State University. The staining of tumor tissues was done by the technician in the advanced imaging and microscopy lab. Paraffin sections were deparaffinized in xylene 3 times for 5 min each time. The slides were rehydrated through graded ethanol solutions followed by PBS 3 times for 5 min each time. Antigen retrieval

was performed by boiling the slides for 20 min in antigen retrieval solution (10 mM sodium citrate, 0.05% Tween-20, pH 6.0) in water bath. Slides were cooled for 30 minutes at room temperature, rinsed with PBS 3 times for 5 min each time. The slides were wiped gently to remove PBS and covered with protein block agent for 30 min. After 30 min incubation. blocking agent was wiped gently from the slides. The slides were incubated with primary antibody (e.g. COX-2, D5D, cleaved PARP, Ki-67, MMP-2 and E-cadherin, dilution 1:1000) overnight at 4°C. After overnight incubation, the slides were washed with PBS 3 time for 5 min each time. The slides were then incubated with secondary fluorescent antibody (e.g. anti-rabbit IgG Alexa Fluor 647) for 30 min at room temperature in the dark room. After 30 min incubation, the slides were washed with PBS 3 time for 5 min each time. Cell nuclei were counter stained with DAPI showing blue staining in the images. The slides were then added with mounting media and covered with cover slip for imaging by a Zeiss Axio Imager M2 microscope which is located in the advanced imaging and microscopy laboratory. For immunofluorescence analysis of D5D, COX-2, MMP-2 and E-cadherin, the mean fluorescence intensity in each sample was measured by Image Pro software which represents the expression levels of proteins in tumor tissues.

For immunofluorescence analysis of cleaved PARP, the number of cleaved PARP positive cells and the total number of cells in each image were measured by Image Pro software. The percentage of apoptotic cells was calculated as percentage of the number of cleaved PARP positive cells compared to the total number of cells in each image. For immunofluorescence analysis of Ki-67, the number of Ki-67 positive cells and the total number of cells were measured by Image Pro software. The percentage of Ki-67 positive cells was calculated as percentage of the number of Ki-67 positive cells compared to the total number of cells in each image.

2.20. Statistics

For *in vitro* studies, the results of multiple observations (at least three separate experiments) were presented as mean ± standard deviation (SD). For in vivo studies, the results of multiple observations (at least six separate experiments) were presented as mean ± SD. Statistical differences between the mean values for different groups were evaluated by analysis of variance (ANOVA) and post hoc t-test. A statistically significant difference was considered with a p-value < 0.05.

The calculation of animal number is based on assuming a 40% difference (in tumor volume) will be observed between the groups, 25% standard deviation, p=0.05 and a power level of 80%. By using the formula sample size = $2\times SD^2(Z^{\alpha/2} + Z^{\beta})^2/d^2$ (SD = standard deviation, $Z_{\alpha/2} = Z_{0.05/2} = Z_{0.025} = 1.96$, $Z_{\beta} = Z_{0.20} = 0.8416$ at 80% power, d = difference between mean values) [138], the sample size equals 6.1. Therefore, we needed 6 mice per group in this study.

3. DIRECT TREATMENT OF 8-HOA CAN INHIBIT PANCREATIC CANCER CELLS GROWTH AND MIGRATION

3.1. Introduction

Pancreatic cancer is one of the most common causes of cancer death in the United States (e.g. over 40000 people died of pancreatic cancer in 2016 [139]). Surgery, radiation therapy and chemotherapy have been used to treat pancreatic cancer patients. A variety of pharmacological and diet care regimens have also been investigated as complementary strategies to improve efficacy of the standard chemotherapy for pancreatic cancer. For example, ω-3s have been proven to possess anti-cancer effects toward pancreatic cancer cells as well as tumors [28-32]. ω-6s, more abundant fatty acids in our daily diet, however, have received much less attention in cancer treatment mainly due to formation of deleterious metabolites (e.g. 2-series prostaglandins) from COX-catalyzed AA peroxidation [64-70]. DGLA, the immediate precursor of AA, may represent an exceptional ω-6 fatty acid as it is related to anti-cancer bioactivities [97-99].

Dr. Qian's lab has developed a HPLC/ESR/MS in combination with spin trapping technique to characterize the individual PUFA-derived free radicals. In this system, spin-trapped free radicals are separated according to their distinct chromatographic polarities by the HPLC column, monitored by ESR, and identified by MS. Using this HPLC/ESR/MS combination approach along with spin trapping technique (POBN as the trapping agent), the common as well as exclusive free radicals generated from COX-catalyzed AA and DGLA peroxidation have been successfully characterized [103-105]. Due to the similar structural moiety (C-8 to C-20), DGLA and AA can form the same free radical byproducts, pentane and HEX (hexanol, the common free radical byproduct that can be generated from both COX-2-catalyzed DGLA and AA peroxidation) *via* C-15 oxygenation (Scheme 5). Due to the different structural moieties, DGLA

can also go through C-8 oxygenation to form two unique free radical byproducts, HTA and 8-HOA from its COX-catalyzed peroxidation (Scheme 6) [104-105].

In this chapter, we first tested the effects of metabolites generated from COX-2-catalyzed DGLA peroxidation, including HEX (the common free radical byproduct), HTA, 8-HOA (two exclusive free radical byproducts) and PGE1 on BxPC-3 cell growth. We found that the direct treatment of certain amounts of 8-HOA can inhibit growth and migration of BxPC-3 cells *via* promoting cell apoptosis and downregulating MMPs. In addition, direct treatment of 8-HOA can be combined with many chemo-drugs such as gemcitabine to kill pancreatic cancer cells. We chose gemcitabine in our study as it is the most common chemo-drug used in pancreatic cancer treatment and many pancreatic cancer patients have develop resistance to it. We expect the results from this chapter could provide a rationale for designing a ω-6-based diet care strategy in combination with chemotherapy for pancreatic cancer.

3.2. Results

3.2.1. Direct treatment 8-HOA inhibited pancreatic cancer cell growth

Two pancreatic cancer cell lines, BxPC-3 (high COX-2 expression) and PANC-1 (deficient COX-2 expression) were selected to tested the effects of free radical byproducts generated from COX-2-catalyzed DGLA peroxidation on their cell viability using MTS assay. Three free radical byproducts were tested on BxPC-3 and PANC-1 cells, including HEX, HTA and 8-HOA (two distinct free radical byproducts from DGLA). The concentration range of treatment was from 0.1 μM to 10 μM, which is physiological relevant based on our previous studies [105].

Results from the MTS assay showed that treatment with 8-HOA (1.0 μM - 10 μM) inhibited cell viability of BxPC-3 cells (cell viability ~88.3% for 1.0 μM 8-HOA and ~ 86.2%

for 10 μM 8-HOA compared to control, **Fig 1**), while treatments of HEX and HTA (0.1 μM -10 μM) did not inhibit cell viability. In addition to free radical byproducts, we also tested the effect of PGE1 on BxPC-3 cancer cell viability. PGE1 is a major and stable metabolite from COX-catalyzed DGLA peroxidation. Studies have shown that PGE1 possesses anti-inflammation and anti-cancer activities and was commonly considered responsible for DGLA's anti-cancer effects [54-57]. However, our results showed that the treatments of PGE1 (0.1 μM – 10 μM, physiological concentration range) did not inhibited cancer cell viability (cell viability above 95% for 0.1 μM – 10 μM PGE1, Fig1). Together these results suggested that, instead of PGE1, 8-HOA is the metabolite responsible for DGLA's anti-cancer activities.

We also used PANC-1 (another pancreatic cancer cell line with deficient COX-2 expression) to test whether 8-HOA can inhibit its cancer cell viability. Treatment of 8-HOA significantly inhibited cancer cell viability in PANC-1 cells (cell viability ~86.3% for 1.0 μM 8-HOA and ~ 85.2% for 10 μM 8-HOA compared to control, **Fig 2**), while treatments of HEX and HTA (0.1 μM -10 μM) did not inhibit cell viability, consistent with the observation in BxPC-3 cells.

A colony formation assay was performed on BxPC-3 cells to further confirm the inhibitory effect of 8-HOA on cancer cell survival. Upon treatment of 8-HOA at 1.0 μM, colony formation of BxPC-3 cells was significantly inhibited with the survival fraction ~ 73.0% compared to control (**Fig 3A**). Data from both MTS assay and colony formation assay demonstrated that 8-HOA is the metabolite that accounts for DGLA's anti-cancer activities and can significantly inhibit cancer cell viability and cell survival.

In order to investigate how 8-HOA caused cell growth inhibition, we tested the effect of 8-HOA on cell apoptosis *via* FITC Annexin V and PI double staining followed by flow

cytometry. Direct treatment 8-HOA induced apoptotic cell population (population of early apoptotic cells, Annexin V positive and PI negative, ~ 6.89%, **Fig 3B**) *vs.* control (e.g., without 8-HOA, population of early apoptotic cells ~2.35%). The results indicated that 8-HOA is the metabolite responsible for DGLA's anti-cancer effects.

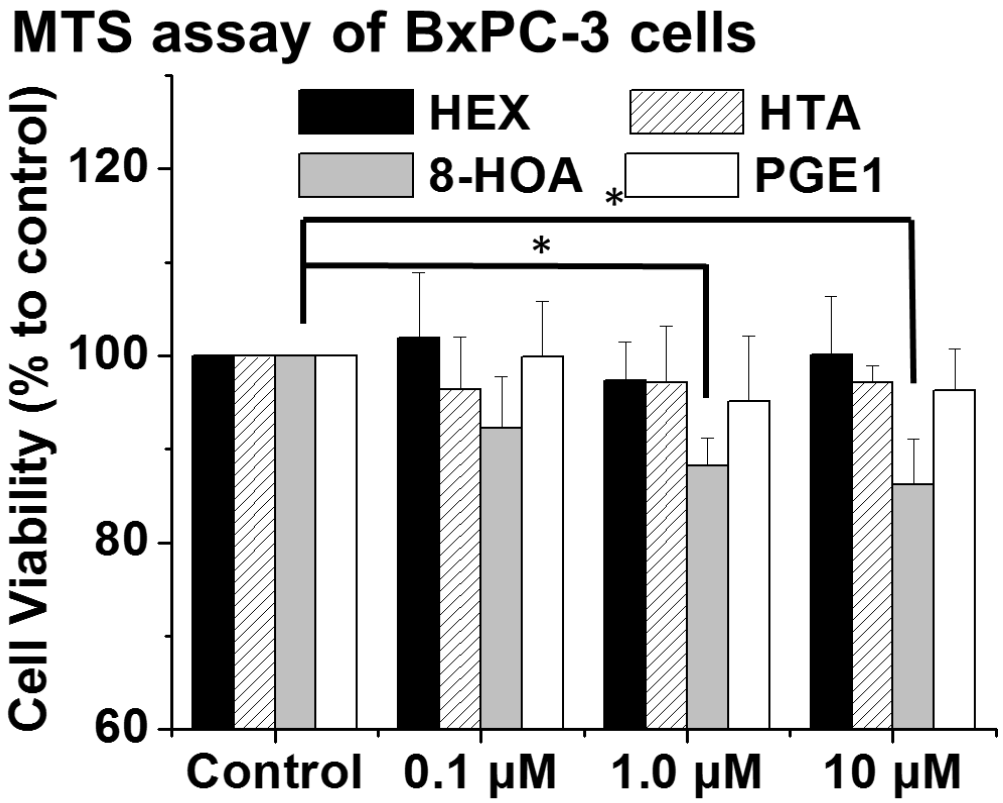

Fig 1. 8-HOA inhibited cell viability in BxPC-3 cells.
MTS assay of BxPC-3 cells after 48 h treatment of HEX (0.1 μM - 10 μM), HTA (0.1 μM - 10 μM), 8-HOA (0.1 μM - 10 μM) and PGE1 (0.1 μM - 10 μM). The BxPC-3 cells treated with vehicle were used as control. (*: significant difference $p < 0.05$ from $n \geq 3$).

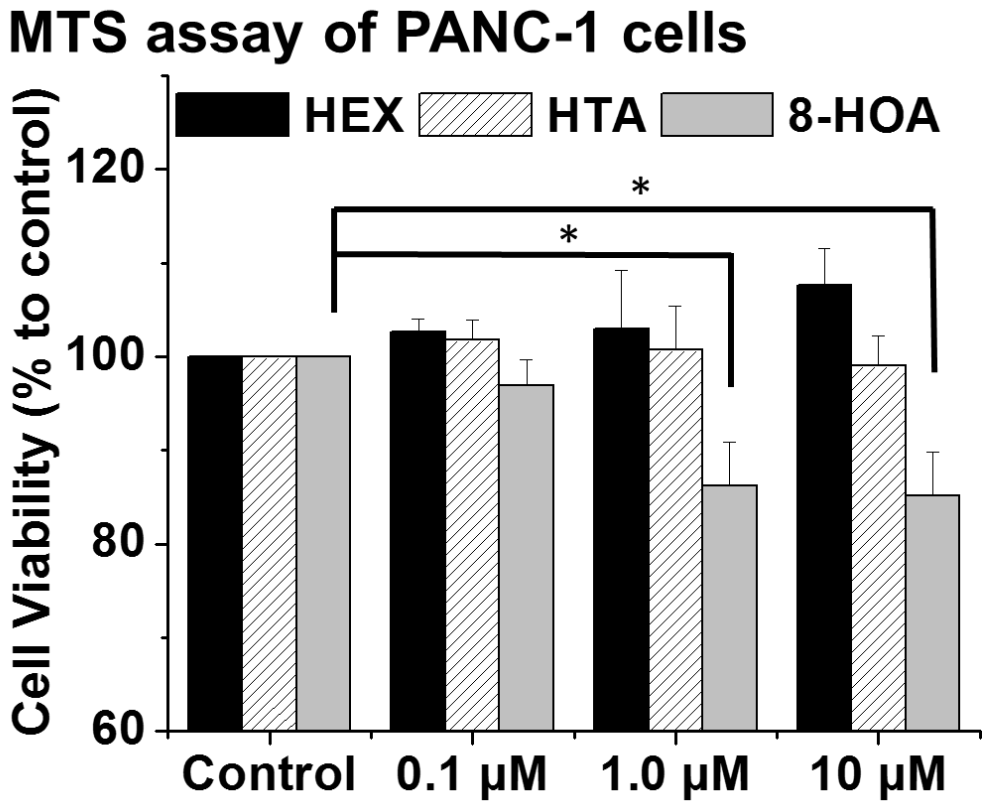

Fig 2. 8-HOA suppressed cell viability in PANC-1 cells.
MTS assay of PANC-1 cells after 48 h treatment of HEX (0.1 μM - 10 μM), HTA (0.1 μM - 10 μM) and 8-HOA (0.1 μM - 10 μM). The PANC-1 cells treated with vehicle were used as control. (*: significant difference $p < 0.05$ from $n \geq 3$).

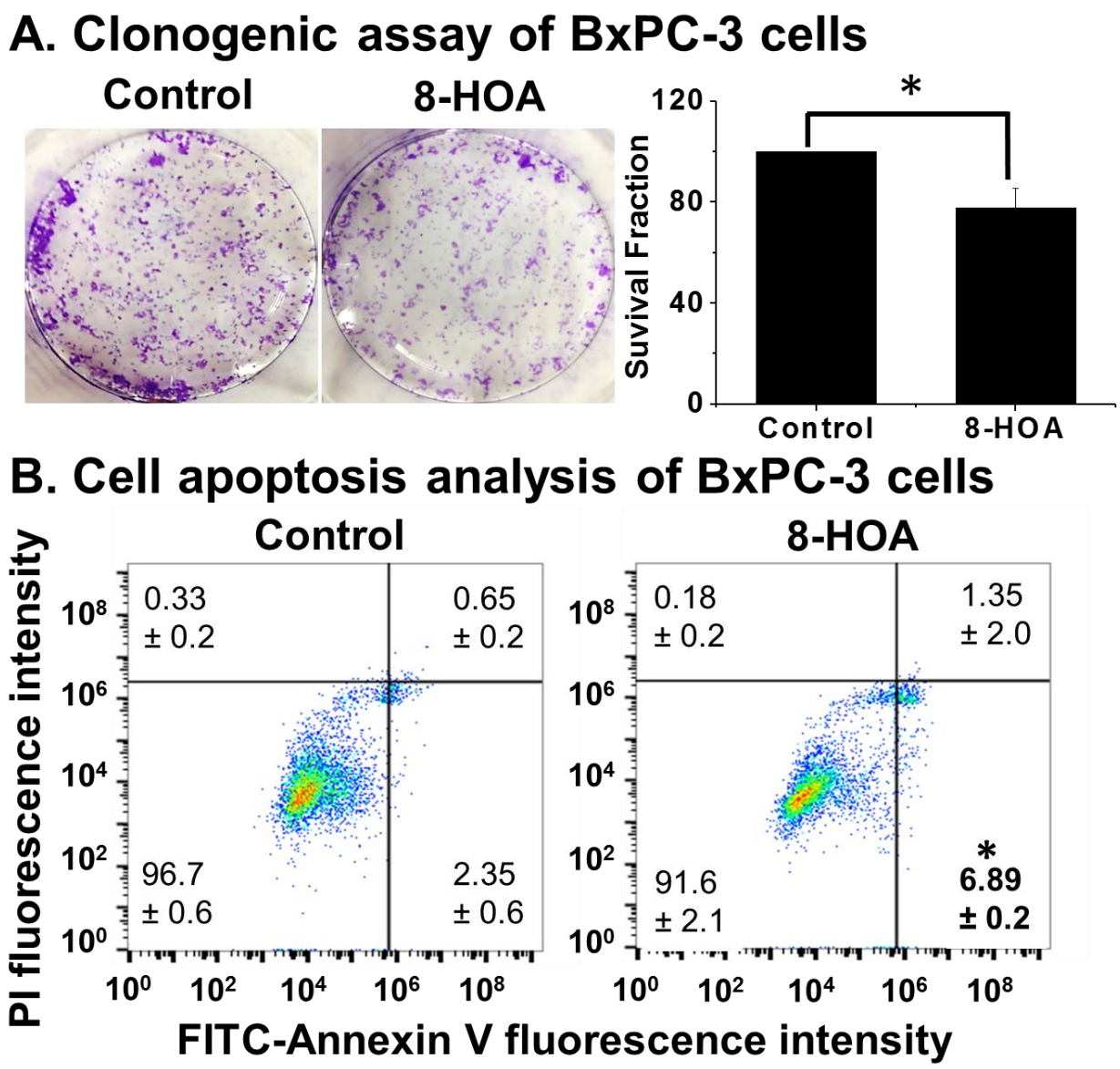

Fig 3. 8-HOA inhibited colony formation and induced cell apoptosis in BxPC-3 cells. A) Clonogenic assay of BxPC-3 cells at 10 days after 48 h of 8-HOA treatment (1.0 μM). The BxPC-3 cells treated with vehicle were used as control. B) Cell apoptosis analysis of BxPC-3 cells. After 48 h treatment of vehicle (control) and 8-HOA (1.0 μM), cells were double stained with FITC-Annexin V/PI and subjected to flow cytometry. (*: significant difference $p < 0.05$ from $n \geq 3$).

3.2.2. 8-HOA inhibited HDAC and caused DNA damage

HDACs are enzymes that can catalyze deacetylation of lysine residues of the core histone [140-142]. Increased expression of HDACs have been found in several types of cancers,

including pancreatic cancer, and play an important role in cancer development and progression [141-142].

A variety of short chain fatty acids such as butyrate and valproate can serve as effective HDAC inhibitors to suppress cancer cell growth and migration, and induced cell cycle arrest and apoptosis in many types of cancer, such as pancreatic cancer [147-150]. Since 8-HOA's structure is similar to some short chain fatty acids that are well-known HDAC inhibitors [151-154], we proposed that 8-HOA can also inhibit HDAC activity, leading to inhibited cancer cell growth and migration.

An HDAC activity assay was conducted to test the effect of 8-HOA on HDAC activity in BxPC-3 cells. Results showed that about 50% of HDAC activity was inhibited in BxPC-3 cells upon treatment with 8-HOA (1.0 μM) compared to cells without 8-HOA treatment (**Fig 4**), indicating that 8-HOA could serve as a HDAC inhibitor.

Results from western blots showed that there is an increase in expression of acetyl histone H3 (substrate for HDAC) in BxPC-3 cells upon 8-HOA treatment, confirming that 8-HOA is an HDAC inhibitor. We observed expression of DNA damage marker γH2AX was increased in BxPC-3 cells treated with 8-HOA compared to cells without 8-HOA treatment, consistent with HDAC inhibitors-induced DNA damage reported in other studies [155].

We tested the possible alternation of proteins involved in regulating cell apoptosis in BxPC-3 cells upon 8-HOA treatment. 8-HOA was found to downregulate protein expressions of procaspase-9 and procaspase-3 (pro-apoptotic proteins that activate the apoptotic pathway, **Fig 5**), which is consistent with the observation of 8-HOA induced apoptosis in FITC Annexin V and PI double staining. We demonstrated that 8-HOA can inhibit cell growth by serving as an

HDACi to prevent histone deacetylation to cause DNA damage, resulting in activation of pro-apoptotic proteins (e.g. procaspase-3 and procaspase-9).

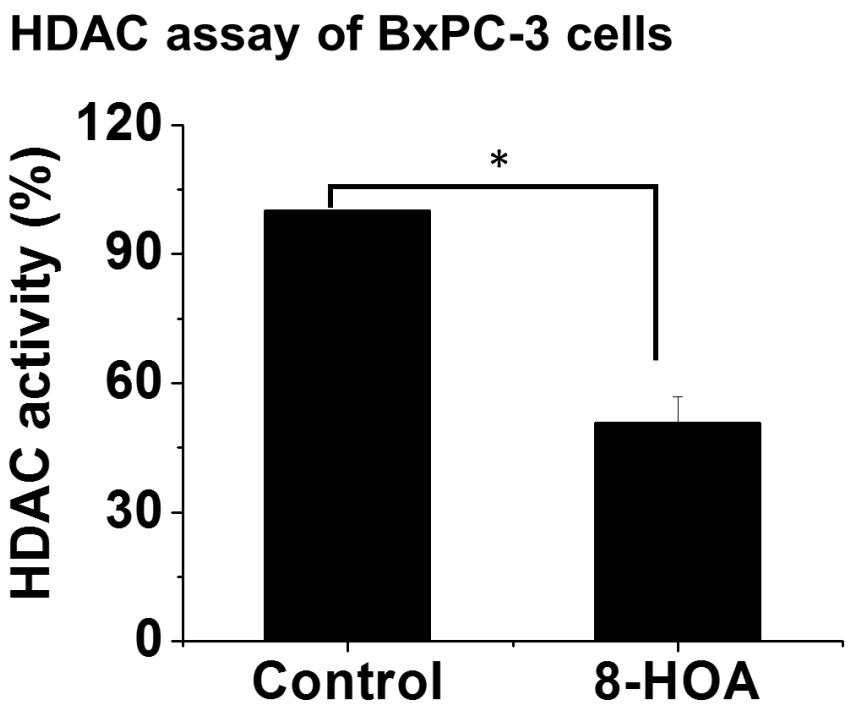

Fig 4. HDAC activity was inhibited by 8-HOA in BxPC-3 cells.
HDAC activity assay of BxPC-3 cells treated with vehicle (control) and 8-HOA (1.0 μM). (*: significant difference with $p < 0.05$ from $n \geq 3$).

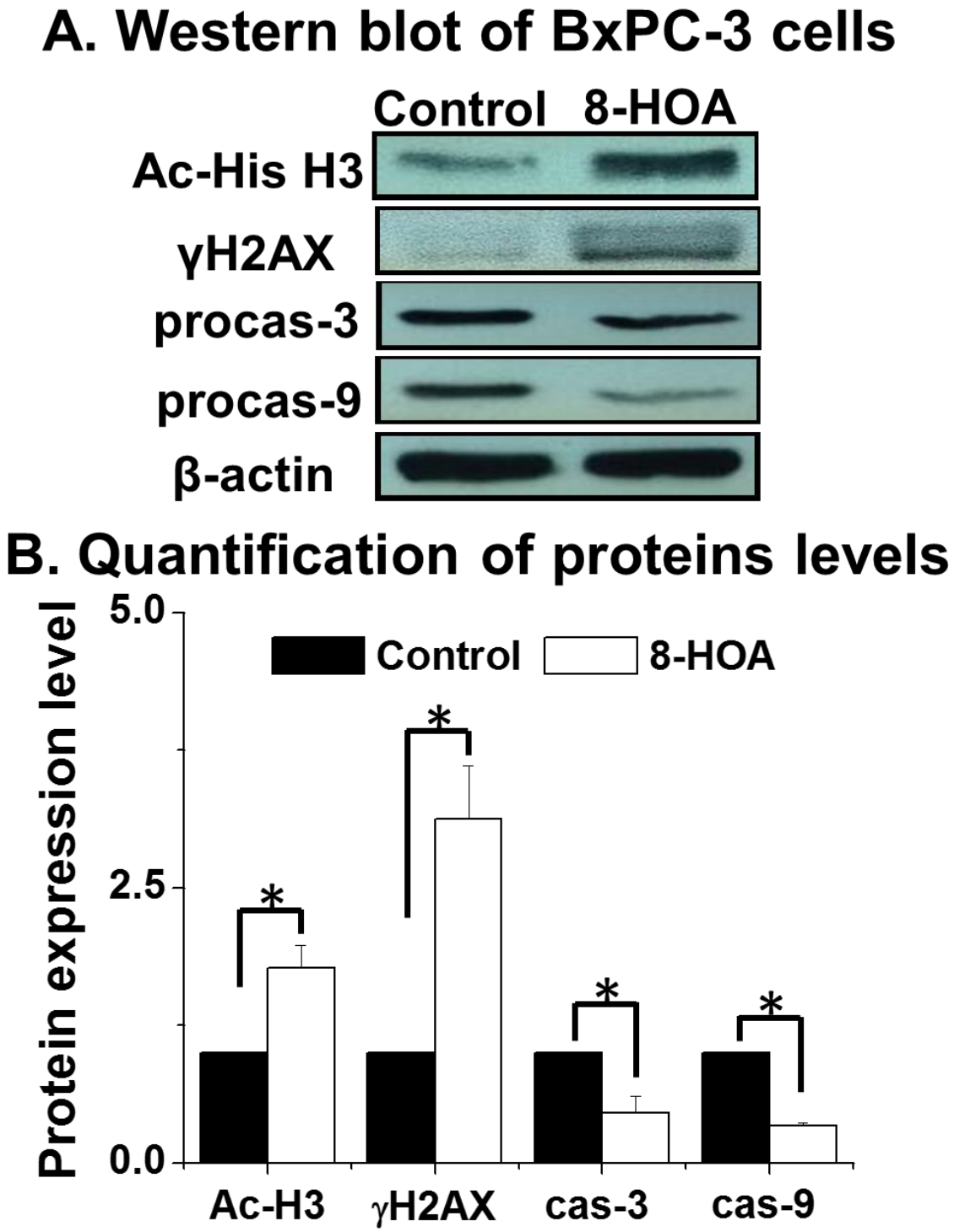

Fig 5. 8-HOA induced DNA damage and activated pro-apoptotic proteins.
A) Western blot of acetyl histone H3, γH2AX, procaspase-3 and procaspase-9 in BxPC-3 cells treated with vehicle and 8-HOA (1.0 μM). B) Quantification of protein expression level. Protein expression level was normalized using histone H3 as loading control (*: significant difference $p < 0.05$ from $n \geq 3$).

3.2.3. Pancreatic cancer cell migration was suppressed by 8-HOA

It is reported that, rather than the primary tumors, cancer metastasis accounts for more than 90% of all cancer death, including pancreatic cancer [156]. A majority of pancreatic cancer patients with cancer metastasis showed a poor survival rate as cancer cells metastasize to important organs such as the liver or lungs. Studies have shown that HDAC inhibitors such as butyrate and valproate can suppress cancer cell migration [149-154]. We proposed that 8-HOA, whose structure is similar to those well-known HDAC inhibitors, can also inhibit pancreatic cancer cell migration.

We used a wound healing assay to test whether the direct treatment 8-HOA could inhibit migration of pancreatic cancer cells BxPC-3. Upon treatment of 8-HOA (1.0 μM) for 48 h, BxPC-3 cells migration was significantly inhibited with the wound area ~ 81.1% at 48h compared to control ~ 58.3% (**Fig 6**).

We also investigated the possible molecular mechanism of the inhibition of cancer cell migration caused by 8-HOA. Results from western blot showed that 8-HOA decreased expressions of MMP-2 and MMP-9, two proteins involved in degradation of extracellular matrix (**Fig 7**). Our study indicated that 8-HOA could serve as a HDAC inhibitor to suppress breakdown of extracellular matrix, resulting in inhibition of cancer cell migration.

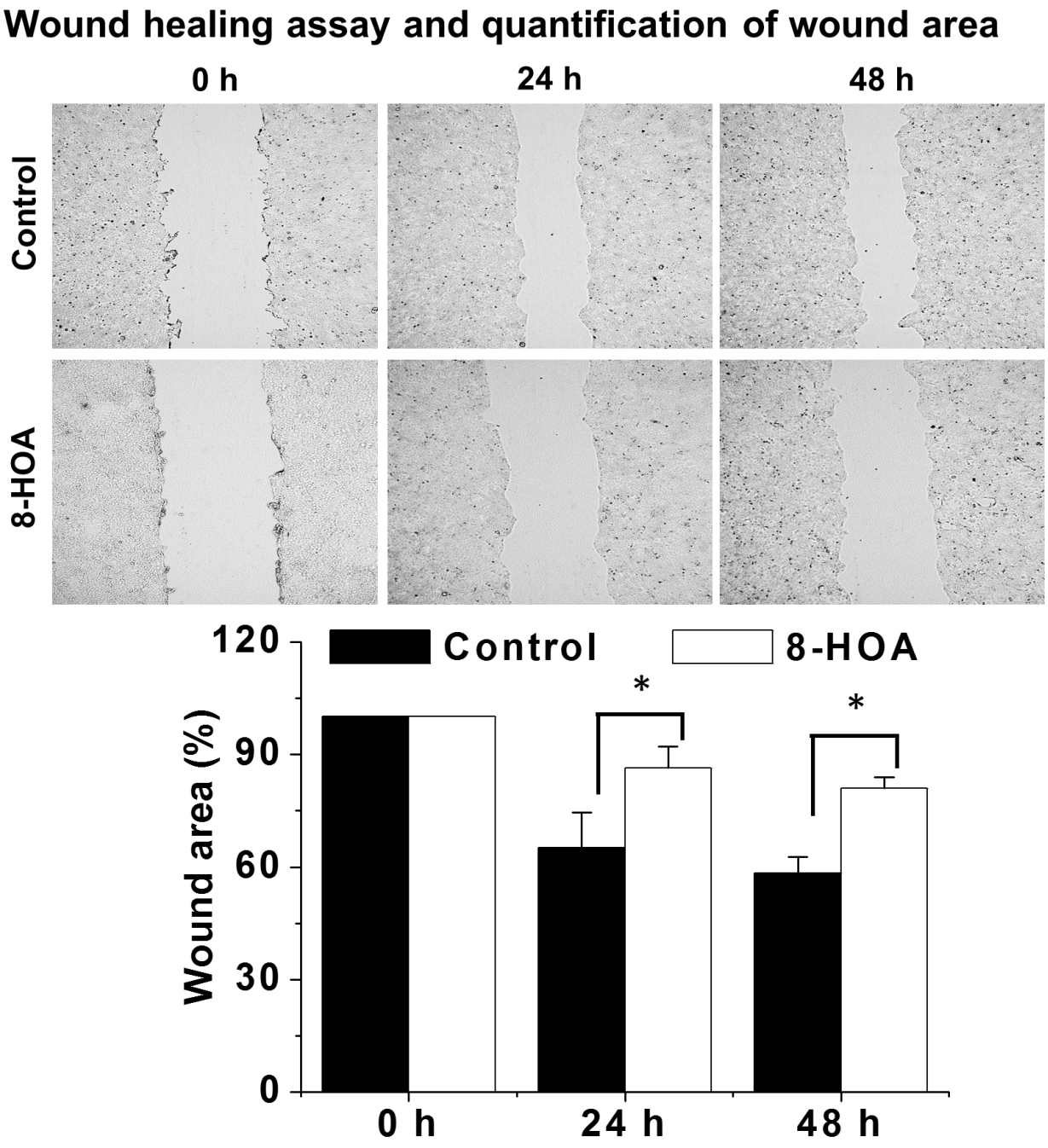

Fig 6. Cell migration of BxPC-3 cells was suppressed by 8-HOA.
Wound healing assay and quantification of wound area of BxPC-3 cells upon 8-HOA treatment (1.0 μM) for 48 h. The BxPC-3 cells treated with vehicle were used as control. (*: significant difference with $p < 0.05$ from $n \geq 3$).

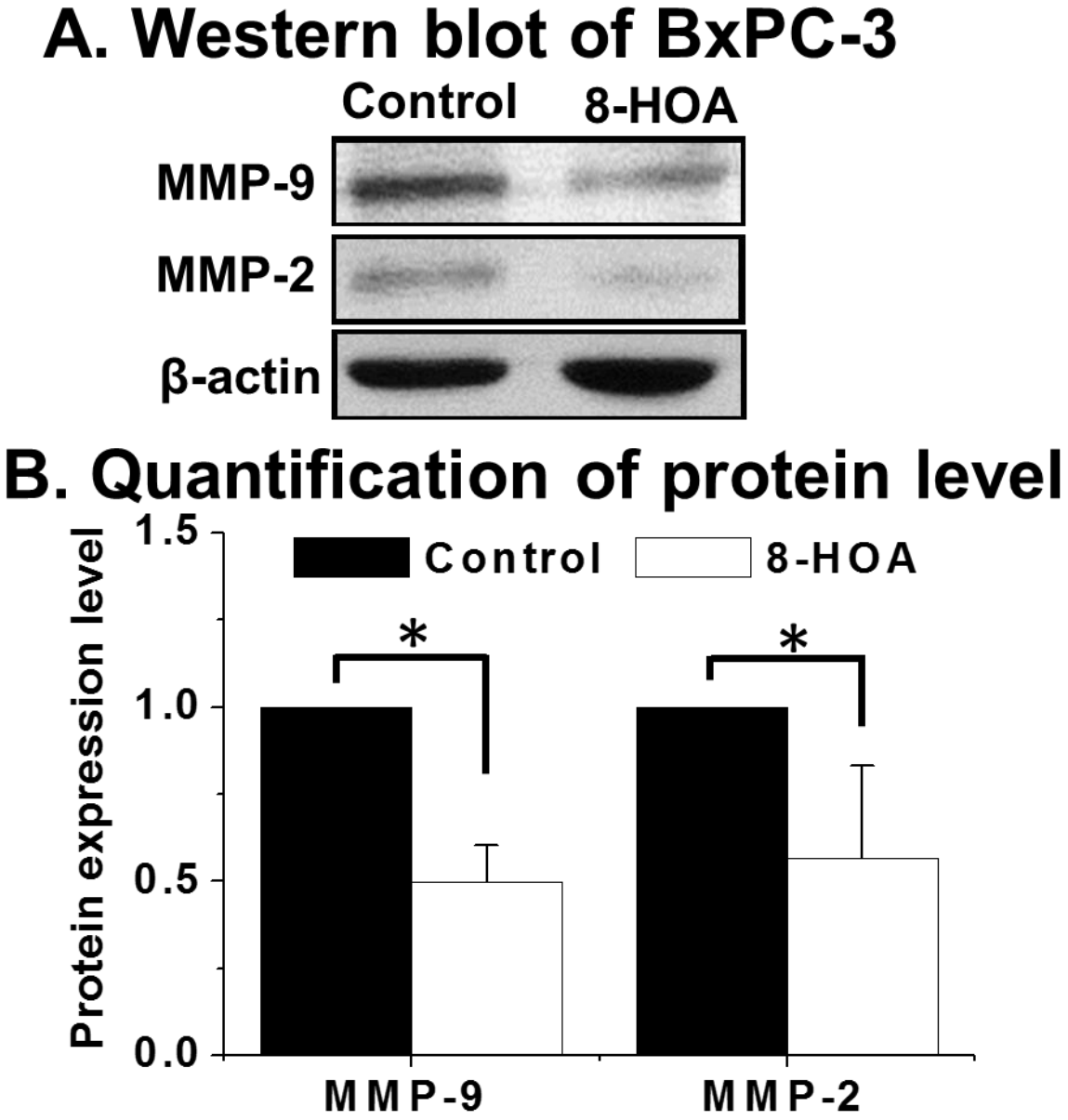

Fig 7. 8-HOA decreased levels of MMP-9 and MMP-2.
A) Western blot of MMP-2 and MMP-9 in BxPC-3 cells treated with vehicle and 8-HOA. B) Quantification of protein expression level of MMP-2 and MMP-9 in BxPC-3 cells treated with vehicle and 8-HOA (1.0 μM). Protein expression level was normalized using β-actin as loading control. (*: significant difference with $p < 0.05$ from $n \geq 3$).

3.2.4. Treatment 8-HOA enhanced the efficacies of chemotherapy drugs

Various chemotherapy drugs are used in clinical practices for treatment of pancreatic cancer [118-127]. However, drug resistance has been major obstacle for successful pancreatic cancer chemotherapy, as many types of pancreatic cancer cells are insensitive to chemo-drugs.

For example, many pancreatic cancer cell lines have been reported resistant to gemcitabine, a nucleoside analog that has been used as a front-line chemo-drug for pancreatic cancer treatment [129-133]. Thus, a variety of regimens such as ω-3 fatty acids and COX-2 inhibitors have been used to enhance efficacy of chemotherapy drugs on pancreatic cancer [34-35, 75-81].

We here tested whether 8-HOA can improve the efficacy of chemo-drugs on BxPC-3 cells. When cells were co-treated with 8-HOA and gemcitabine, 8-HOA could significantly enhance efficacy of gemcitabine on BxPC-3 cells. Significantly inhibited colony formations were observed in BxPC-3 cells upon treatment of gemcitabine and 8-HOA (survival fraction ~31.1% vs. 50.6% for gemcitabine only, **Fig 8**).

In addition to gemcitabine, we also tested whether direct treatment of 8-HOA could sensitize BxPC-3 cells to chemotherapeutic drugs, e.g., erlotinib (tyrosine kinase inhibitor used as targeted therapy drug for pancreatic cancer [120-125]) and oxaliplatin (platinum-based antineoplastic agent used for pancreatic cancer therapy [126-127]). Results showed that 8-HOA (1.0 μM) improved the cytotoxicity of erlotinib on BxPC-3 cells as shown in MTS assays (~37.8% cell viability for treatment 8-HOA plus 10 μM erlotinib vs. 49.7% for erlotinib only **Fig 9**). Treatment with 8-HOA also sensitized BxPC-3 cells to oxaliplatin as we observed in a MTS assay (cell viability 36.8 % for co-treatment of 8-HOA and 20 μM oxaliplatin vs. 52.4 % for oxaliplatin only, Fig 8).

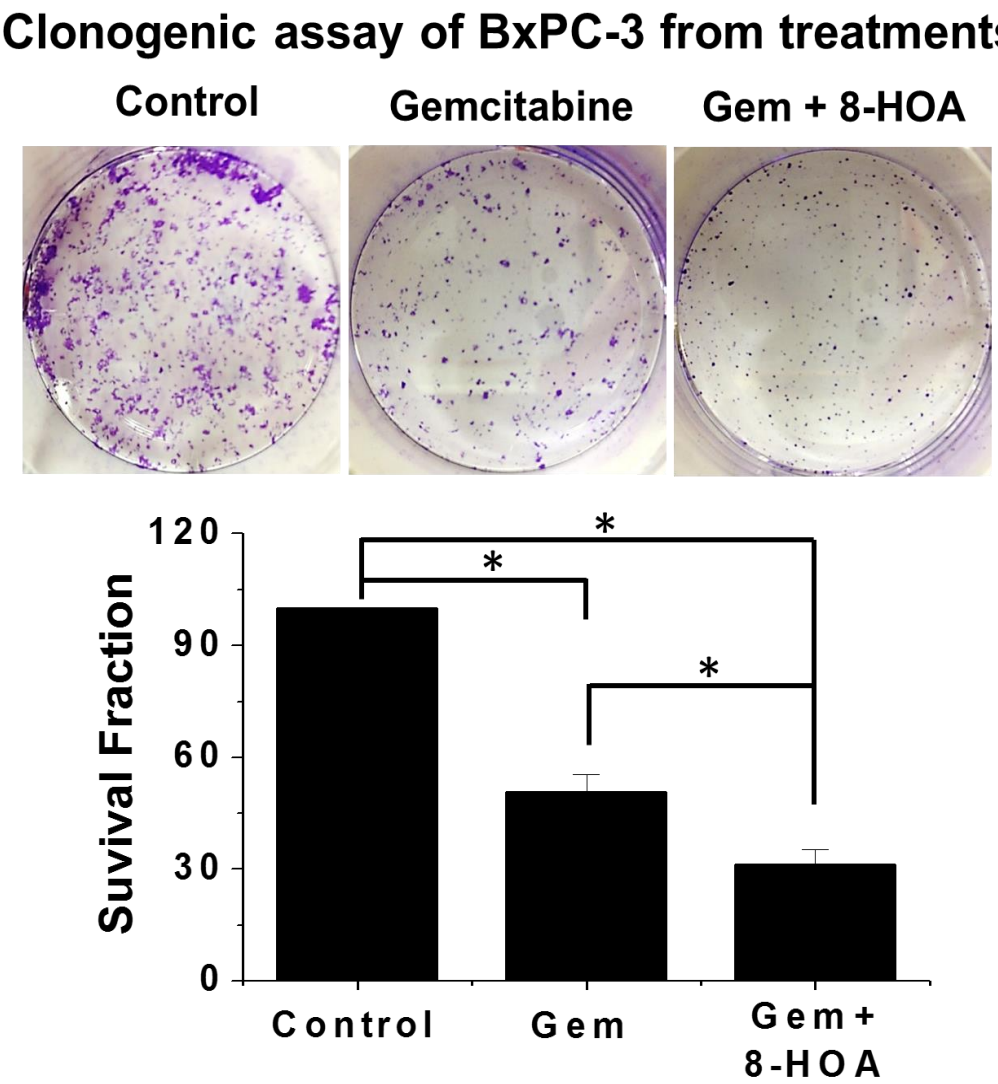

Fig 8. 8-HOA inhibited colony formation in BxPC-3 cells.
Clonogenic assay of BxPC-3 cells at 10 days after 48 h of 8-HOA treatment (1.0 μM), gemcitabine (0.1 μM), and 8-HOA + gemcitabine. The BxPC-3 cells treated with vehicle were used as control. (*: significant difference with $p < 0.05$ from $n \geq 3$).

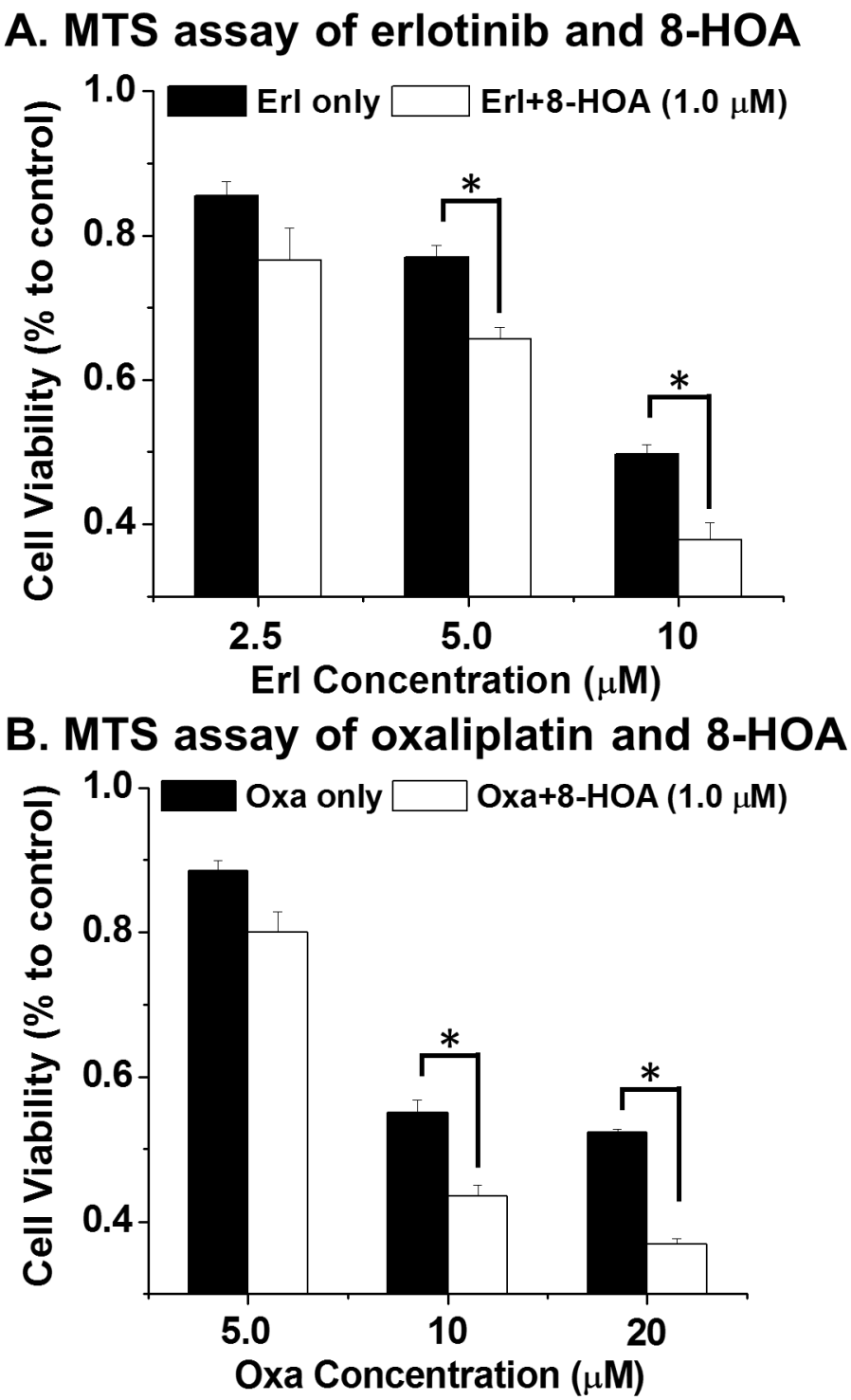

Fig 9. Improved cytotoxicities of erlotinib and oxaliplatin by 8-HOA in BxPC-3 cells.
A) MTS assay of BxPC-3 cells upon treatment of erlotinib (2.5 μM -10 μM) alone or erlotinib (2.5 μM -10 μM) + 8-HOA (1.0 μM) as well as oxaliplatin (5.0 μM - 20 μM) alone or oxaliplatin (5.0 μM -20 μM) + 8-HOA (1.0 μM) for 48 h. The cells without 8-HOA and drug treatment were used as controls and their cell viability was normalized 100%. (*: significant difference with $p < 0.05$ from $n \geq 3$).

3.3. Discussion

Our previous study showed that DGLA can produce unique free radical byproducts e.g. 8-HOA from COX-2-catalyzed lipid peroxidation though C-8 oxygenation. Thus, in this chapter, we investigated the effect of 8-HOA growth and migration of pancreatic cancer cells. In addition, we also tested whether 8-HOA can enhance the efficacies of chemotherapy drugs.

We also tested the effect of PGE1 on pancreatic cancer cell growth as PGE1 is a major metabolite generated from DGLA peroxidation and has been reported to possess anti-cancer and anti-inflammation effects. At physiological concentration range (0.1 μM – 10 μM), PGE1 showed no inhibitory effect on BxPC-3 cancer cell growth, suggesting that PGE1 should not be the metabolite that actually exerts anti-cancer effects on cancer cells. On the other hand, at the same physiological concentration range, DGLA's exclusive free radical byproduct 8-HOA inhibited cancer cell growth from 1.0 μM to 10 μM, suggesting that 8-HOA is the bioactive metabolite that responsible for DGLA's anti-cancer effects.

Mutated p53 is found in majority of pancreatic cancer cell lines (e.g. BxPC-3) and closely associated with pancreatic cancer development and progression [157]. Thus, we investigated whether 8-HOA can inhibit pancreatic cancer cell growth *via* p53-independent manner. It was found that 8-HOA can induce cell apoptosis *via* activating procaspase-9 and procaspase-3 in BxPC-3 cells, indicating that 8-HOA can cause cancer cell death through p53-independent pathway.

HDAC inhibition can lead to histones hyperacetylation, affecting chromatin assembly as histones required deacetylation after deposition onto the newly synthesized DNA [153]. The failure to deposit newly synthesized histones onto DNA or to remove acetyl residues from the histones can cause defects in chromatin assembly, leading to DNA damage [153]. The DNA

damage in cancer cells can trigger caspase activation and the execution of apoptosis [153]. The 8-HOA-induced apoptosis *via* p53-independent pathway is not only associated with direct activation of apoptosis executioners (e.g. procaspase-9 and procaspase-3) by DNA damage, but also related to transcriptional downregulation of anti-apoptotic protein Bcl-2, which is involved in regulating mitochondrial membrane integrity [143].

The molecular mechanism of HDAC inhibitors' anti-metastatic effect has not yet been completely elucidated. The possible pathway is that, when acetylated, relaxed structure of chromatin may allow transcriptional repressors to access the chromatin, resulting in transcriptional repression of key MMPs, including as MMP-2 and MMP-9 (proteins that degrade extracellular matrix and facilitate cancer cell migration) [155].

Gemcitabine, acting as a nucleoside analog to replace one of the building blocks of nucleic acids in the process of DNA replication [128], has been widely used as front line chemo-drug to treat patients with advanced pancreatic cancer. However, pancreatic cancer cells can develop resistance to gemcitabine due to a variety of factors (e.g. decreased expression of hENT1 [129]). Various regimens such as COX-2 inhibitors (e.g., celecoxib) as well as ω-3 fatty acids have been used to sensitize pancreatic cancer cells to gemcitabine [34-35, 75-80]. Our study demonstrated that 8-HOA could also enhance the efficacy of gemcitabine to control pancreatic cancer cell growth (Fig 8).

Erlotinib, a reversible tyrosine kinase inhibitor, has been used as a targeted therapeutic drug for treating a variety of cancers including pancreatic cancer. Targeted therapy is emerging as a promising strategy for cancer treatment *via* using drugs to more precisely target and attack cancer cells. Our study showed that treatment of 8-HOA can significantly improve the efficacy of erlotinib (Fig 9).

In this chapter, we demonstrated that the exclusive free radical byproduct 8-HOA from COX-2-catalyzed DGLA peroxidation can serve as a HDAC inhibitor to control growth and migration of pancreatic cancer cell lines as well as improve the efficacies of chemo-drugs. In next chapter, we promoted the formation of 8-HOA from COX-2-catalyzed DGLA peroxidation by exploiting overexpressed COX-2 as well as knocking down D5D (the rate-limiting enzyme to convert DGLA to AA) to control cancer growth and migration.

4. KNOCKING DOWN D5D SUPPRESSED CANCER GROWTH AND MIGRATION IN COX-2 OVEREXPRESSED PANCREATIC CANCER CELLS

4.1. Introduction

In chapter 3, we demonstrated that direct treatment of 8-HOA can inhibit pancreatic cancer cell growth and migration. In this chapter, we aimed to take advantage of high COX-2 expression in cancer cells and manipulate ω-6 fatty acids metabolism to promote formation of 8-HOA to suppress pancreatic cancer cell growth and migration.

COX-2, the inducible form of COX, can be readily induced by stresses, growth factors, and pro-inflammatory signals in diseases such as inflammation and cancer [59-62]. COX-2 has been found to be overexpressed in ~ 70% pancreatic cancer patients [81]. COX-2 overexpression is positively correlated with pancreatic cancer development and progression as it can metabolize AA to form deleterious metabolite PGE2 [64-70]. PGE2 has shown to facilitate cellular proliferation, migration and angiogenesis of pancreatic cancer [65-70]. COX-2 inhibition *via* using COX-2 inhibitors has been used as the classic strategy to target COX-2 in cancer therapy [75-80]. However, COX-2 inhibitors have never achieved the desirable anti-cancer effects over the past decades and suffer from some safety issues in patients, e.g., increased risks of cardiovascular disease and gastrointestinal injury [82-85].

In our research, instead of COX-2 inhibition, we exploited the commonly high COX-2 expression to kill cancer cells by promoting formation of anti-cancer metabolite 8-HOA from COX-2 catalyzed DGLA peroxidation. In order to promote the formation of 8-HOA, we genetically knocked down D5D (rate-limiting enzyme to convert DGLA to AA) *via* siRNA/shRNA transfection. We proposed that, by knocking down D5D, we can not only limit the production of deleterious metabolites such as PGE2 from COX-2 catalyzed AA peroxidation,

but also reserve more DGLA to improve the formation of 8-HOA from COX-2 catalyzed DGLA peroxidation to a threshold level to deliver growth and migration inhibitory effects on pancreatic cancer cells.

The outcome of this work is expected to provide a guidance to make use of the hallmark of cancer (high COX-2 expression) to work against cancer itself and challenge the current paradigm of COX-2 biology in cancer treatment.

4.2. Results

4.2.1. Knockdown of D5D promoted formation of 8-HOA from DGLA

D5D is the key enzyme that converts DGLA to AA (Scheme 1). In order to manipulate DGLA metabolism to promote formation of 8-HOA, BxPC-3 cells were transfected with D5D-siRNA to knock down D5D. About 70% inhibition of D5D in siRNA transfected BxPC-3 cells was observed compared to negative control siRNA (NC-si) transfected cells (**Fig 10**).

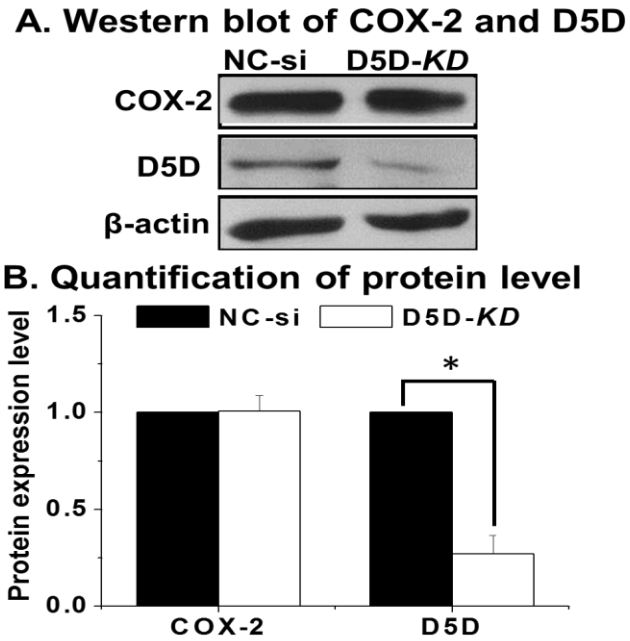

Fig 10. Western blot of COX-2 and D5D in NC-si and D5D-*KD* BxPC-3 cells.
A) Western blot and protein expression level of COX-2 and D5D expression in NC-si transfected *vs.* D5D-*KD* cells. B) Quantification of protein expression level of COX-2 and D5D in NC-si transfected vs D5D-*KD* cells. Protein expression level was normalized using β-actin as loading control. (*: significant difference with $p < 0.05$ from $n \geq 3$).

To determine whether formation of 8-HOA can be promoted by D5D-*KD* to a threshold level for inhibiting cancer cell growth and migration, we used GC/MS to detect 8-HOA (PFB-derivative form) generated from both D5D-*KD* and NC-si BxPC-3 cells treated with DGLA for 48 h. GC/MS, a well-known analytical technique, has been used for the analysis of trace levels of fatty acids in biological samples. For GC/MS analysis, 8-HOA must be derivatized to PFB derivative to increase volatility [135].

In D5D-*KD* BxPC-3 cells, the level of endogenous 8-HOA maintained above the threshold level 0.5 μM during 48 h treatment due to continuous COX-catalyzed DGLA peroxidation (**Fig 11**). However, the level of endogenous 8-HOA never reached 0.5 μM in NC-si transfected BxPC-3 cells upon DGLA treatment for 48 h.

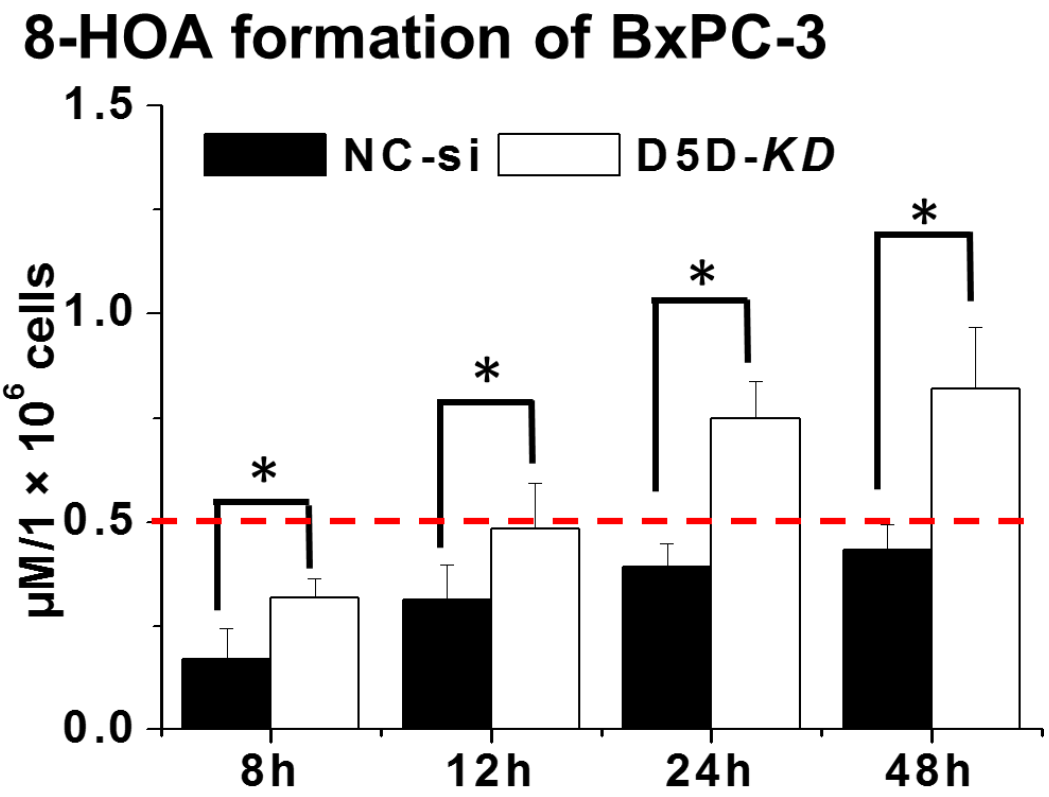

Fig 11. D5D-*KD* promoted formation of 8-HOA in BxPC-3 cells.
GC/MS quantification of 8-HOA from NC-si or D5D-*KD* BxPC-3 cells treated with 100 μM DGLA. The red line is the threshold level of 8-HOA (0.5 μM) that can be reached in D5D-*KD* BxPC-3 cells. Data represent as mean ± SD. (*: significant difference with $p < 0.05$ from $n \geq 3$).

Our strategy not only resulted in formation of a threshold level of 8-HOA, but also caused alterations in the levels of DGLA, AA and their metabolites PGE1 and PGE2 in D5D-*KD* BxPC-3 cells treated with DGLA for 48 h (**Table 4**). As the conversion from DGLA to AA was suppressed by D5D-*KD*, higher level of DGLA and decreased level of AA were detected in D5D-*KD* BxPC-3 compared to those in NC-si BxPC-3 cells. Consistently, increased formation of PGE1 and decreased formation of PGE2 were also detected in D5D-*KD* BxPC-3 compared to those in NC-si BxPC-3 cells, suggesting that D5D-*KD* can not only promote the formation of 8-HOA (cancer inhibitor) from DGLA, but also achieve the similar effect of COX-2 inhibitor to limit the generation of PGE2 (cancer promoter) from AA.

The results again indicated that PGE1 is not the key metabolite that delivers anti-cancer effects as the higher concentration of PGE1 (up to 10 μM) had no effect on cell viability when BxPC-3 cells were directly treated with PGE1 (Fig 1).

Table 4. Levels of DGLA, AA, PGE1 and PGE2 in BxPC-3 cells.

	NC-si BxPC-3 (μM in 1×10^6 cells)			D5D-*KD* BxPC-3 (μM in 1×10^6 cells)		
	12 h	24 h	48 h	12 h	24 h	48 h
DGLA	8.25 ± 1.14	4.62 ± 1.34	0.59 ± 0.17	12.17 ± 1.51	7.27 ± 1.45	1.93 ± 0.26
AA	0.65 ± 0.03	0.54 ± 0.07	0.41 ± 0.13	0.48 ± 0.04	0.37 ± 0.04	0.27 ± 0.06
PGE1	0.17 ± 0.02	0.21 ± 0.05	0.27 ± 0.03	0.37 ± 0.09	0.48 ± 0.08	0.67 ± 0.06
PGE2	0.43 ± 0.05	0.61 ± 0.05	0.91 ± 0.21	0.31 ± 0.11	0.41 ± 0.08	0.56 ± 0.15

Profile of fatty acid and metabolites. LC/MS quantification of DGLA, AA, PGE1 and PGE2 from cell medium of NC-si transfected or D5D-*KD* BxPC-3 cells treated with 100 μM DGLA for 48 h. Data represent as mean ± SD for $n \geq 3$.

4.2.2. Pancreatic cancer cell growth was inhibited by D5D-*KD* and DGLA

We then assessed whether D5D-*KD* and DGLA treatment can inhibit pancreatic cancer cell growth and induce cancer cell apoptosis. Results from clonogenic assay showed that DGLA treatment (48 h) significantly inhibited colony formation in D5D-*KD* BxPC-3 cells (~ survival fraction of 70.6%, **Fig 12A**), but had no effect on cell growth of the cells transfected with NC-si (~survival fraction of 101.1%, Fig 12A). The growth inhibition in D5D-*KD* BxPC-3 cells upon treatment of DGLA is consistent with the inhibited cell growth when BxPC-3 cells were directly treated with 8-HOA in chapter 3 (Fig 1).

FITC-Annexin V-PI double staining was also used to test whether D5D-*KD* along with DGLA treatment can also induce BxPC-3 cells apoptosis. We observed that DGLA treatment significantly increased apoptotic cell population in D5D-*KD* BxPC-3 cells (FITC-Annexin V positive and PI negative, 8.12 %) vs. the control (e.g., D5D-*KD* cells without DGLA treatment, ~2.71 %, **Fig 12B**).

Together these results suggested that D5D-*KD* and DGLA treatment resulted in promoted formation of 8-HOA (> 0.5 μM, Fig 11) from COX-2-catalyzed DGLA peroxidation which in turn can inhibit cancer cell growth and induce cancer cell apoptosis.

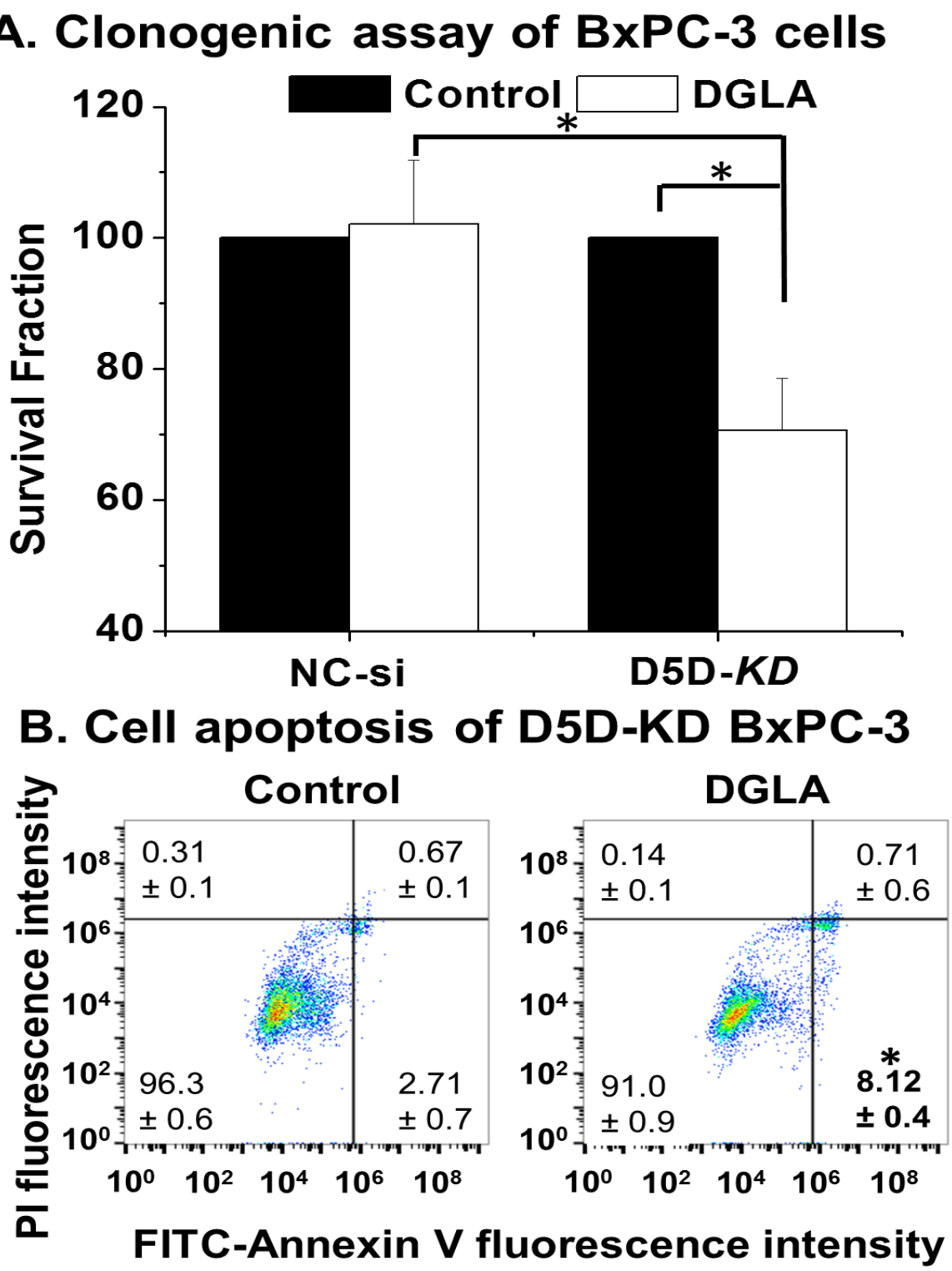

Fig 12. D5D-*KD* improved DGLA's growth inhibitory effect in BxPC-3 cells.
A) Clonogenic assays of NC-si and D5D-*KD* BxPC-3 cells at day 10 upon the DGLA (100 μM, 48 h) treatment vs. controls (without DGLA). B) Cell apoptosis analysis of D5D-*KD* cells treated with vehicle (control) or DGLA (100 μM). (*: significant difference with $p < 0.05$ from $n \geq 3$).

4.2.3. Pancreatic cancer cell migration was suppressed by D5D-*KD* and DGLA

Pancreatic cancer cells often metastasize to the liver, lungs, bone, brain, and other organs. Once pancreatic cancer is metastasized, the survival rate of the patients dropped significantly as these spread cancers cannot be removed by surgery. Therefore, there is an urgent need for regimen to suppress cancer metastasis.

In chapter 3, we demonstrated that direct treatment of 8-HOA can inhibit BxPC-3 cells migration, therefore, we further tested whether D5D-*KD* along with DGLA treatment can also inhibit cell migration of BxPC-3 cells. Wound healing assay was used to test the effect of D5D-*KD* and DGLA on cell migration in BxPC-3 cells. D5D-*KD* significantly inhibited cell migration in BxPC-3 cells treated with DGLA (~ wound area of 83.4% at 48 h compared to control 55.3%, **Fig 13**). DGLA treatment had no inhibitory effects on cell migration of the negative control BxPC-3 cells (~wound area of 57.9% vs. ~ 58.1% in control, **Fig 14**), indicating that 8-HOA formed in negative control BxPC-3 cells is not sufficient (below 0.5 μM, Fig 11) to inhibit cancer cell migration.

In addition, a transwell assay was also conducted to assess the effect of D5D-*KD* and DGLA treatment on pancreatic cancer cell migration and invasion. Consistent with the wound healing assay, treatment of DGLA for 48 h resulted in significant inhibition on D5D-*KD* BxPC-3 cell migration (~ 102 cells migrated for treatment DGLA vs. ~ 146 cells migrated for control, **Fig 15A**) and invasion (~ 79 cells invaded for treatment DGLA vs. ~ 121 cells invaded for control, **Fig 15B**).

These results have demonstrated that D5D-*KD* can promoted formation of 8-HOA from COX-2-catalyzed DGLA peroxidation to reach the threshold level (> 0.5 μM, Fig 11), resulting in inhibited cancer cell migration and invasion.

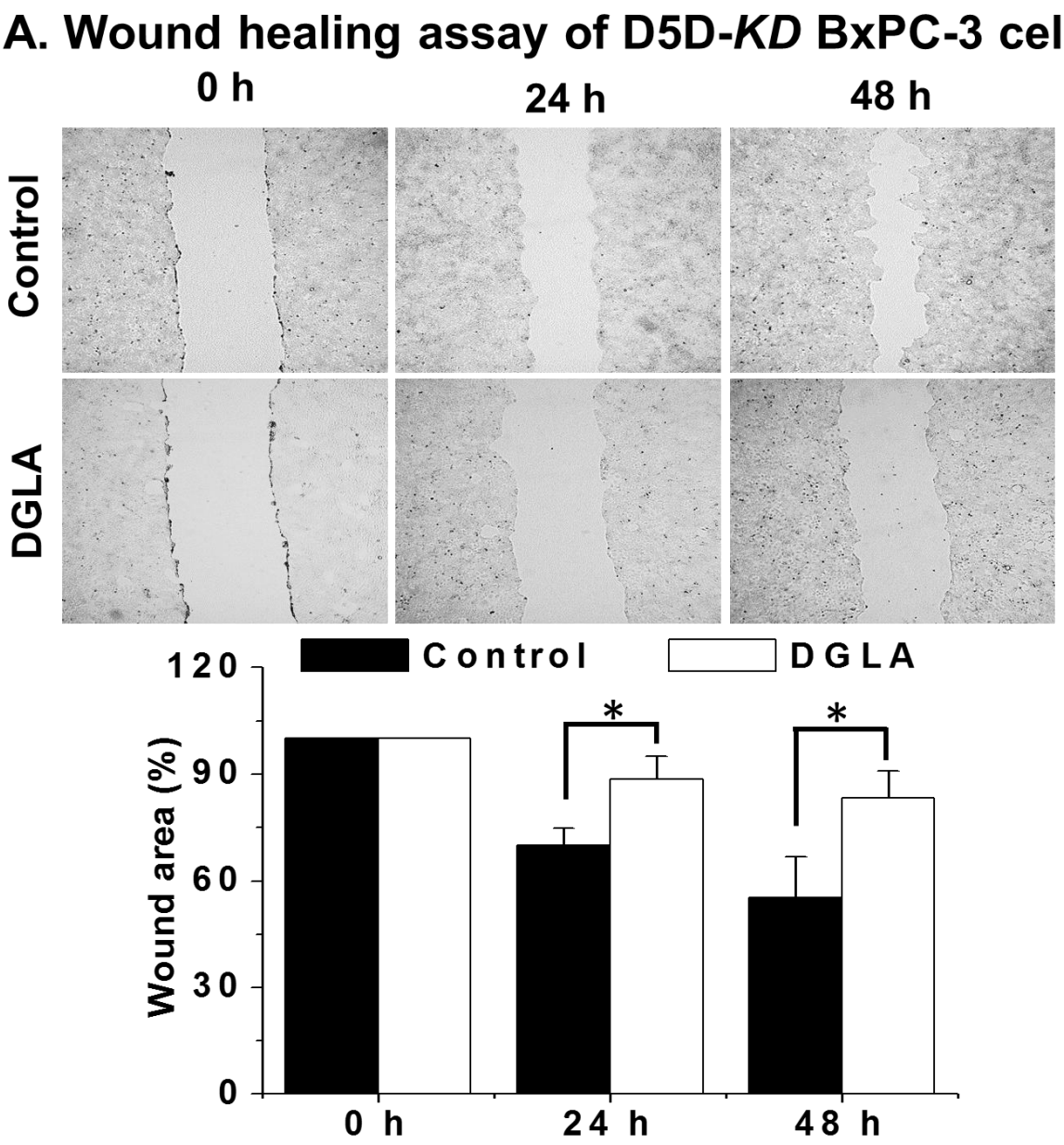

Fig 13. D5D-*KD* and DGLA supplement inhibited cell migration in BxPC-3 cells.
A) Wound healing assays and quantification of wound area of D5D-*KD* BxPC-3 cells upon DGLA (100 μM, 48 h) treatment vs. controls (without DGLA). (*: significant difference with $p < 0.05$ from $n \geq 3$).

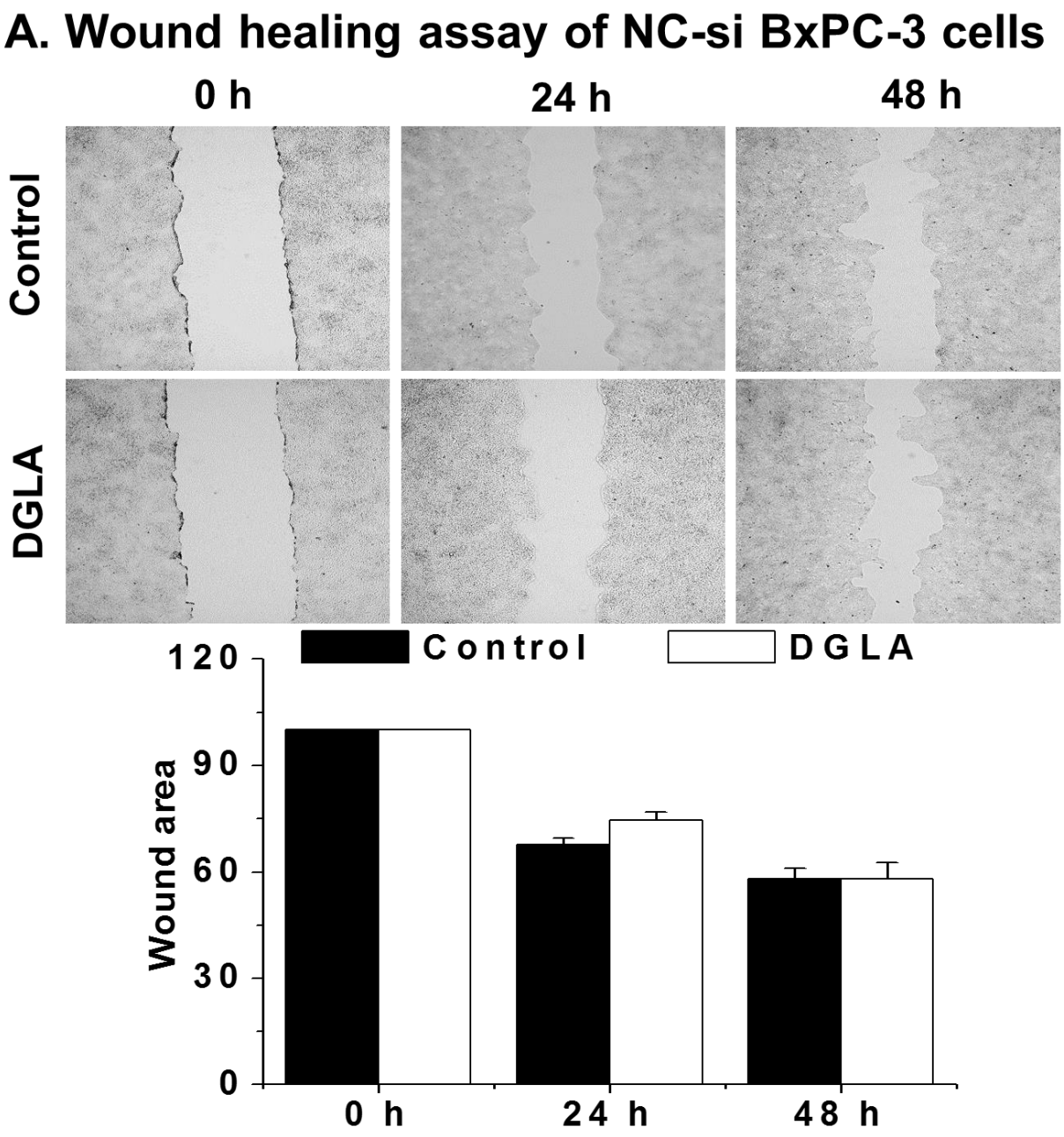

Fig 14. DGLA treatment did not inhibit cell migration in negative control BxPC-3 cells. A) Wound healing assays and quantification of wound area of negative control BxPC-3 cells upon DGLA (100 μM, 48 h) treatment vs. controls (without DGLA, there is no significant statistical difference between controls and cells with DGLA treatment from $n \geq 3$).

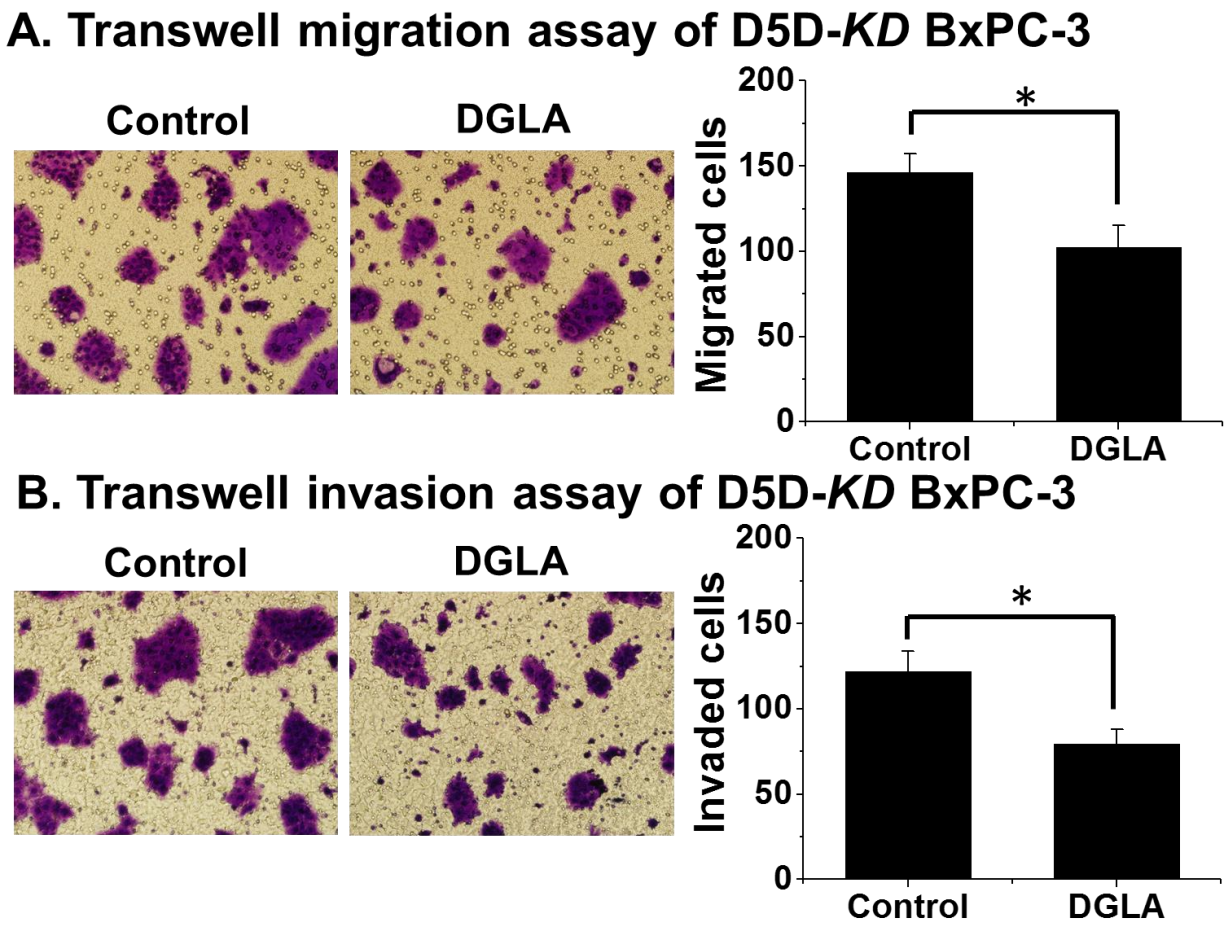

Fig 15. D5D-*KD* and DGLA inhibited cell migration and invasion in BxPC-3 cells.
A) Transwell migration assay of D5D-*KD* BxPC-3 cells upon treatment of DGLA (100 μM). The D5D-*KD* cells without fatty acid treatment were used as controls; B) Transwell invasion assay of D5D-*KD* BxPC-3 cells upon treatment of DGLA (100 μM). The D5D-*KD* cells without fatty acid treatment were used as controls. (*: significant difference with $p < 0.05$ from $n \geq 3$).

4.2.4. DGLA's anti-cancer effects were associated with its COX-2-catalyzed peroxidation

To further confirm that DGLA's anti-cancer effects were associated with its COX-2-catalyzed peroxidation, we knocked down D5D and COX-2 separately or simultaneously in BxPC-3 cells. We used MTS assay to test their cell growth response upon 48 h DGLA treatment. Results showed that treatment with DGLA significantly inhibited cell viability in D5D-*KD* BxPC-3 cells. However, the growth inhibitory effect was abolished in D5D/COX-2 double-KD BxPC-3 cells (**Fig 16**), indicating that COX-2 is essential for delivering the anti-cancer effects.

This observation also provide evidence to support our hypothesis that 8-HOA produced from COX-2-catalyzed DGLA peroxidation is responsible for DGLA's anti-cancer activities.

We also tested our strategy (i.e. D5D-*KD* and DGLA treatment) on cancer cell growth in another pancreatic cancer cell line PANC-1 with deficient COX-2 expression. Results showed that after 48 h, DGLA treatment (100 μM) did not inhibit cell growth in D5D-*KD* PANC-1 cells (~98.3% cell viability compared to control, **Fig 17**).

These results taken together indicated that overexpressed COX-2 is essential for promoting formation of 8-HOA from DGLA peroxidation to control pancreatic cancer cell growth. Therefore, overexpressed COX-2 is considered as a benefit rather than a problem in our study, shifting the paradigm of COX-2 biology in cancer as the classic strategy to target COX-2 in cancer is to inhibit it.

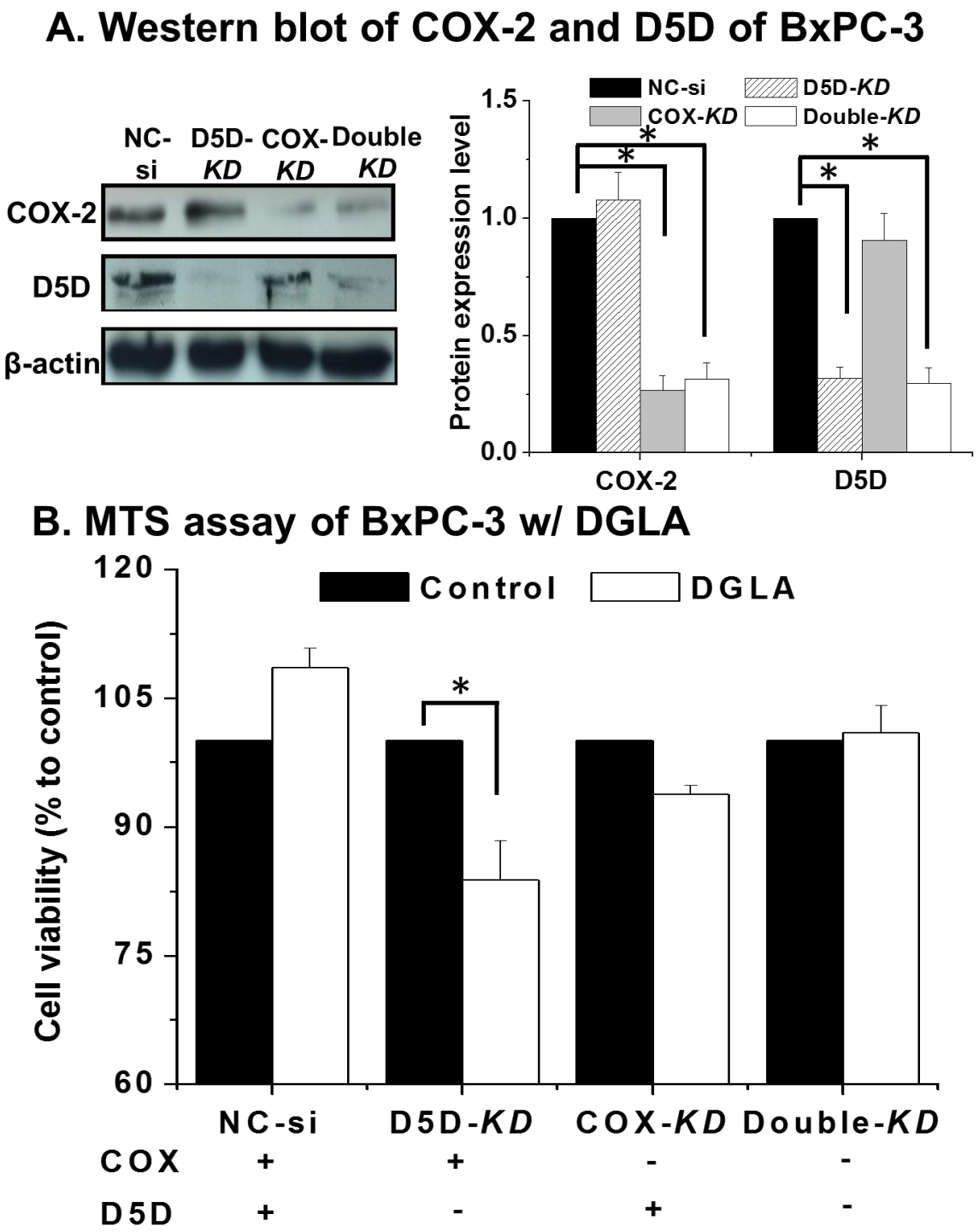

Fig 16. D5D and COX-2 expression levels and their effects on growth of BxPC-3 cells treated DGLA.

A) Western blot and protein expression level of COX-2 and D5D in BxPC-3 cells with COX-2 and D5D siRNA transfection. Protein expression level was normalized using β-actin as loading control; B) MTS assay of NC-si transfected, D5D-*KD*, COX-*KD* and double *KD* BxPC-3 cells upon treatment of 100 μM DGLA. (*: significant difference compared to NC-si with $p < 0.05$ from $n \geq 3$).

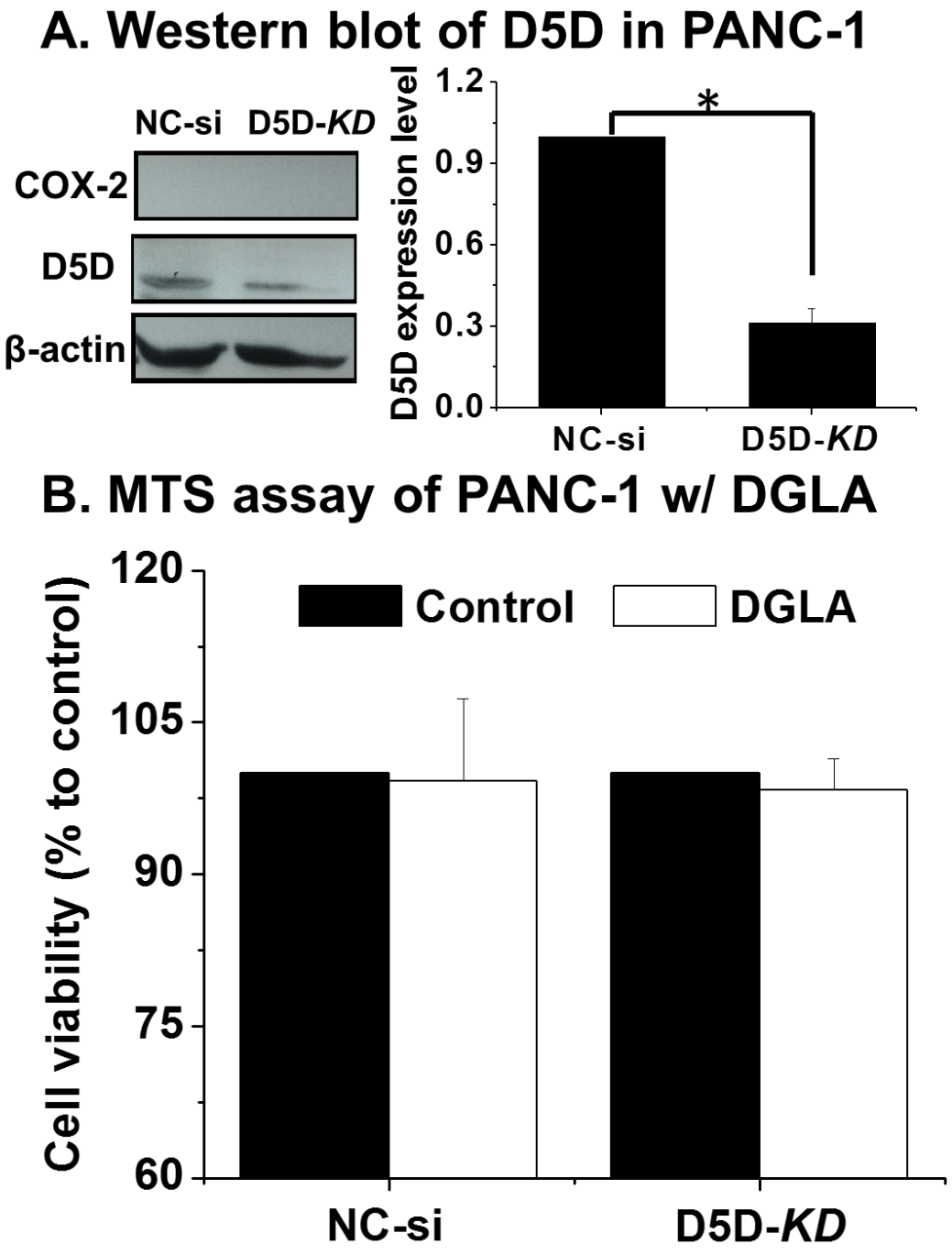

Fig 17. DGLA treatment did not inhibit cell viability of D5D-*KD* PANC-1 cells.
A) Western blot and protein expression level of D5D in NC-si transfected vs D5D-*KD* PANC-1 cells. Protein expression level was normalized using β-actin as loading control. B) MTS assay of NC-si transfected and D5D-*KD* PANC-1 cells upon treatment of DGLA (100 μM). The NC-si transfected and D5D-*KD* cells without fatty acid were used as controls. (*: significant difference with $p < 0.05$ from $n \geq 3$).

4.2.5. DGLA treatment and D5D-*KD* enhanced the efficacies of gemcitabine on inhibiting pancreatic cancer cell growth

Gemcitabine is used as a front-line chemotherapy drug for pancreatic cancer patients. A variety of regimens such as ω-3 fatty acids and COX-2 inhibitors have been combined with gemcitabine to further kill cancer cells [34-35, 75-81]. In chapter 3, we have previously shown that direct treatment of 8-HOA can sensitize BxPC-3 cells to gemcitabine. In this chapter, we further tested whether the threshold of 8-HOA formed from COX-catalyzed DGLA peroxidation can also enhance the efficacy of gemcitabine.

When cells were co-treated with DGLA and gemcitabine, DGLA could significantly enhance efficacy of gemcitabine on D5D-*KD* BxPC-3 cells as we observed in MTS assay (cell viability 41.3 % for co-treatment vs. 54.6 % for gemcitabine only, **Fig 18A**). Significantly inhibited colony formation was also observed in D5D-*KD* BxPC-3 cells upon treatment of gemcitabine and DGLA (survival fraction ~30.8% vs. 51.3% for gemcitabine only, **Fig 18B**). For NC-si BxPC-3 cells, DGLA treatment could not improve efficacy of gemcitabine as shown in MTS assay and colony formation assays in Fig 16A-16B. The further inhibited cancer cell growth in D5D-KD BxPC-3 cells was attributed to 8-HOA reaching the threshold level (above 0.5 μM, Fig 15), consistent with the observed further growth inhibition upon treatment of gemcitabine and 8-HOA.

Lower concentration of gemcitabine was used in clonogenic assay (0.1 μM) compared to MTS assay (1.0 μM) as the same high concentration of gemcitabine used in MTS assay (48 h) can kill all the cells in clonogenic assay and leave no cells to form colonies (48 h treatment, 10 days incubation).

We also used FITC-Annexin V and PI double staining to the effect of gemcitabine and DGLA treatment on cell apoptosis in D5D-*KD* BxPC-3 cells. Results showed that gemcitabine alone can induce cell apoptosis in D5D-*KD* BxPC-3 cells as demonstrated as FITC-Annexin V positive and PI negative staining (population of early apoptotic cells ~12.6%, **Fig 18C**). Gemcitabine-induced cell apoptosis was further promoted by DGLA treatment on D5D-*KD* BxPC-3 cells (population of early apoptotic cells, ~18.0%, Fig 18C).

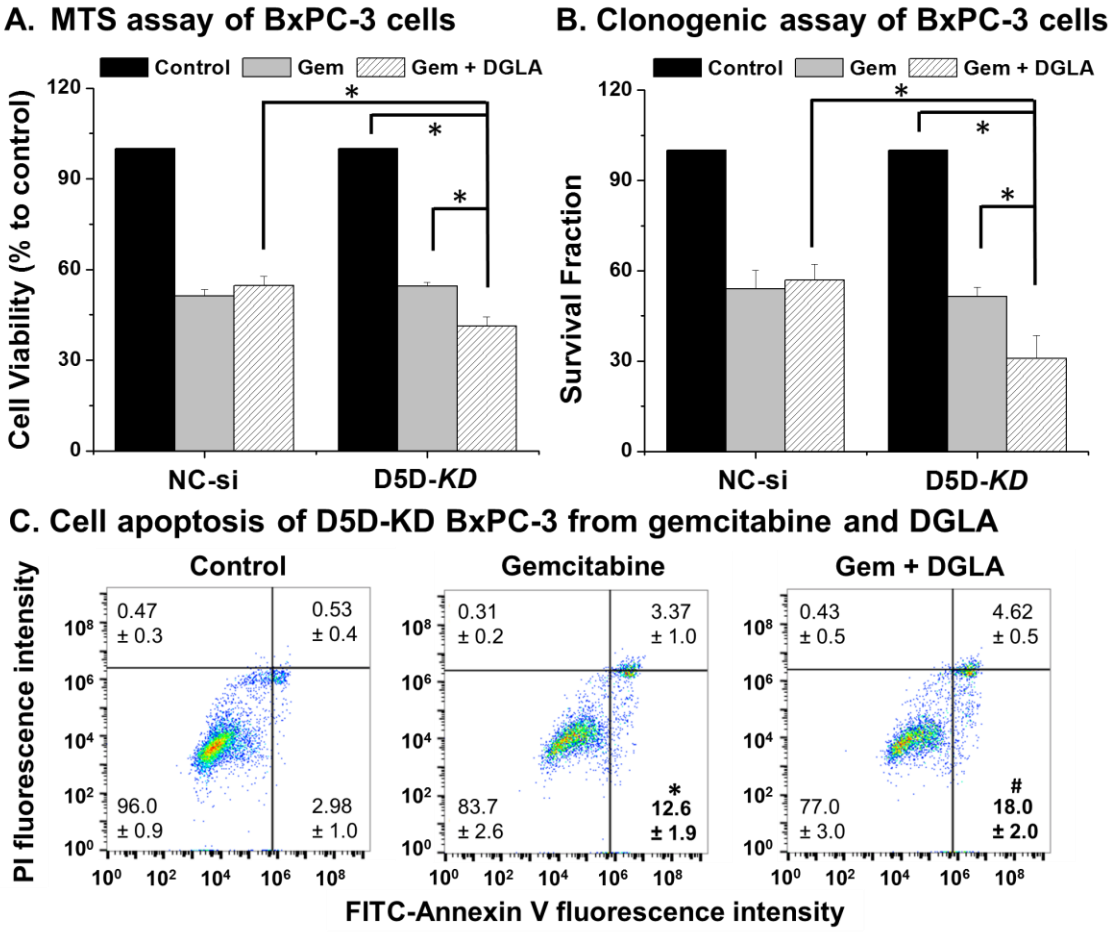

Fig 18. D5D-*KD* and DGLA treatment enhanced efficacies of gemcitabine to kill BxPC-3 cells.

A) MTS assay of NC-si and D5D-*KD* BxPC-3 cells upon treatment of gemcitabine (1.0 μM) alone or gemcitabine + DGLA (100 μM). B) Clonogenic assay of NC-si and D5D-*KD* BxPC-3 cells at 10 days with treatment of DGLA (100 μM), gemcitabine (0.1 μM) or gemcitabine + DGLA for 48 h. The NC-si and D5D-*KD* cells without fatty acid and drug treatment were used as controls. C) Cell apoptosis of D5D-*KD* BxPC-3 cells treated with vehicle (control), DGLA (100 μM), gemcitabine (0.1 μM) alone or gemcitabine + DGLA. (*: significant difference vs. control with $p < 0.05$; and #: significant difference *vs.* gemcitabine with $p < 0.05$ from $n \geq 3$).

Gemcitabine has been known to suppress cancer cell growth by inducing p53-dependent as well as p53-independent cell apoptosis [158-159]. In order to assess the possible molecular mechanism of gemcitabine efficacy promoted by DGLA, D5D-*KD* BxPC-3 cells (mutated p53) were treated by DGLA, gemcitabine alone, and their combination, respectively.

We found that gemcitabine alone could down regulate Bcl-2 (anti-apoptotic proteins) as well as activate procaspase 9 and procaspase 3 (pro-apoptotic proteins, **Fig 19**). Increased expressions of acetyl histone H3 and γH2AX were observed in D5D-*KD* BxPC-3 cells treated with DGLA, consistent with Fig 4, and confirmed that 8-HOA can serve as a histone deacetylase inhibitor to induce DNA damage. Further increased expression of γH2AX and down-regulated expressions of Bcl-2, procaspase 9 and procaspase 3 (Fig 19) were observed when D5D-*KD* BxPC-3 cells were co-treated by DGLA and gemcitabine (vs. gemcitabine alone). The data indicated that combination of DGLA and D5D-*KD* can significantly enhance gemcitabine's efficacy potentially by 8-HOA which can induce DNA damage, and then decrease expressions of anti-apoptotic proteins (e.g., Bcl-2) and activate pro-apoptotic proteins (e.g., caspase-9 and caspase-3).

From what we observed in clonogenic assay and apoptosis assay, the growth inhibition effect was additive when D5D-*KD* BxPC-3 cells were treated with the combination of DGLA and gemcitabine. The combination of gemcitabine and DGLA showing additive rather than synergistic effects on cancer cells may be attributed to both gemcitabine and 8-HOA inducing cancer cell apoptosis by causing DNA damage. Therefore, in the future, we can combine our strategy with other drugs that inhibit cancer growth *via* a different mechanism such as targeted therapeutic drugs to treat cancer cells. In addition, in order for the combination of our strategy

and drug to exert synergistic effect, we should use the drug at a low concentration as the high concentration may mask the effect of our strategy on cancer cell growth inhibition.

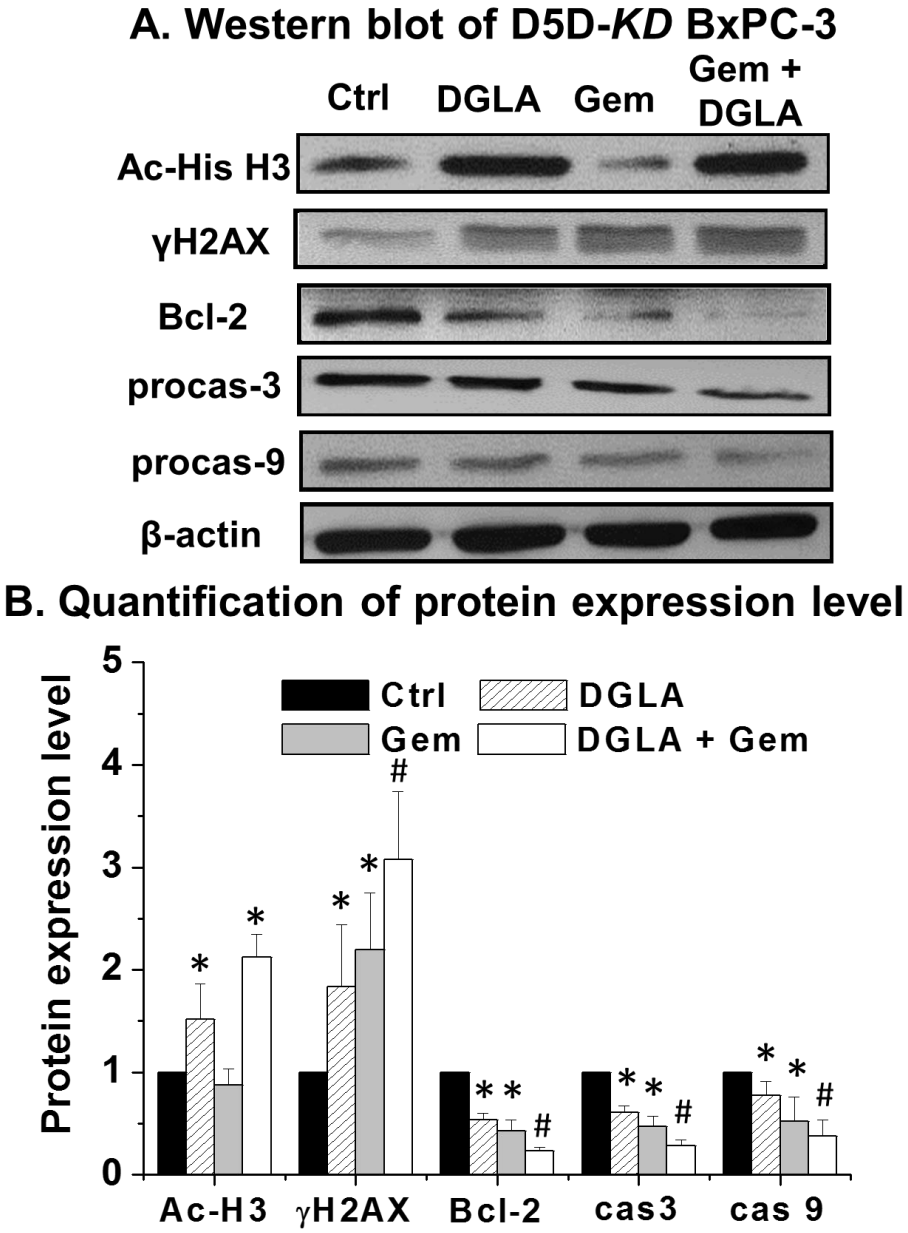

Fig 19. D5D-*KD* and DGLA treatment promoted gemcitabine-induced apoptosis *via* p53 independent pathway.

A) Western blot of acetyl histone H3, γH2AX, Bcl-2, procaspase-3 and procaspase-9 from D5D-*KD* BxPC-3 cells treated with vehicle (control), DGLA (100 μM), gemcitabine (0.1 μM) or gemcitabine (0.1 μM) + DGLA (100 μM) for 48 h. B) Quantification of protein expression level of acetyl histone H3, γH2AX, Bcl-2, procaspase-3 and procaspase-9 from D5D-*KD* BxPC-3 cells treated with vehicle, DGLA, gemcitabine or gemcitabine + DGLA for 48 h. Protein expression level was normalized using β-actin as loading control. (*: significant difference vs. control with $p < 0.05$; and #: significant difference vs. gemcitabine with $p < 0.05$ from $n \geq 3$).

4.2.6. D5D-*KD* and DGLA treatment improved efficacies of other chemotherapy drugs on inhibiting pancreatic cancer cell growth

Erlotinib, a reversible tyrosine kinase inhibitor acting on epidermal growth factor receptor, has been used as a targeted therapeutic drug for a variety of cancers including pancreatic cancer. Oxaliplatin, a platinum-based anti-neoplastic agent, has been also used as a common chemotherapy drug for pancreatic cancer. Besides gemcitabine, we also tested whether our strategy (i.e. D5D-*KD* and DGLA treatment) could sensitize BxPC-3 cells to erlotinib and oxaliplatin.

Our data showed that DGLA treatment improved the cytotoxicity of erlotinib and oxaliplatin on D5D-*KD* BxPC-3 cells as shown in their MTS assays (~39.6% and 34.3% cell viability for treatment DGLA plus chemo-drugs vs. 52.1% and 46.9% for erlotinib and oxaliplatin only **Fig 20A**). The results suggested that D5D-*KD* can promote the formation of 8-HOA to reach a threshold level (> 0.5 μM), leading to enhanced efficacy of chemotherapeutic drugs.

The clonogenic assays also demonstrated that co-treatment of DGLA with erlotinib and oxaliplatin further inhibited colony formation (~34.5% and 36.7% survival fraction for treatment DGLA plus chemo-drugs vs. ~52.2% and 62.9% for erlotinib and oxaliplatin alone **Fig 20B**). In NC-si transfected BxPC-3 cells, treatment of DGLA could not enhance the efficacies of erlotinib and oxaliplatin.

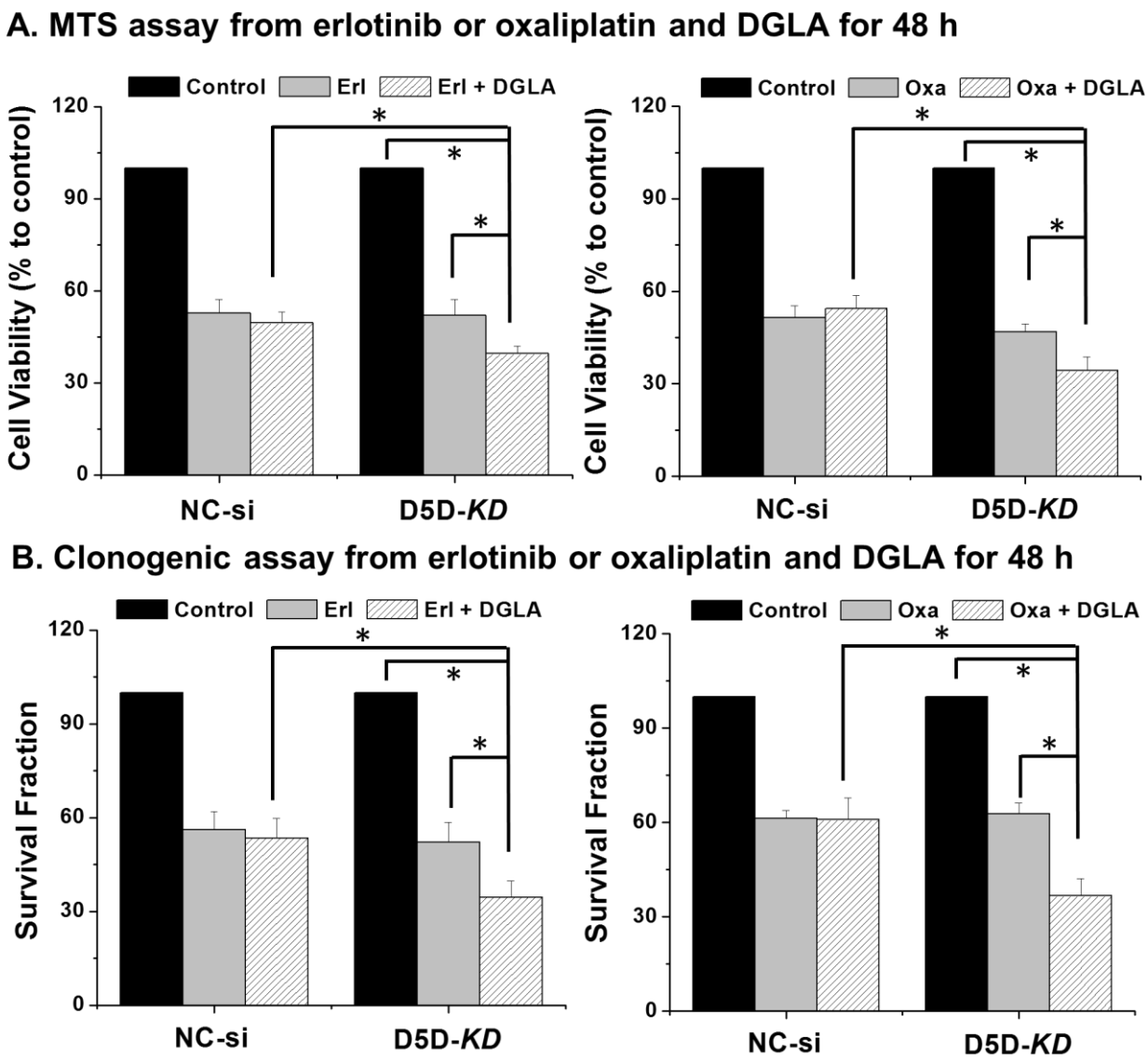

Fig 20. Improved cytotoxicities of erlotinib and oxaliplatin by DGLA in D5D-*KD* BxPC-3 cells.

A) MTS assay of NC-si and D5D-*KD* BxPC-3 cells treated with erlotinib (10 μM) alone or erlotinib + DGLA as well as oxaliplatin (20 μM) alone or oxaliplatin + DGLA for 48 h. B) Clonogenic assay of NC-si and D5D-*KD* BxPC-3 cells at 10 days treated with erlotinib (2.0 μM) or erlotinib + DGLA as well as oxaliplatin (2.0 μM) or oxaliplatin + DGLA for 48 h. The NC-si and D5D-*KD* cells without fatty acid and drug treatment were used as controls. (*: significant difference with $p < 0.05$ from $n \geq 3$).

4.2.7. The efficacy of gemcitabine was enhanced by D5D-*KD* on suppressing cancer cell migration

Gemcitabine, a nucleoside analog, replaces one of the building blocks of nucleic acids during DNA replication. Gemcitabine has been used to treat pancreatic cancer metastasis in clinical patients [160]. Thus, we further tested whether the strategy of D5D-*KD* and DGLA treatment can also enhance the efficacy of gemcitabine on suppressing pancreatic cancer cell migration and invasion. Results showed that D5D-*KD* and DGLA treatment could improve the efficacy of gemcitabine on BxPC-3 cells as shown in transwell migration assays (~ 63 cells migrated for treatment DGLA plus gemcitabine vs. ~ 87 for gemcitabine only **Fig 21A**). The transwell invasion assays also showed that co-treatment of DGLA with gemcitabine further inhibited cell invasion in D5D-*KD* BxPC-3 cells (~ 40 cells invaded for treatment DGLA plus gemcitabine vs. ~62 cells for gemcitabine alone **Fig 21B**).

Gemcitabine has been shown to suppress cancer migration and invasion by altering MMP-2 expression and epithelial mesenchymal transition (EMT) protein levels [161-175]. We found that gemcitabine alone could decrease expression of MMP-2, vimentin (mesenchymal marker) and Snail (transcriptional factor inducing EMT) as well as increase expression of epithelial marker E-cadherin (**Fig 22**). Increased expressions of acetyl histone H3 was observed in D5D-*KD* BxPC-3 cells treated with DGLA, confirming that 8-HOA can serve as a histone deacetylase inhibitor to inhibit cancer cell migration and invasion (Fig 22). When D5D-*KD* BxPC-3 cells were co-treated with DGLA and gemcitabine, further decreased expressions of MMP-2, vimentin and snail as well as further increased expression of E-cadherin were observed in D5D-*KD* BxPC-3 cells compared to treatment gemcitabine alone (Fig 22).

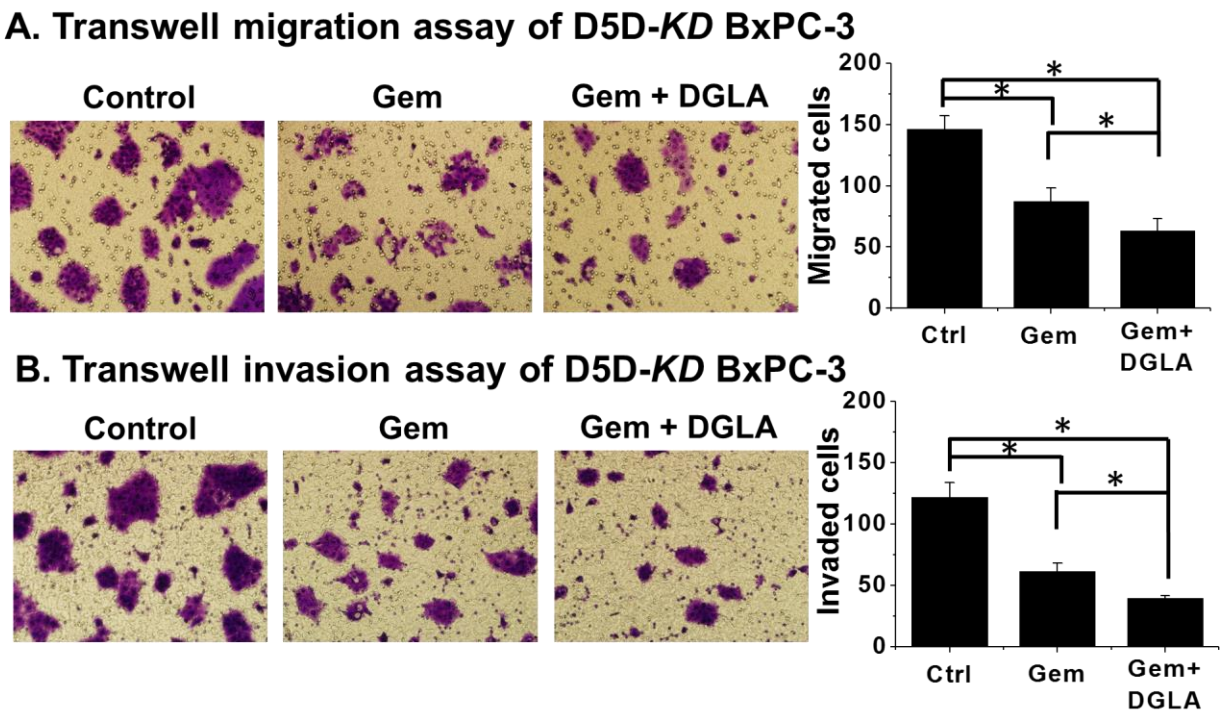

Fig 21. D5D-*KD* and DGLA treatment enhanced efficacy of gemcitabine on cell migration and invasion in BxPC-3 cells.
A) Transwell migration assay of D5D-*KD* BxPC-3 cells upon treatment of DGLA (100 μM), gemcitabine (0.1 μM) alone or gemcitabine + DGLA. The D5D-*KD* cells without fatty acid and drug treatment were used as controls. B) Transwell invasion assay of D5D-*KD* BxPC-3 cells upon treatment of DGLA (100 μM), gemcitabine (0.1 μM) alone or gemcitabine + DGLA. The D5D-*KD* cells without fatty acid and drug treatment were used as controls. (*: significant difference with $p < 0.05$ from $n \geq 3$).

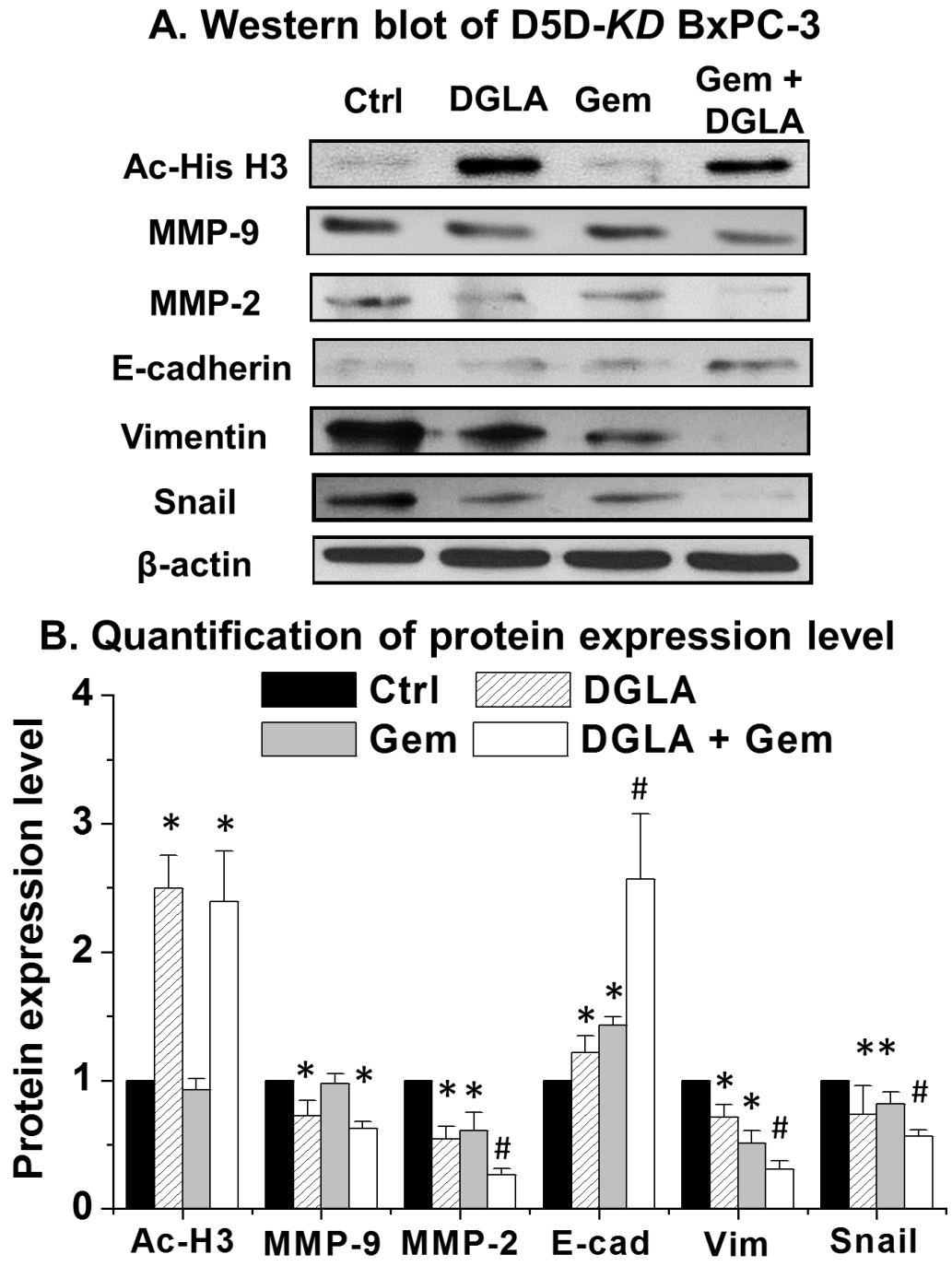

Fig 22. D5D-*KD* and DGLA treatment improved efficacy of gemcitabine *via* altering expressions of proteins involved in cell migration and invasion in BxPC-3 cells.
A) Western blot and protein expression level of acetyl histone H3, MMP-9, MMP-2, E-cadherin, vimentin and snail from D5D-*KD* BxPC-3 cells treated with vehicle (control), DGLA (100 μM), gemcitabine (0.1 μM) or gemcitabine + DGLA. B) Quantification of protein expression level of acetyl histone H3, MMP-9, MMP-2, E-cadherin, vimentin and Snail from D5D-*KD* BxPC-3 cells treated with vehicle, DGLA, gemcitabine or gemcitabine + DGLA. Protein expression level was normalized using β-actin as loading control (*: significant difference vs. control with $p < 0.05$; and #: significant difference vs. gemcitabine group with $p < 0.05$ from $n \geq 3$).

4.3. Discussion

In chapter 3, we showed that direct treatment of DGLA's unique free radical byproduct 8-HOA can not only inhibit cell growth and migration, but can also enhance the efficacy of chemotherapy drugs e.g., gemcitabine on pancreatic cancer cells. In this chapter, we further tested whether D5D-KD can promote formation of 8-HOA to inhibit growth and migration of pancreatic cancer cells.

We detected the levels of 8-HOA in D5D-*KD* BxPC-3 cells treated with DGLA for 48 h using GC/MS. A threshold level of endogenous 8-HOA (> 0.5 μM) was found essential to exert its anti-cancer effect on pancreatic cancer cells (Fig 11). Our results suggested that, in cancer cells with high COX-2 expression, the endogenous formation of 8-HOA can inhibit cancer growth and migration in an autocrine manner once a threshold level (> 0.5 μM) was reached.

In addition, for cancer cells with deficient COX-2 expression, our strategy (i.e. D5D-KD and DGLA treatment) can also be used to inhibit their cell growth and migration. This is because 8-HOA, continually generated from nearby cancer cells (overexpress COX-2), can suppress the growth and migration of cancer cells with deficient COX-2 expression in a paracrine manner.

Gemcitabine, acting as a nucleoside analog to replace one of the building blocks of nucleic acids in the process of DNA replication, has been widely used as front line chemo-drug to treat patients with advanced pancreatic cancer. However, drug resistance has been a major obstacle for successful chemotherapy (e.g. gemcitabine) for pancreatic cancer. Our study demonstrated that promoted formation of 8-HOA from DGLA treatment along with D5D-*KD* could enhance the efficacy of gemcitabine to control pancreatic cancer cell growth by further promoting gemcitabine-induced cell apoptosis though a p53-independent pathway (Fig 21).

Considering that the common low efficacy of chemotherapy for pancreatic cancer patients, our strategy can be used to improve many frontline chemo-drugs to kill cancer.

In this study we demonstrated that 8-HOA can inhibit cancer cell migration and invasion. The molecular mechanism behind the observation is that 8-HOA can act as an HDACi to prevent histone deacetylation, leading to relaxed chromatin and transcriptional alternation of targeted genes (e.g. MMP-2 and MMP-9). Our study also showed that the improved formation of 8-HOA can enhance efficacy of gemcitabine on suppressing D5D-*KD* BxPC-3 cell migration and invasion by further increasing expression of E-cadherin and decreased expression of MMP-2, vimentin and snail (Fig 22).

For the first time, we have demonstrated that high COX-2 expression could be used to improve formation of 8-HOA from DGLA peroxidation *via* D5D-*KD* for the inhibition of cancer cell growth and migration, as well as for the improvement of efficacy of chemotherapy on pancreatic cancer cells. The outcome of our work will reinforce our translational efforts to develop a novel ω-6 based dietary strategy in combination with modified COX-2-catalyzed DGLA peroxidation and D5D-mediated ω-6 conversion, and therefore improving the efficacies of chemotherapy.

5. D5D KNOCKDOWN AND DGLA INHIBITED GROWTH OF PANCREATIC TUMOR OVEREXPRESSING COX-2 IN MOUSE XENOGRAFT MODEL

5.1. Introduction

In chapter 4, we demonstrated that genetic knockdown of D5D promoted formation of 8-HOA (cancer inhibitor) from COX-catalyzed DGLA peroxidation, leading to cancer cell growth and migration inhibition. Our strategy also enhanced efficacy of gemcitabine, a front-line chemotherapy drug, on suppressing pancreatic cancer cell growth and migration. In this chapter, we further extended our strategy to *in vivo* studies to confirm whether knockdown of D5D and DGLA supplementation can also inhibit pancreatic tumor growth and metastasis potential.

We established a xenograft tumor model using immune-deficient mice, which are the standard *in vivo* model in cancer researches [166-167]. The immune-deficient mice are athymic and hairless due to homozygous mutation of Foxn1 ($Foxn1^{nu}/Foxn1^{nu}$) [168]. The absence of a thymus blocks the development of T cells, resulting in an immunodeficiency which allows transplantation of tumor cell xenografts [168]. In addition, nude mice are also ideal for measurement of subcutaneous tumor volume and whole body imaging.

In present study, a stable D5D-*KD* BxPC-3 cell line was created and subcutaneously injected into the flank of nude mice to establish a D5D-*KD* xenograft tumor model. For comparison, wild-type BxPC-3 cells were also injected into nude mice and subjected to same treatments. Following a 2-week standard diet to allow tumors grow, the mice were further divided into four sub-groups and received different treatments for 4 weeks, including 1) vehicle (control), 2) DGLA supplementation (8 mg/mice, oral gavage, twice a week), 3) gemcitabine injection (30 mg/kg, intraperitoneal, twice a week), and 4) combination of DGLA and gemcitabine (**Scheme 9**).

For the first time, we demonstrated that increased formation of 8-HOA from COX-2-catalyzed DGLA peroxidation *via* D5D-*KD* can significantly inhibit pancreatic tumor growth and metastasis potential, as well as improve the efficacy of gemcitabine. The outcome of our study is expected to provide guidance for developing a new diet care strategy to improve current chemotherapy by taking advantage of abundant dietary ω-6s and commonly overexpressed COX-2 in cancer.

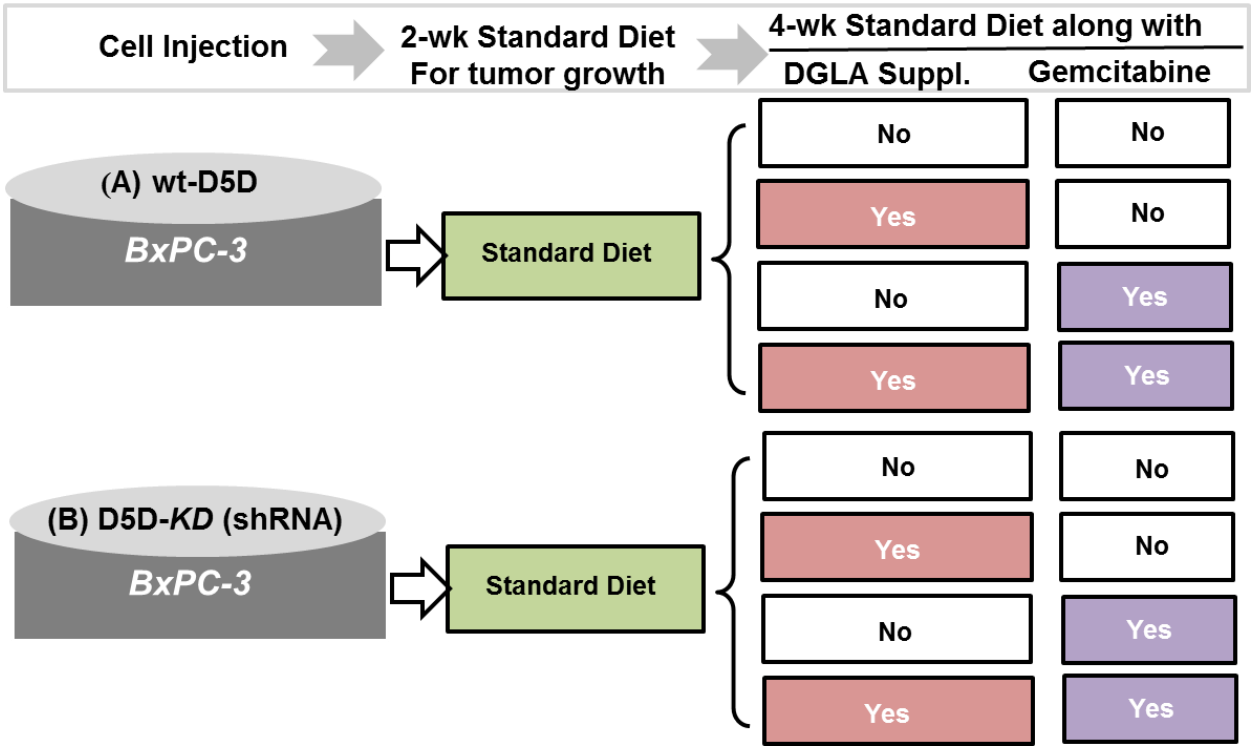

Scheme 9. Animal experiment design.
A total of 48 mice (8 groups and 6 mice each group) were used in this study to confirm the anti-cancer effects of DGLA treatment and D5D-*KD* on pancreatic tumors. Wt-D5D and D5D-*KD* BxPC-3 cells were subcutaneously injected into the hind flank of immuno-deficient mice to establish a xenograft tumor model. After two weeks for tumor growth, the mice bearing wt-D5D or D5D-*KD* tumor were further divided into four sub groups and received different treatment for 4 weeks, including 1) vehicle control, 2) DGLA supplementation, 3) gemcitabine injection, and 4) combination of DGLA and gemcitabine. The tumor size and mice body weights were measured twice a week to test whether D5D-*KD* and DGLA supplementation could inhibit pancreatic tumor growth. At the end of the treatment, the mice were euthanized and the tumors were collected for further analysis.

5.2. Results

5.2.1. DGLA supplementation suppressed tumor growth in mice bearing D5D-*KD* tumors

Due to the lack of thymus, the cancer cells injected into the immune-deficient mice can readily form solid tumors. The hairless phenotype of nude mice is also ideal for evaluating tumor growth. Mice were injected with wild-type or D5D-*KD* BxPC-3 cells to establish tumors. After 2-week standard diet to allow tumors to grow, the mice were subjected to different treatments (e.g. DGLA, gemcitabine, combination of DGLA and gemcitabine) for 4 weeks.

The body weights of mice bearing wt-D5D tumors were measured twice a week to monitor the toxicity effect of DGLA and gemcitabine treatments. Results showed that DGLA and gemcitabine administered to mice bearing wt-D5D tumors for 4 weeks did not cause any significant loss in body weights of mice (**Fig 23A**). In future animal studies, the livers and kidneys will be collected for histology to assess organ toxicity.

In groups of mice bearing wt-D5D tumors, 4-week DGLA supplementation (8 mg/mice, oral gavage, twice a week) did not suppress tumor growth, but even increase the tumor volume compared to control group (tumor volume 146.9 mm^3 for DGLA supplementation *vs.* 135.4 mm^3 for control at the end of experiment, **Fig 23B**-**Fig 23C**). The results suggested that, in mice bearing wt-D5D tumors, D5D can readily convert DGLA to AA, limiting formation of 8-HOA from COX-2-catalyzed DGLA peroxidation to suppress tumor growth.

Gemcitabine, a front-line chemo-drug used for pancreatic cancer therapy, was given to mice with or without DGLA supplementation. Treatment of gemcitabine (30 mg/kg, intraperitoneal, twice a week) significantly inhibited tumor growth (tumor volume 87.0 mm^3), while co-treatment of gemcitabine and DGLA did not further reduced tumor growth in wt-D5D tumors (tumor volume 96.9 mm^3), suggesting that the suppressed tumor growth in mice treated

with gemcitabine or the combination of gemcitabine and DGLA only comes from the growth inhibitory effect of gemcitabine.

The 4-week supplementation of DGLA and gemcitabine did not cause any change in the body weight of mice bearing D5D-*KD* tumors compared to mice in control group (**Fig 24A**), indicating that the treatments (e.g. DGLA and gemcitabine) has no severe toxicity of on mice.

In groups of mice bearing D5D-*KD* tumors, DGLA supplementation significantly decreased tumor growth in mice compared to those without DGLA treatment **(**tumor volume 90.2 mm^3 for DGLA treatment vs. 129.1 mm^3 for control at the end of experiment, **Fig 24B-Fig 24C**). In addition, injection of gemcitabine alone also resulted in a significant decrease of tumor growth in D5D-*KD* tumors (tumor volume 81.6 mm^3). When mice bearing D5D-*KD* tumors treated with combination of DGLA and gemcitabine, the tumor volume was further significantly reduced (tumor volume 37.7 mm^3) compared to mice treated with gemcitabine alone (tumor volume 81.6 mm^3). The data suggested that D5D-*KD* and DGLA supplementation could enhance the efficacy of gemcitabine on inhibiting tumor growth, which is consistent with the conclusion in *in vitro* study.

Note, when comparing tumors from both D5D-*KD* group and wt-D5D group without DGLA supplementation, the size of tumors from D5D-*KD* group (tumor volume: 129.1 mm^3, Fig 24) was smaller compared to that from wt-D5D group (tumor volume 135.4 mm^3, Fig 23). This may be because D5D-*KD* blocked the conversion from upstream ω-6 fatty acids (e.g. DGLA) to AA, leading to limited production of PGE2 from COX-2-catalyzed AA peroxidation (**Fig 25**).

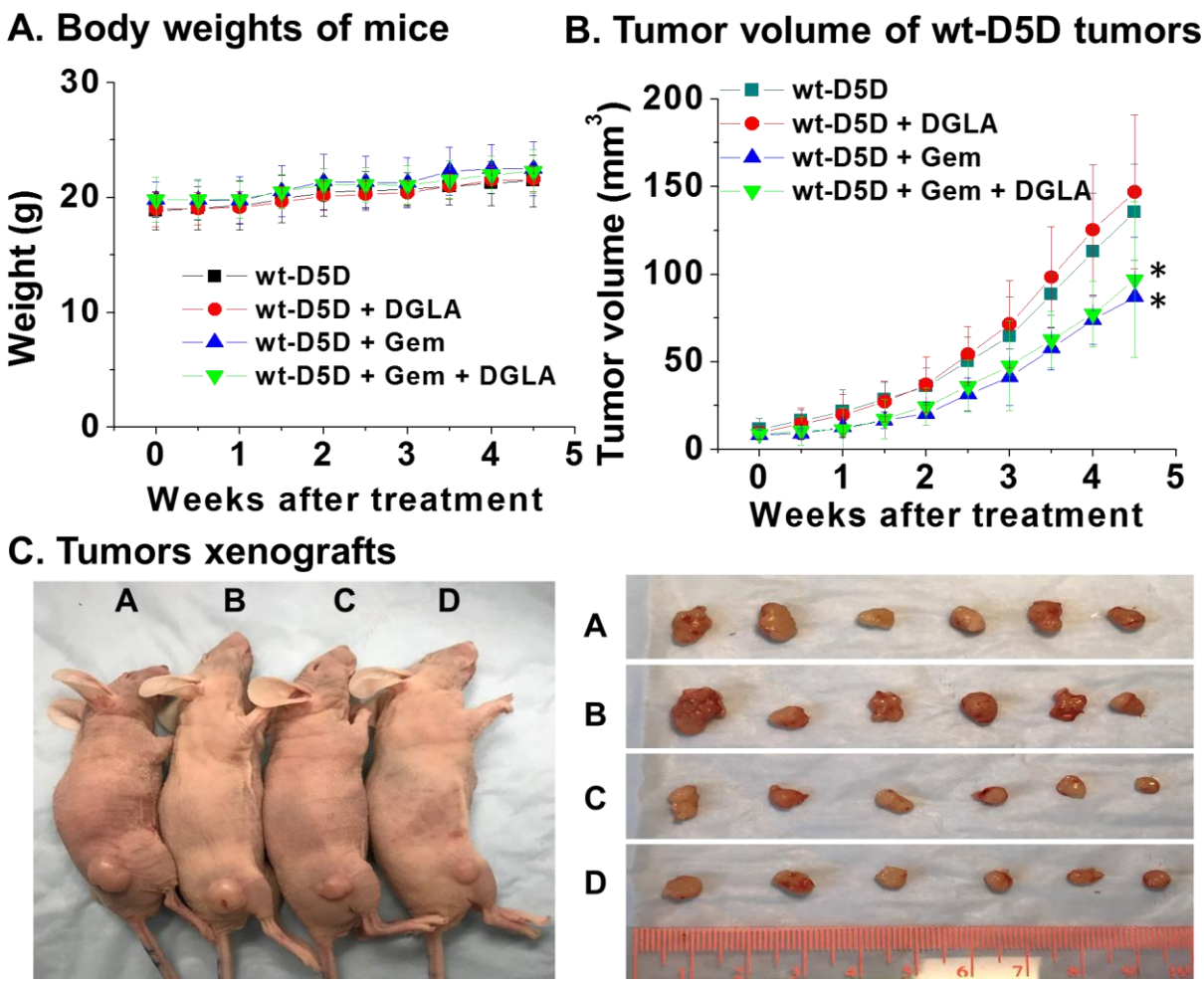

Fig 23. Tumor growth of wt-D5D tumors.
A) Body weight of mice from wt-D5D tumors treated with vehicle (control), DGLA (8 mg/mouse), gemcitabine (30 mg/kg) or gemcitabine + DGLA; B) Tumor volume of wt-D5D tumors treated with vehicle, DGLA, gemcitabine or gemcitabine + DGLA. C) Mice with tumors xenografts from wt-D5D tumors treated with A: vehicle, B: DGLA, C: gemcitabine and D: gemcitabine + DGLA. (*: significant difference vs. control with $p < 0.05$ from $n = 6$).

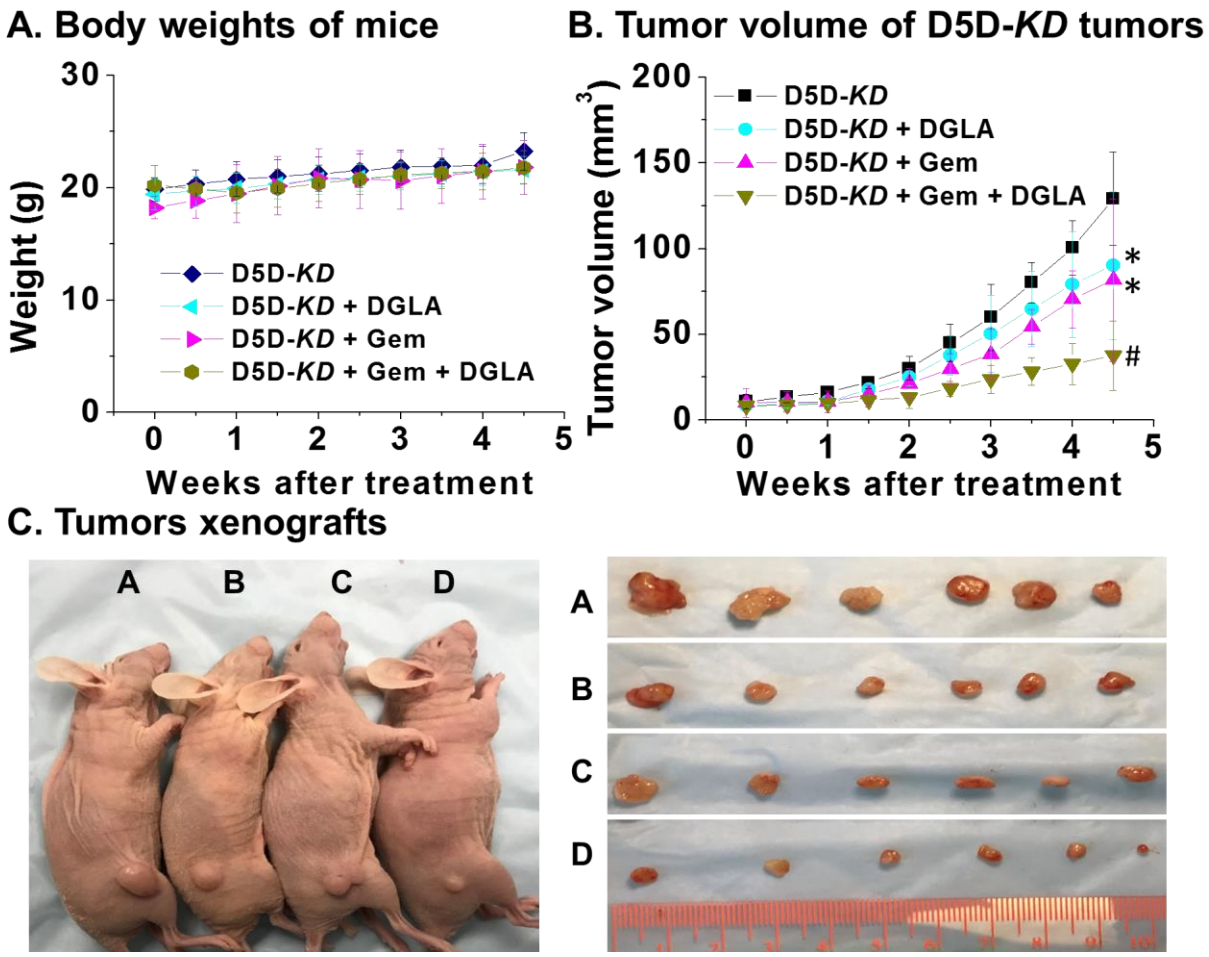

Fig 24. DGLA supplementation suppressed tumor growth in mice bearing D5D-*KD* tumors. A) Body weight of mice from D5D-*KD* tumors treated with vehicle (control), DGLA (8 mg/mouse), gemcitabine (30 mg/kg) or gemcitabine + DGLA. B) Tumor volume of D5D-*KD* tumors treated with vehicle, DGLA, gemcitabine or gemcitabine + DGLA. C) Tumor xenografts from D5D-*KD* tumors treated with A: vehicle, B: DGLA, C: gemcitabine or D: gemcitabine + DGLA. (*: significant difference vs. control with $p < 0.05$; and $^{\#}$: significant difference vs. gemcitabine group with $p < 0.05$ from $n = 6$).

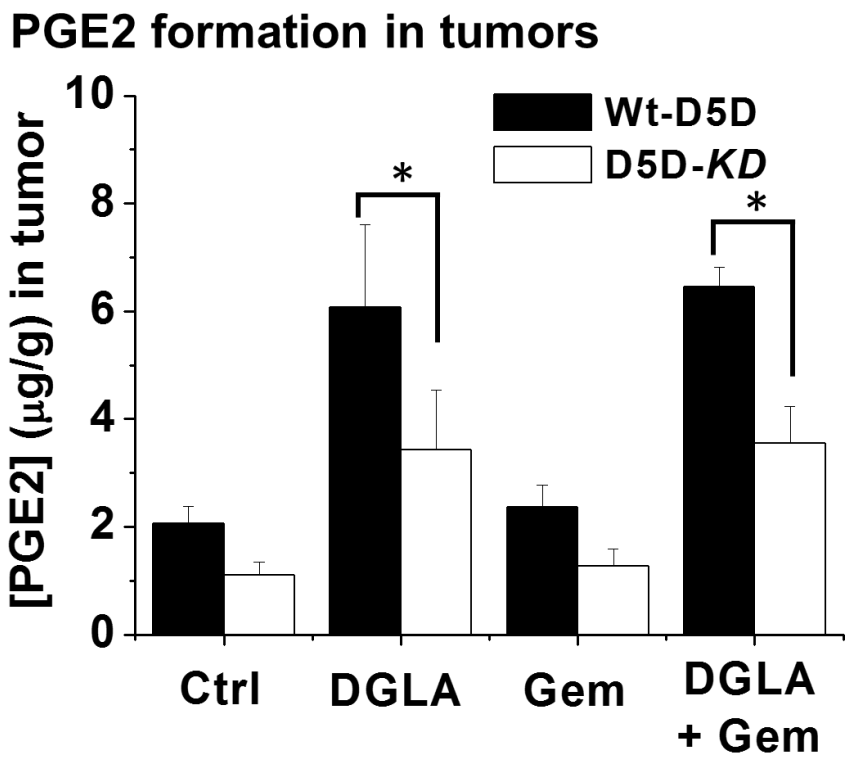

Fig 25. D5D-*KD* decreased level of PGE2 in tumors.
LC/MS quantification of PGE2 in tumors from wt-D5D and D5D-*KD* groups treated with vehicle, DGLA, gemcitabine, or gemcitabine + DGLA. Data represent as mean ± SD from n = 6. (*: significant difference with $p < 0.05$).

5.2.2. Formation of 8-HOA was promoted from COX-catalyzed DGLA peroxidation in mice bearing D5D-*KD* tumors

In chapter 4, our strategy (i.e. D5D-*KD* and DGLA treatment) promoted formation of 8-HOA to a threshold level (above 0.5 μM), which leads to inhibited cancer cell growth, migration and invasion. Here, we assessed whether the reduced tumor growth in D5D-*KD* groups with DGLA supplementation is associated the promoted formation of 8-HOA from COX-catalyzed DGLA peroxidation *via* D5D-*KD*. The expression of COX-2, D5D as well as the associated mechanism were assessed by immunofluorescence analysis.

We firstly used immunofluorescence analysis to assess the expression of D5D and COX-2 in wt-D5D and D5D-*KD* tumors. The results showed that ~65% expression of D5D (the pink

color) was inhibited in tumors from D5D-*KD* groups compared to the tumors from wt-D5D groups (**Fig 26**), while COX-2 expression (the green color) remained at similar level in tumors from both D5D-*KD* and wt-D5D groups. The data demonstrated that D5D shRNA transfection can stably knock down D5D expression in tumors without affecting COX-2 expression.

We then detected the levels of DGLA and AA in tumors from both wt-D5D and D5D-*KD* groups *via* LC/MS to investigate whether D5D-*KD* altered DGLA metabolism in tumors. In mice without DGLA supplementation (e.g. control groups and gemcitabine groups), the ratio of DGLA *vs.* AA in D5D-*KD* tumors is similar compared to that in wt-D5D tumors (DGLA/AA range from 0.15 to 0.2, with DGLA level ~0.7 μg/g in both wt-D5D and D5D-*KD* tumors, **Fig 27A**). In wt-D5D tumors with DGLA supplementation, we found the ratio of DGLA *vs.* AA remains unchanged compared to that in wt-D5D tumors without DGLA treatment (~0.16, with DGLA level ~1.5 μg/g, **Fig 27B**). However, the ratio of DGLA *vs.* AA increased more than 2-fold in D5D-*KD* tumors from mice supplemented with DGLA (~0.35, with DGLA level ~3.1 μg/g, Fig 27B). These results indicated that, when mice were supplemented with DGLA, D5D-*KD* can effectively suppress the conversion from DGLA to AA in tumors, which could be essential for promoting formation of 8-HOA in D5D-*KD* tumors

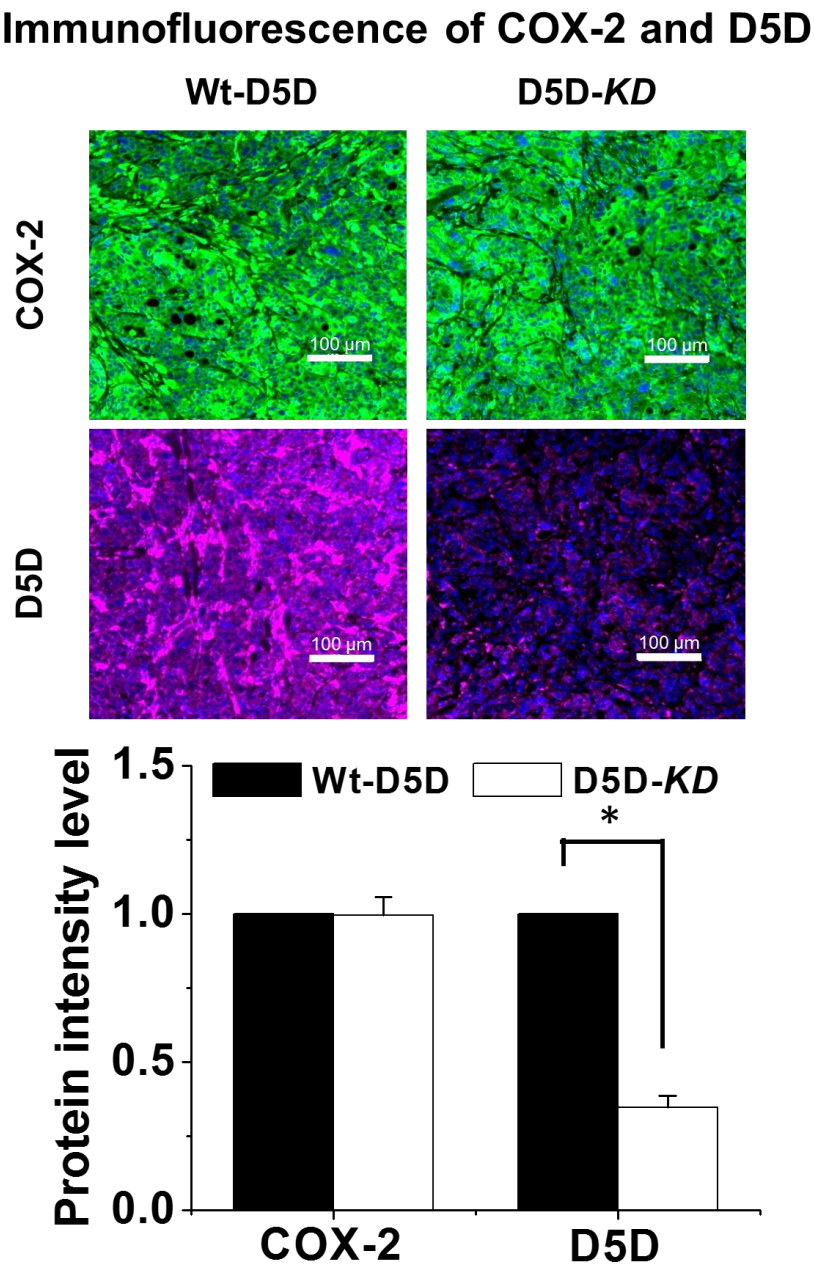

Fig 26. Immunofluorescence analysis of COX-2 and D5D in tumors.
Immunofluorescence analysis of COX-2 (green color) and D5D expression (pink color) in tumors from wild-type and D5D-*KD* groups treated with vehicle (control), DGLA (8 mg/mouse), gemcitabine (30 mg/kg) or gemcitabine + DGLA. Protein intensity rate was calculated by comparing the immunofluorescence intensity of COX-2 and D5D in D5D-*KD* groups to those in wild-type groups. (*: significant difference with $p < 0.05$ from $n = 6$).

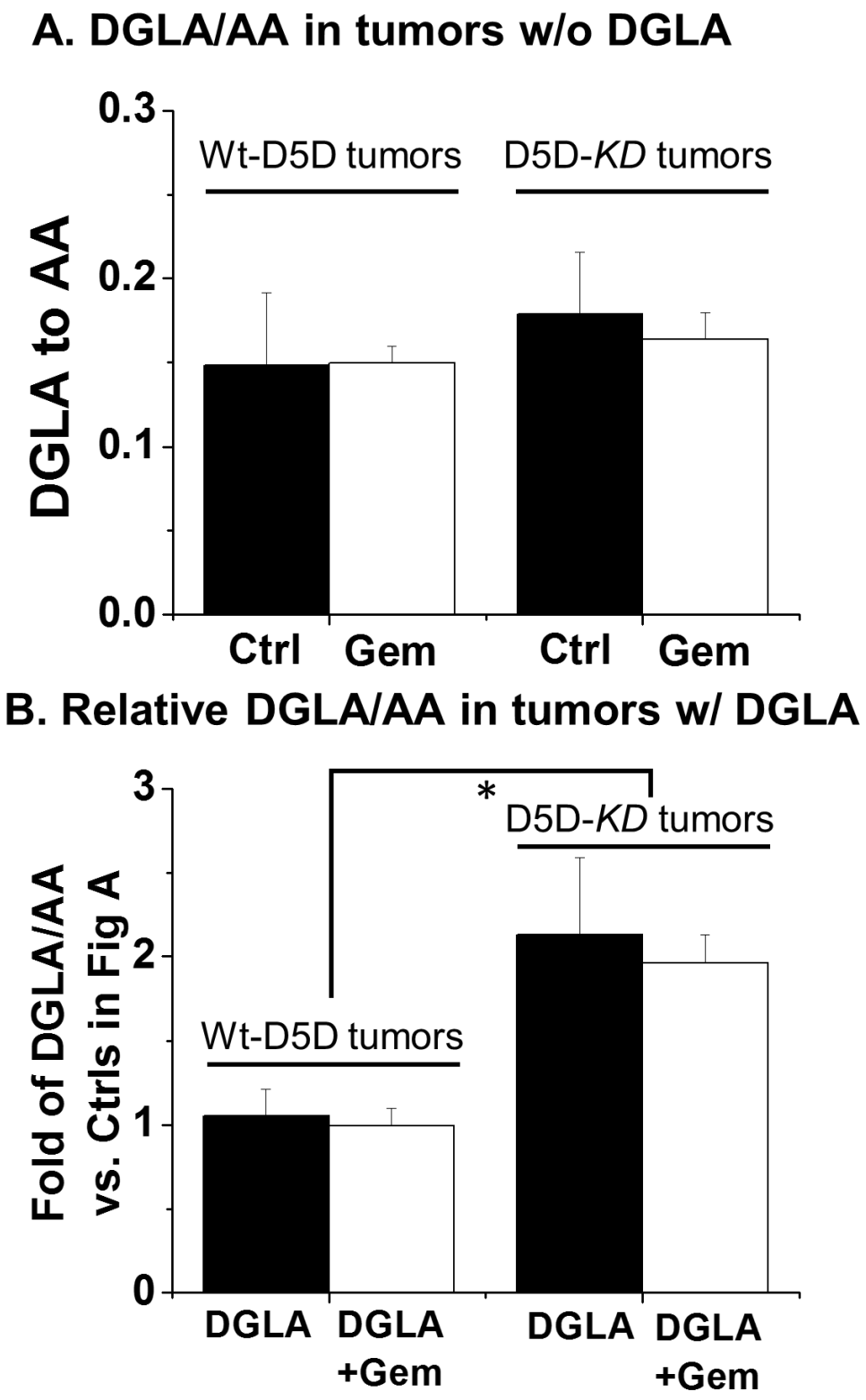

Fig 27. D5D-*KD* increased the ratio of DGLA/AA in tumors supplemented with DGLA. A) Ratio of DGLA/AA in tumors without DGLA supplementation from wt-D5D and D5D-*KD* groups; B) Relative ratio of DGLA/AA in tumors with DGLA supplementation from wt-D5D and D5D-*KD* groups. (*: significant difference with $p < 0.05$).

GC/MS was performed to measure the PFB-derivative form of 8-HOA generated from tumors in both D5D-*KD* and wt-D5D groups with or without DGLA supplementation. The levels of 8-HOA in tumors of D5D-*KD* groups reached ~ 0.5 µg/g during the 4-week DGLA treatment (**Fig 28**). The results suggested that, once reached the threshold level (> 0.25 µg/g), 8-HOA can inhibit tumor growth. However, the levels of 8-HOA in wt-D5D groups only reached ~ 0.15 µg/g with DGLA supplementation, thus in mice bearing wt-D5D tumors, even treated with combination of DGLA and gemcitabine, the tumor growth was similar to that in mice treated only with gemcitabine (Fig 23). The results indicated that, in order for 8-HOA to suppress tumor growth, it is necessary to reach a threshold level (above 0.25 µg/g) in tumor.

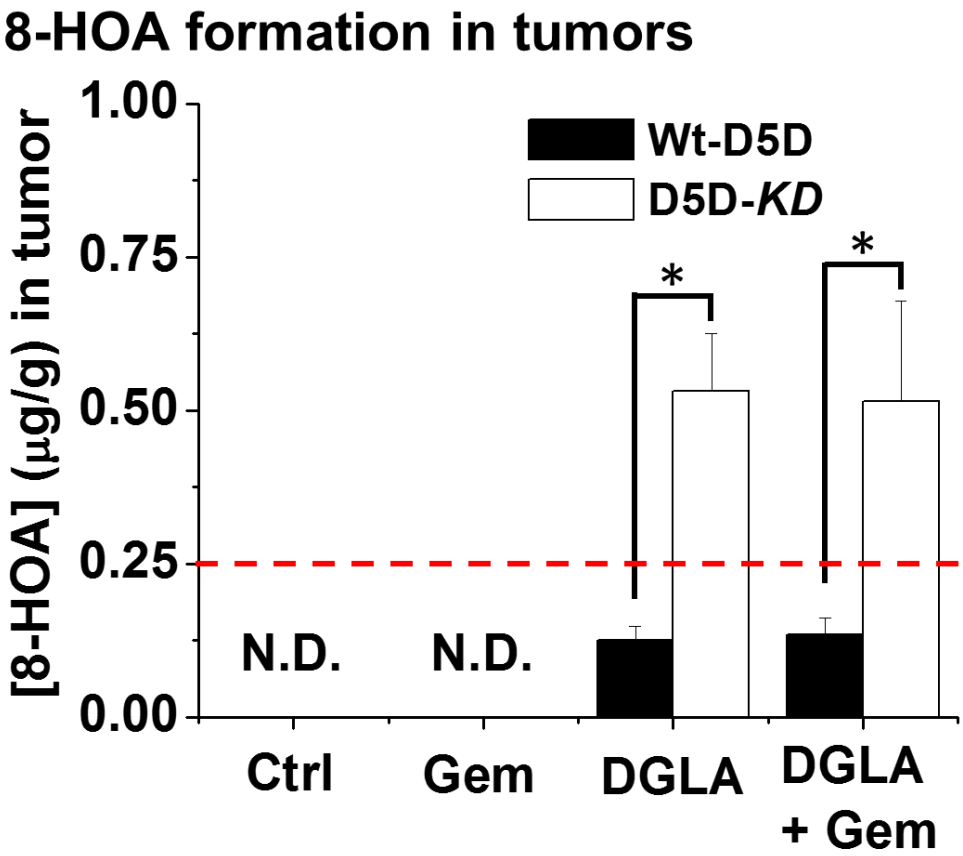

Fig 28. D5D-*KD* promoted formation of 8-HOA in pancreatic tumors.
GC/MS quantification of 8-HOA in tumors from wild-type and D5D-*KD* groups treated with vehicle (control), (8 mg/mouse), gemcitabine (30 mg/kg), or gemcitabine + DGLA. N.D.: not detected. The red line indicates the threshold level of 8-HOA to inhibit tumor growth. Data represent as mean ± SD from n = 6. (*: significant difference with $p < 0.05$).

5.2.3. Supplementation of DGLA induced tumor cell apoptosis in D5D-*KD* tumors

The protein expression of Ki-67 is closely related to cell proliferation. Ki-67 has been commonly used as a marker for detecting proliferating cell [169-171]. Studies from chapter 4 have shown that promoted formation of 8-HOA from COX-catalyze DGLA peroxidation *via* D5D-*KD* can inhibit pancreatic cancer cell viability. Tumor sections from wt-D5D and D5D-*KD* groups were stained with Ki-67 (orange dots) to investigate the effect of D5D-*KD* and DGLA treatment on pancreatic tumor cell proliferation.

Results showed that in wt-D5D tumors, DGLA supplementation did not reduce Ki-67 positive cells compared to control (percentage of Ki-67 positive cells ~85.2 for DGLA vs. 89.0 for control, **Fig 29**), which could be associated with insufficient generation of 8-HOA. The combination of DGLA and gemcitabine caused a significant decrease of tumor cell proliferation in wt-D5D tumors similar to treatment of gemcitabine alone (percentage of Ki-67 positive cells ~37.6% for DGLA and gemcitabine *vs.* ~35.7% for gemcitabine alone, Fig 29). The data suggested that, when the formation of 8-HOA did not reach the threshold level (0.25 μg/g), the efficacy of gemcitabine cannot be enhanced.

In D5D-*KD* tumors, treatment of DGLA significantly decreased the percentage of Ki-67 positive cells in D5D-*KD* tumors (~58.1 % for DGLA vs. 80.6 % for control, Fig 29), suggesting that, once formation of 8-HOA reached the threshold level (above 0.25 μg/g), 8-HOA can inhibit tumor cell proliferation. Gemcitabine treatment alone resulted in a significant decrease in the percentage of Ki-67 positive cells of D5D-*KD* tumors (~39.6%, Fig 29). Further reduction of Ki-67 positive cells was observed in D5D-*KD* tumors treated with DGLA and gemcitabine (~20.7%, Fig 29), indicating that our strategy can improve the efficacy of gemcitabine on inhibiting cancer cell proliferation, consistent with the *in vitro* study in chapter 4.

Cleaved PARP has been used as a marker for detecting cell apoptosis in tumors [172-173]. We also stained tumor tissues with cleaved PARP (pink dots) to test the effect of our strategy on tumor cell apoptosis. Immunofluorescence analysis of cleaved PARP showed that DGLA had no effect inducing tumor cell apoptosis in wt-D5D tumor (percentage of apoptotic cells ~5.1% for DGLA vs. ~4.0% for control, **Fig 30**). The combination of gemcitabine and DGLA induced tumor cell apoptosis in wt-D5D tumors similar to treatment of gemcitabine alone (percentage of apoptotic cells ~ 10.7 for DGLA and gemcitabine *vs.* ~9.4% for gemcitabine alone, Fig 30). The results demonstrated that the efficacy of gemcitabine cannot be improved in wt-D5D tumors as the formation of 8-HOA did not reach the threshold level (0.25 μg/g).

In D5D-*KD* tumors, supplementation of DGLA significantly induced tumor cell apoptosis (percentage of apoptotic cells ~6.2% for DGLA vs. 3.6% for control, Fig 30). In addition, treatment of gemcitabine alone also induced tumor cell apoptosis in D5D-*KD* tumors (percentage of apoptotic cells ~9.2%, Fig 30), indicating that formation of 8-HOA reaching the threshold level (> 0.25 μg/g) is essential for inducing tumor cell apoptosis. When mice were co-treated with DGLA and gemcitabine, promoted formation of 8-HOA from DGLA and D5D-*KD* could significantly enhance efficacy of gemcitabine on D5D-*KD* tumors as we observed in cleaved PARP staining (percentage of apoptotic cells ~16.0 %, Fig 30).

The decreased percentage of Ki-67 (marker for detecting proliferating tumor cells) positive cells in tumors from mice supplemented with DGLA and gemcitabine could be attributed to the increased apoptotic cells in tumors, suggesting that improved formation of 8-HOA from D5D-*KD* and DGLA supplementation can enhance the efficacy of gemcitabine on inducing tumor cell apoptosis, consistent with the *in vitro* study in chapter 4.

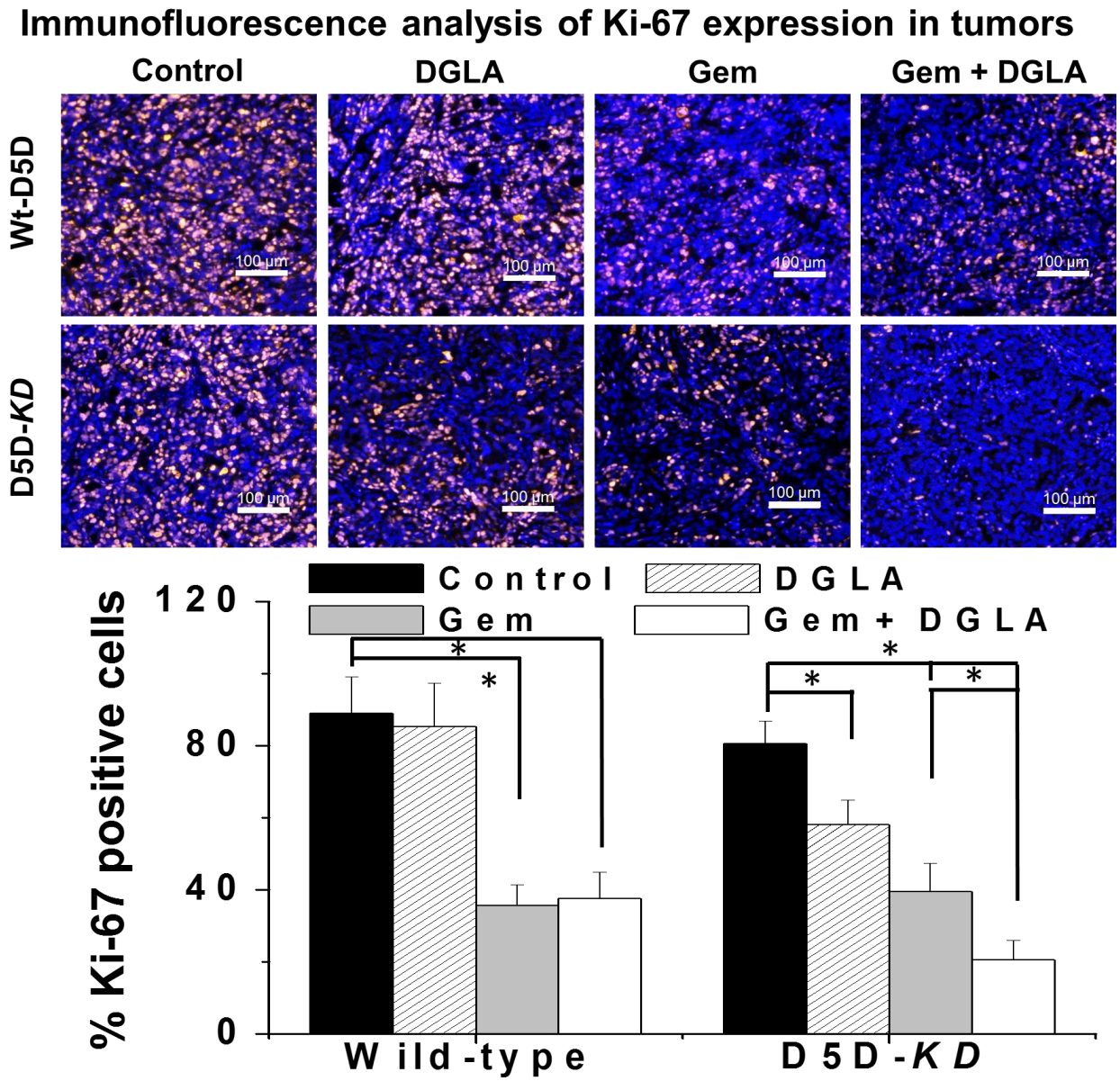

Fig 29. D5D-*KD* and DGLA supplement decreased Ki-67 positive cells.
Immunofluorescence analysis of Ki-67 expression (orange dots) in tumors from wild-type and D5D-*KD* groups treated with vehicle (control), DGLA (8 mg/mouse), gemcitabine (30 mg/kg) or gemcitabine + DGLA. The orange dots indicate Ki-67 positive tumor cell. (*: significant difference with $p < 0.05$ from $n = 6$).

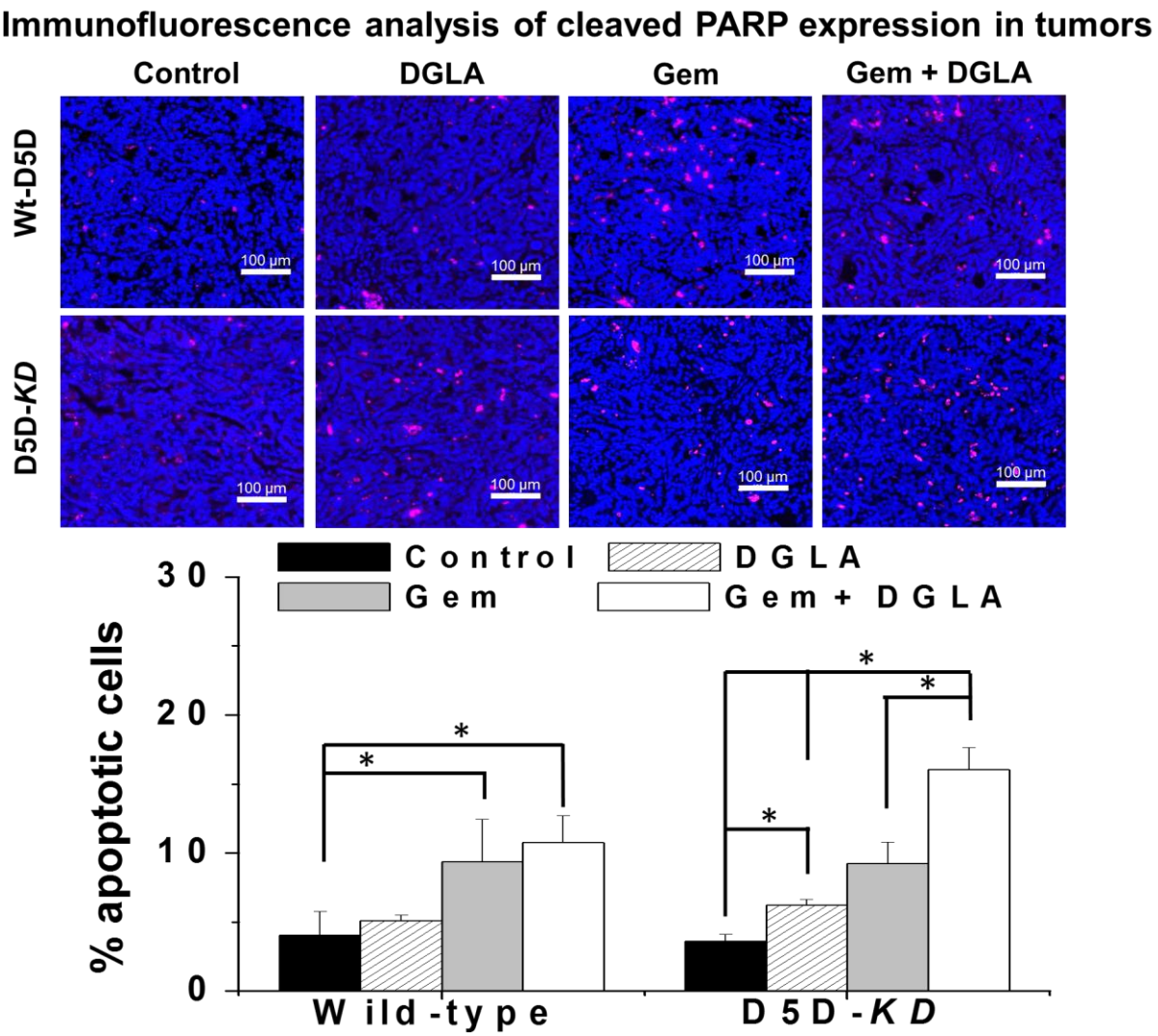

Fig 30. D5D-*KD* and DGLA supplement induced tumor cell apoptosis.
Immunofluorescence analysis of cleaved PARP expression (pink dots) in tumors from wild-type and D5D-*KD* groups treated with vehicle (control), DGLA (8 mg/mouse), gemcitabine (30 mg/kg) or gemcitabine + DGLA. The pink dots indicate the apoptotic tumor cells. (*: significant difference with $p < 0.05$ from $n = 6$).

A western blot was performed to investigate the molecular mechanism of observed tumor growth inhibition. We observed no alternation in expression of acetyl histone H3, γH2AX, Bcl-2, procaspase-9 and procaspase-3 in wt-D5D tumors with DGLA supplementation. The data indicated that, in wt-D5D tumors supplemented with DGLA, there is not enough 8-HOA generated to inhibit HDAC and cause DNA damage (**Fig 31**).

Gemcitabine was known to suppress cancer cell growth by inducing p53-dependent as well as p53-independent cell apoptosis [165-166]. Treatment of gemcitabine downregulated expressions of Bcl-2 (anti-apoptotic protein) and procaspase 9 and procaspase 3 (pro-apoptotic proteins) in wt-D5D tumors (Fig 31). However, there is no further alternation in expression of γH2AX, Bcl-2, procaspase-9 and procaspase-3 in wt-D5D tumors treated with the combination of DGLA and gemcitabine (Fig 31).

Increased expression of acetyl histone H3 and γH2AX as well as decreased expressions of Bcl-2 (anti-apoptotic protein), procaspase-9 and procaspase-3 (pro-apoptotic proteins) were observed in D5D-*KD* tumors treated with DGLA, confirming that 8-HOA could act as a histone deacetylase inhibitor to cause DNA damage (**Fig 32**). These data suggested that D5D-*KD* can promote formation of 8-HOA from DGLA in tumors, which can in turn inhibit HDAC activity and induce DNA damage, leading to activation of cell apoptotic pathways and resulting in induced tumor cell apoptosis.

In addition, gemcitabine also down-regulated Bcl-2 as well as activated procaspase 9 and procaspase 3 in D5D-*KD* tumors (Fig 32). Further increased expression of γH2AX and down-regulated expressions of Bcl-2, procaspase 9 and procaspase 3 (Fig 32) were observed when mice in D5D-*KD* tumors were co-treated by DGLA and gemcitabine.

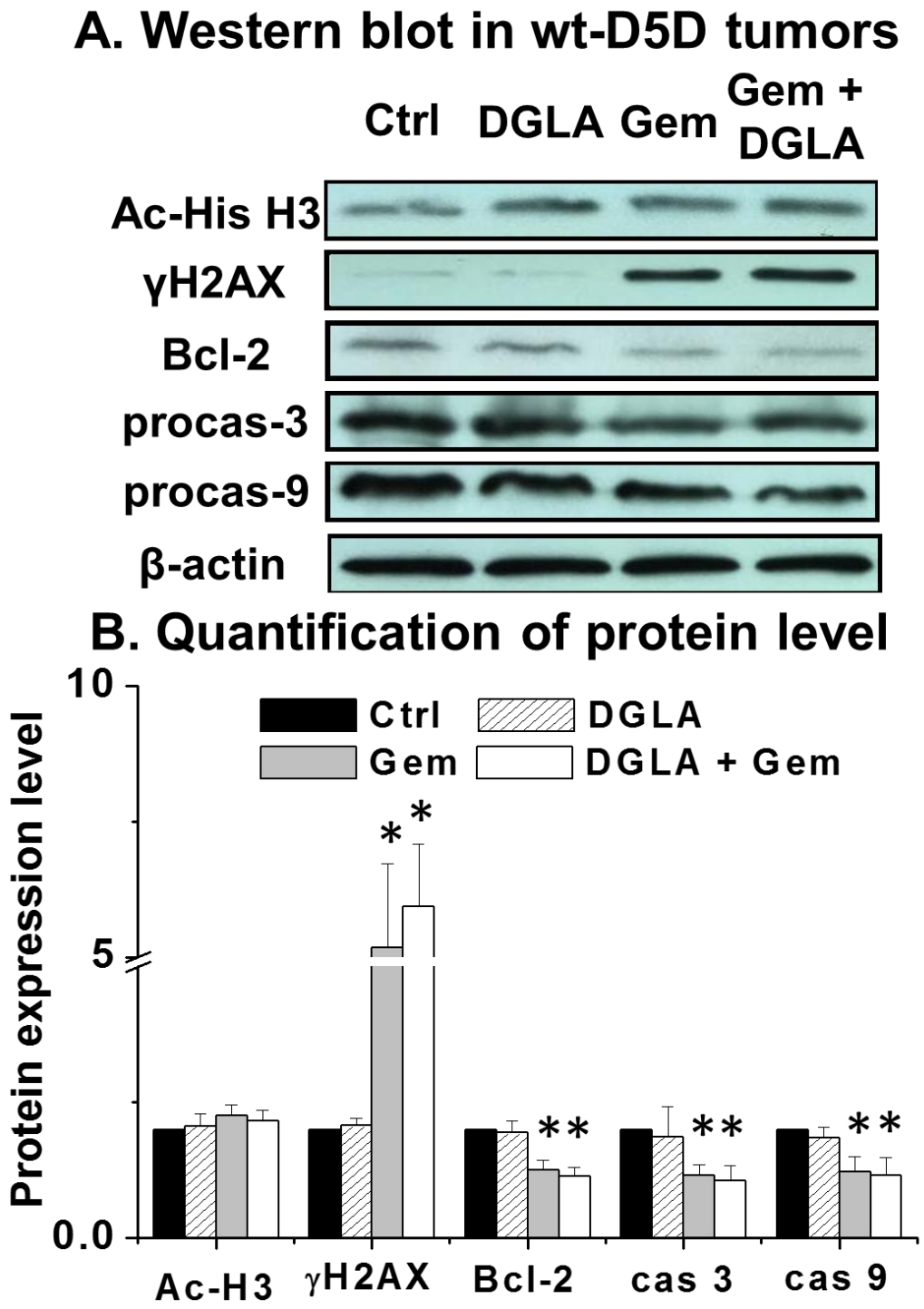

Fig 31. Western blot and quantification of protein level in wt-D5D tumors.
A) Western blot of acetyl histone H3, γH2AX, Bcl-2, procaspase-3 and procaspase-9 in tumors from wild-type groups treated with vehicle (control), DGLA (8 mg/mouse), gemcitabine (30 mg/kg) or gemcitabine + DGLA. B) Quantification of protein expression level. Protein expression level was normalized using β-actin as loading control (*: significant difference vs. control with $p < 0.05$; and #: significant difference vs. gemcitabine group with $p < 0.05$ from $n = 6$).

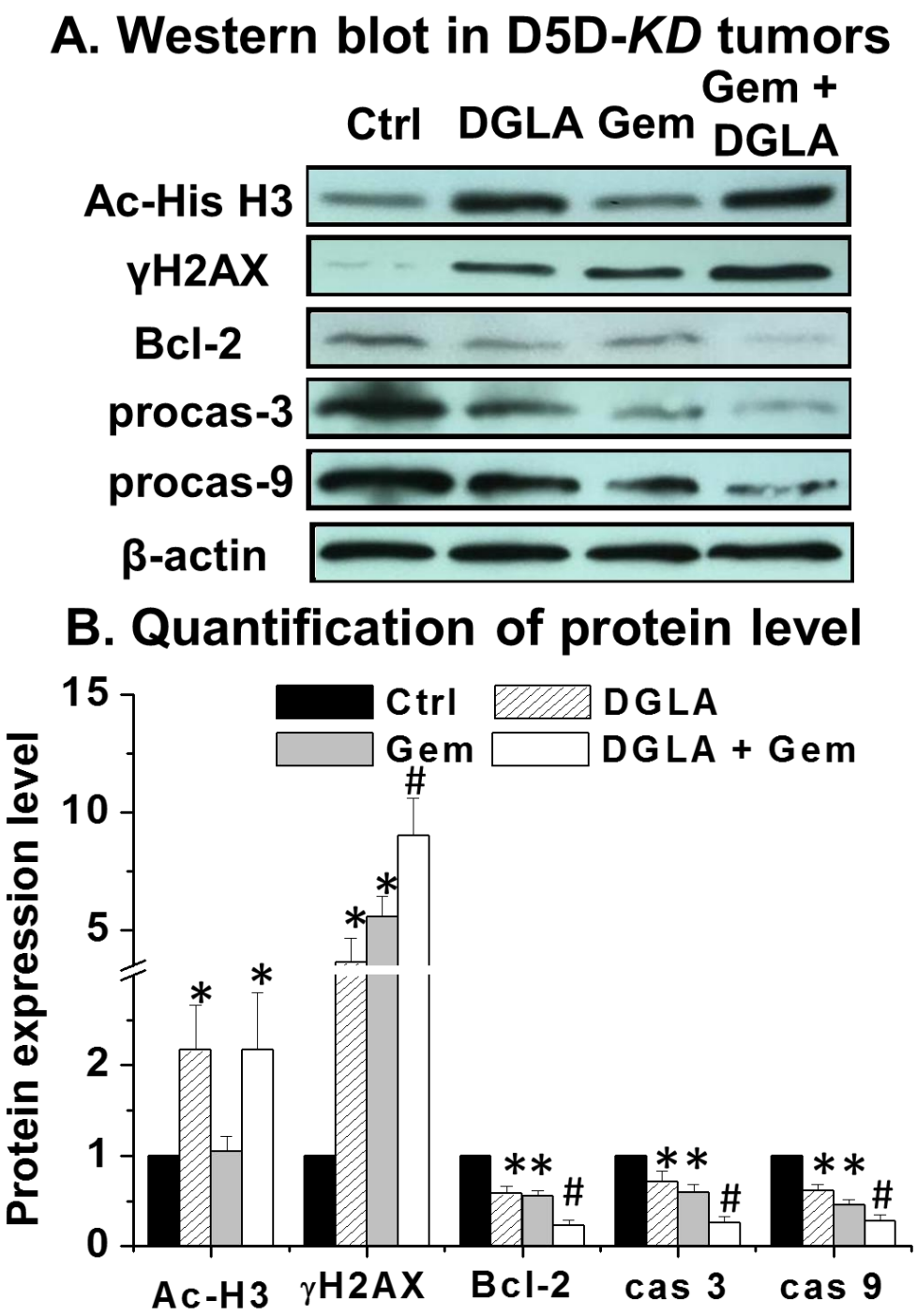

Fig 32. D5D-*KD* and DGLA treatment promoted gemcitabine-induced apoptosis *via* p53 independent pathway.

A) Western blot of acetyl histone H3, γH2AX, Bcl-2, procaspase-3 and procaspase-9 in tumors from D5D-*KD* groups treated with vehicle (control), DGLA (8 mg/mouse), gemcitabine (30 mg/kg) or gemcitabine + DGLA. B) Quantification of protein expression level. Protein expression level was normalized using β-actin as loading control (*: significant difference vs. control with $p < 0.05$; and #: significant difference vs. gemcitabine group with $p < 0.05$ from n = 6).

5.2.4. DGLA supplementation altered expressions of markers involved in cancer metastasis in mice bearing D5D-*KD* tumors

Tumors from wt-D5D and D5D-*KD* groups were tested *via* immunofluorescence for expression of protein markers that play an important role in cancer metastasis such as MMP-2 and E-cadherin. MMP-2 participates in degradation of extracellular matrix, facilitating tumor cell migration. The epithelial marker E-cadherin plays an important role in maintaining the integrity of tissue architecture. Loss of E-cadherin can lead to increased potential for tumor cells to metastasize.

When mice in D5D-*KD* groups were supplemented with DGLA, there is a decrease in the expression of MMP-2 (the pink color), which is involved in the degradation of extracellular matrix, (mean fluorescence intensity ~ 114.4 for DGLA vs. 154.4 for control, **Fig 33**), suggesting that the formation of 8-HOA in D5D-*KD* tumors (above 0.25 μg/g) can inhibit tumor metastasis potential. In wt-D5D tumors, DGLA did not decrease the MMP-2 expression (mean fluorescence intensity ~ 167.7 for DGLA vs. 160.3 for control, Fig 33). Results also showed that treatment of gemcitabine alone can downregulate the MMP-2 level in wt-D5D (mean fluorescence intensity ~ 99.8, Fig 33) and D5D-*KD* tumors (mean fluorescence intensity ~ 104.7, Fig 33). In wt-D5D tumors, the combination of DGLA and gemcitabine did not further downregulate MMP-2 expression (mean fluorescence intensity ~ 106.6, Fig 33). Further decreased expression of MMP-2 was only observed in D5D-*KD* tumors treated with the combination of DGLA and gemcitabine (mean fluorescence intensity ~ 50.9, Fig 33). The data demonstrated that our strategy can improve the efficacy of gemcitabine on inhibiting tumor metastasis potential.

Results showed that DGLA did not affect the expression level of E-cadherin (the green color) in wt-D5D tumors (mean fluorescence intensity ~ 61.4 for DGLA *vs.* 56.2 for control, **Fig**

34). In D5D-*KD* tumors, DGLA supplementation significantly upregulated expression of E-cadherin (mean fluorescence intensity ~ 77.7 for DGLA vs. 55.8 for control, Fig 34). The results suggested that formation of 8-HOA to reach the threshold level (> 0.25 μg/g) was essential to increase the expression level of E-cadherin. Treatment of gemcitabine alone upregulated the level of E-cadherin in wt-D5D (mean fluorescence intensity ~ 94.3, Fig 34) and D5D-*KD* tumors (mean fluorescence intensity ~ 90.0, Fig 34). Further increased expression of E-cadherin was observed in D5D-*KD* tumors co-treated with DGLA and gemcitabine (mean fluorescence intensity ~ 109.2, Fig 34) compared to treatment with gemcitabine alone, while in wt-D5D tumors, the combination did not further upregulate E-cadherin (mean fluorescence intensity ~ 92.7, Fig 34). Taken together, the results demonstrated that promoted formation of 8-HOA from D5D-*KD* and DGLA supplementation can enhance the efficacy of gemcitabine on suppressing cancer metastasis potential by decreasing MMP-2 expression and increase E-cadherin expression.

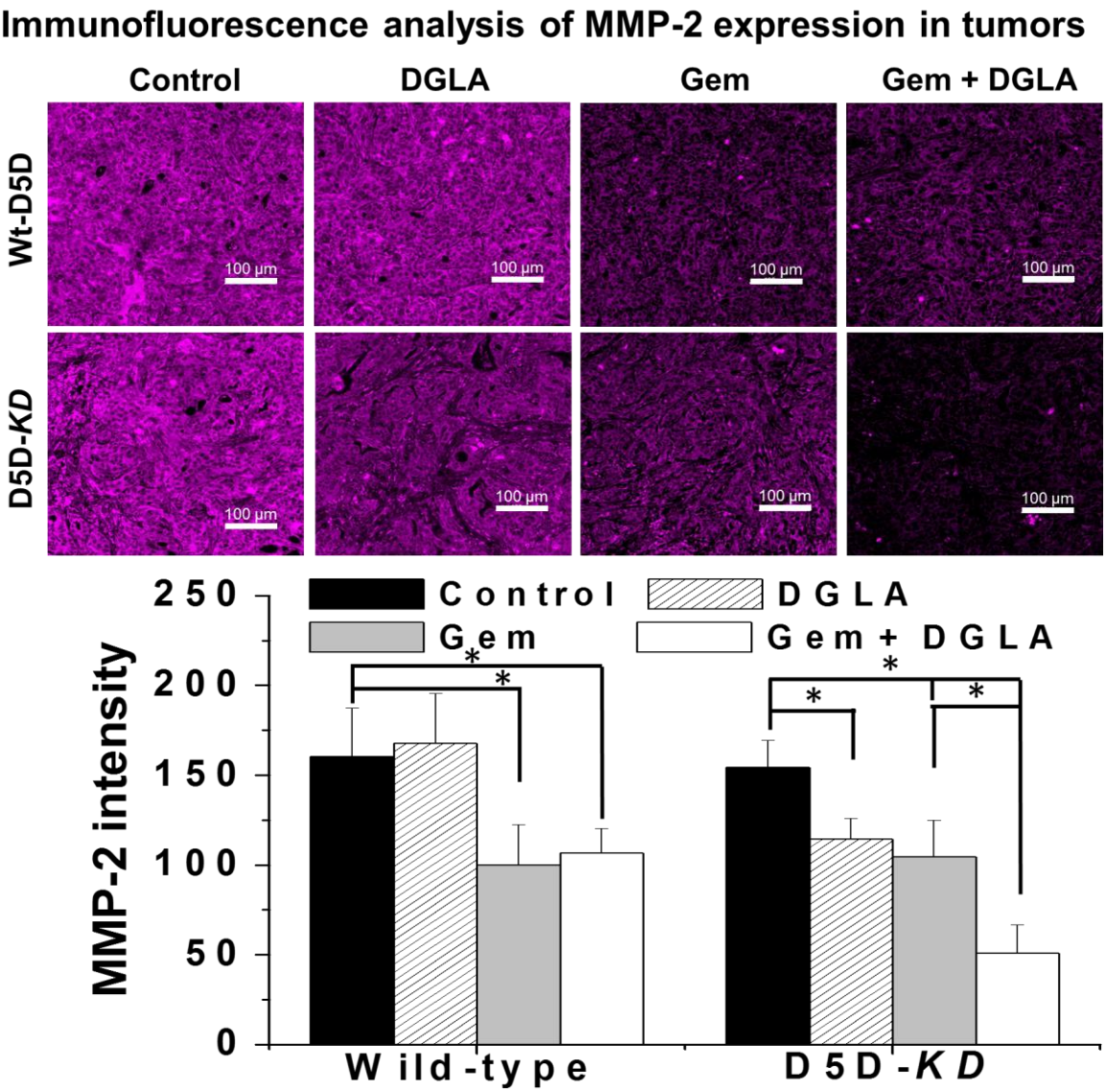

Fig 33. D5D-*KD* and DGLA treatment downregulated MMP-2 expression.
Immunofluorescence analysis of MMP-2 expression (pink color) in tumors from wild-type and D5D-*KD* groups treated with vehicle (control), DGLA (8 mg/mouse), gemcitabine (30 mg/kg) or gemcitabine + DGLA. The pink area indicates the expression of MMP-2. (*: significant difference with $p < 0.05$ from $n = 6$).

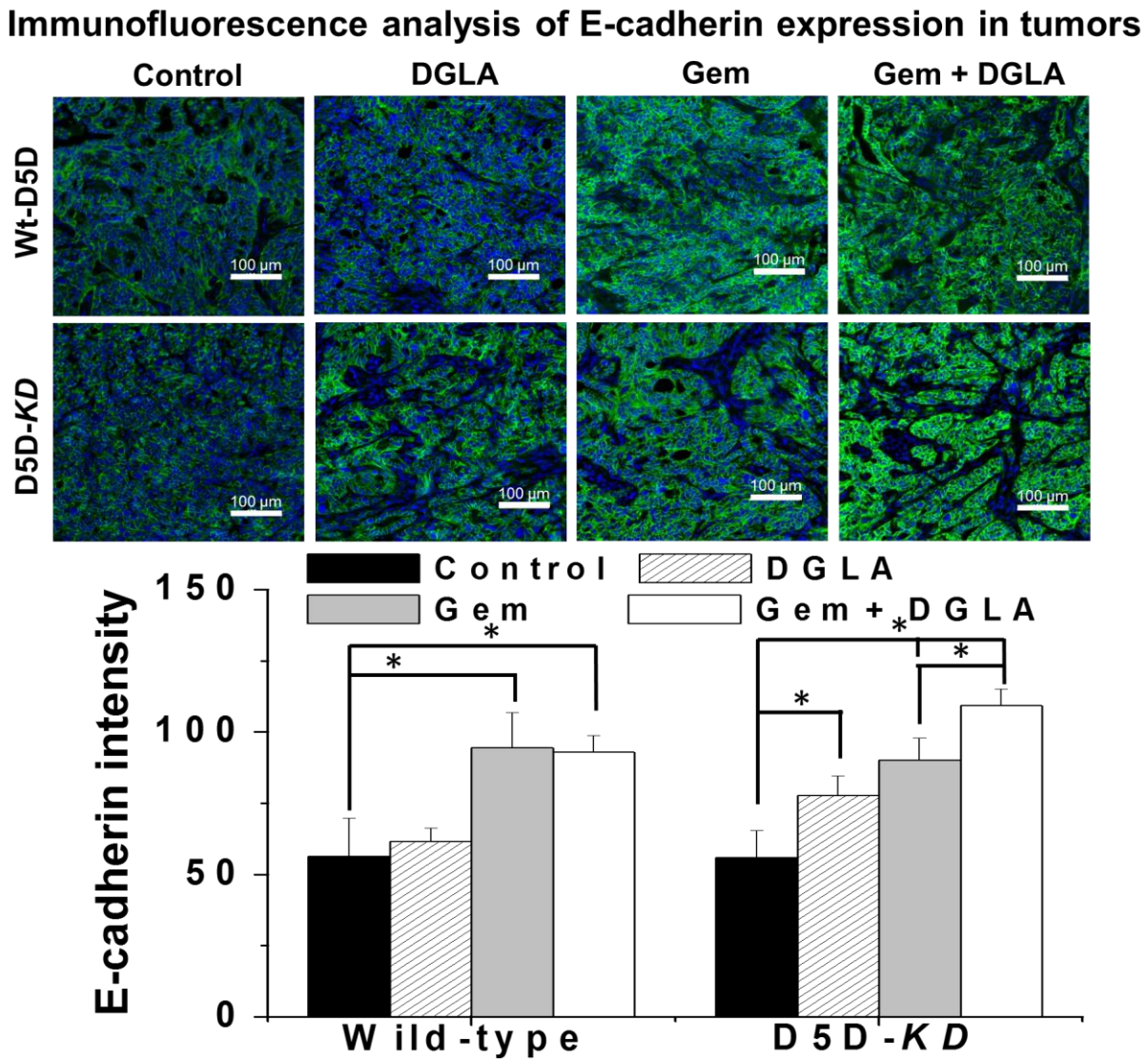

Fig 34. D5D-*KD* and DGLA treatment upregulated E-cadherin expression.
Immunofluorescence analysis of E-cadherin expression (green color) in tumors from wild-type and D5D-*KD* groups treated with vehicle (control), DGLA (8 mg/mouse), gemcitabine (30 mg/kg) or gemcitabine + DGLA. The green area indicates the expression of E-cadherin. (*: significant difference with $p < 0.05$ from $n = 6$).

5.3. Discussion

In chapter 3 and chapter 4, we have shown that direct treatment of 8-HOA as well as formation of endogenous 8-HOA from D5D-*KD* and COX-catalyzed DGLA peroxidation could not only inhibit cancer cell growth and metastasis in pancreatic cancer cells, but also enhance the efficacy of chemotherapy drugs e.g. gemcitabine. In this chapter, we further investigated whether

the strategy of D5D-*KD* and DGLA treatment can also inhibit pancreatic tumor growth and metastasis in mice models.

We detected the levels of 8-HOA in tumors from wt-D5D and D5D-*KD* groups supplemented with DGLA using GC/MS. In *in vitro* studies, a threshold level of endogenous 8-HOA (> 0.5 μM) was determined for inhibiting pancreatic cancer cells growth and metastasis. Similarly, a threshold level of 8-HOA (> 0.25 μg/g) was also found essential to exert anti-cancer effect on pancreatic tumors (Fig 28). The decreased levels of PGE2 as well as the increased levels of 8-HOA in D5D-*KD* tumors (Fig 25 and Fig 28) suggested that knockdown of D5D could not only promote the formation of 8-HOA, but also limit the generation of deleterious metabolites from AA.

Mutated p53 is found in majority of pancreatic cancer patients and it is urgent to identify a strategy that can inhibit growth of cancer cells with mutated p53 [157]. We thus tested whether D5D-*KD* and DGLA treatment can induce pancreatic tumor cell apoptosis *via* p53-independent manner. The results demonstrated that our strategy can enhance the efficacy of gemcitabine to control pancreatic cancer cell growth by further promoting gemcitabine-induced cell apoptosis through a p53-independent pathway (Fig 32), which is consistent with our *in vitro* studies.

In general, cancer patients have a much higher expression level of COX-2 than the noncancerous population, and COX-2 can be readily induced by various agents, such as growth factors and tumor promoters. Thus, the prostaglandins from AA may continue to form at deleterious levels despite using COX inhibitors in cancer patients. D5D-*KD* not only prevents the buildup of AA to limit prostaglandin formation, but also promotes DGLA to generate 8-HOA, which suppresses cancer growth and metastasis. Therefore, the higher expression of COX-2 in cancer is actually a benefit in our strategy rather than a problem.

Our strategy can be used to inhibit growth and metastasis of tumor cells possessing high COX-2 expression as well as those with low or deficient COX-2 expression. For tumors with high COX-2 expression, 8-HOA formed from D5D-*KD* and DGLA can inhibit cancer growth and metastasis in an autocrine manner. For tumors cells with low or deficient COX-2 expression, 8-HOA can be continuously produced from most nearby tumor cells and stromal cells that overexpress COX-2, and suppress cancer growth and metastasis in a paracrine manner. Our theory is supported by several studies showing that increased level of COX-2 can be found in the cancer associated fibroblasts that make up the bulk of cancer stroma [174-175].

For the first time, we have demonstrated that high COX-2 expression could be taken advantage to promote formation of 8-HOA from DGLA peroxidation *via* D5D-*KD* for the inhibition of pancreatic tumors growth and metastasis, as well as to improve the efficacy of chemotherapy. The outcome of our work will reinforce our translational efforts to develop a novel ω-6 based dietary anti-cancer strategy in combination with modified COX-2-catalyzed DGLA peroxidation and D5D-mediated ω-6 conversion, and therefore improving the efficacies of chemotherapy.

6. SUMMARY, CONCLUSION AND FUTURE DIRECTION

6.1. Summary of research data

6.1.1. Summary of chapter 3: DGLA's exclusive byproduct 8-HOA inhibited pancreatic cancer cell growth and migration

In chapter 3, we assessed the potential effect and molecular mechanism of DGLA's exclusive byproducts using pancreatic cancer cell line BxPC-3. Results showed that among all of the tested DGLA's byproducts, 48 h treatment with 8-HOA (1.0 μM-10 μM, physiological relevant concentration), can significantly inhibit the viability and colony formation of BxPC-3 cells. Other DGLA byproducts from COX-2 peroxidation, including HEX, HTA and PGE1, did not suppress cancer cell viability in BxPC-3 cells in the same concentration range. In addition, it was also found that 8-HOA (1.0 μM, 48 h) can induce BxPC-3 cell apoptosis. As 8-HOA shared similar structure with some short chain fatty acids serving as HDAC inhibitors, we tested 8-HOA's effect on HDAC. Results showed that 8-HOA can inhibit the activity of HDAC and cause DNA damage, resulting in activation of pro-apoptotic proteins procaspase-9 and procaspase-3, which are responsible for the cell growth inhibition and cell apoptosis induction in BxPC-3 cells. In addition, we also tested 8-HOA's effect on cancer cell migration and found that 8-HOA can suppress cancer cell migration in BxPC-3 cells by downregulating MMP-2 and MMP-9.

6.1.2. Summary of chapter 4: D5D-*KD* and DGLA treatment inhibit pancreatic cancer cell migration and invasion

In chapter 4, D5D expression was knocked down in BxPC-3 cells by transfecting the cells with D5D targeted siRNA. The results from GC/MS demonstrated that a threshold range of endogenous 8-HOA above 0.5 μM is essential for exerting DGLA's anti-cancer activities. We

then investigated whether this strategy (i.e. DGLA treatment and D5D-*KD*) can inhibit pancreatic cancer cell growth and migration as we observed from direct 8-HOA treatment in chapter 3. Results showed that DGLA treatment (100 μM) significantly inhibited the growth and migration, and induced cell apoptosis in D5D-*KD* BxPC-3 cells as the formation of 8-HOA reached the threshold level (0.5 μM). No inhibitory effect was observed from DGLA treatment on the negative control siRNA transfected cells because 8-HOA cannot accumulate in negative control cells.

The strategy of D5D-*KD* along with DGLA treatment could also sensitize BxPC-3 cells to various chemotherapy drugs such as gemcitabine, likely *via* p53-independent pathway through downregulating of anti-apoptotic proteins (e.g., Bcl-2) and activating pro-apoptotic proteins (e.g., procaspase 3, -9). In addition, D5D-*KD* and DGLA treatment can also inhibit BxPC-3 cells' migration and invasion as promoted formation of 8-HOA can act as an HDAC inhibitor to downregulate cancer metastasis promotors, e.g., MMP-2, MMP-9, vimentin and snail as well as upregulate cancer metastasis suppressor, e.g. E-cadherin

6.1.3. Summary of chapter 5: D5D-*KD* and DGLA treatment inhibit pancreatic tumor growth and metastasis

In chapter 5, we further extended our strategy to *in vivo* studies by testing the effect of formation of 8-HOA from D5D-*KD* and DGLA treatment in a mouse xenograft tumor model. We found that DGLA supplementation can significantly suppress tumor growth compared to that in the control group for mice bearing D5D-*KD* tumors, while in wt-D5D tumors, no significant difference in tumor volume was observed between control and DGLA supplementation groups.

In D5D-*KD* tumors with DGLA supplementation, we detected that formation of 8-HOA can reach the threshold level (0.25 μg/g), which in turn inhibit tumor growth, while in wt-D5D tumors, the production of 8-HOA is insufficient to suppress tumor growth.

DGLA supplementation can enhance the efficacy of gemcitabine by further inhibiting tumor volume in D5D-*KD* tumors compared to treatment of gemcitabine alone, while in wt-D5D tumors, supplementation of DGLA did not further inhibit tumor growth.

Supplementation of DGLA significantly decreased Ki-67 positive cells and induced apoptosis in in D5D-*KD* tumors. The molecular mechanism of the observations is that 8-HOA can act as a HDAC inhibitor to cause DNA damage, resulting in downregulation of anti-apoptotic protein and activation of pro-apoptotic proteins.

In addition, we also tested the effect of D5D-*KD* and DGLA treatment on expression of proteins involved in tumor metastasis. Consistent with the *in vitro* studies, we observed that there is a decreased expression of MMP-2 and an increased expression of E-cadherin in D5D-*KD* tumors with DGLA supplementation, suggesting improved formation of 8-HOA from DGLA and D5D-*KD* can also inhibit tumor metastasis potential.

6.2. Conclusion

COX-2 is overexpressed in 70% of pancreatic cancer patients, and it can promote pancreatic cancer development and progression by catalyzing AA peroxidation to generate deleterious metabolite PGE2. Therefore, COX-2 inhibition, which aims at limiting generation of PGE2, has been extensively studied as a complementary strategy for pancreatic cancer treatment. However, COX-2 inhibitors are not very effective on patients as COX-2 can be stimulated by a variety of factors, including pathological conditions, stresses and pro-inflammatory signals. In addition, COX-2 inhibitors also suffer from severe side-effects such as increased risk of

gastrointestinal tract injury and cardiovascular diseases in patients. Therefore, it is urgent to develop alternative strategies for targeting commonly high COX-2 levels in cancer to improve chemotherapy efficacy.

For the first time, our research showed that, through COX-2 catalyzed lipid peroxidation, DGLA can form a distinct byproduct 8-HOA which serves as an HDAC inhibitor to inhibit pancreatic cancer growth and migration. Based on this novel finding, we proposed and demonstrated that instead of COX-2 inhibition, we consider high COX-2 expression as a benefit and take advantage the high COX-2 expression to promote formation of 8-HOA to control cancer cell growth and migration.

D5D has not been investigated specifically in cancer treatment. For the first time, our studies demonstrated that D5D-*KD* is an effective strategy to promote 8-HOA formation from COX-catalyzed DGLA peroxidation to inhibit cancer cell and tumor growth. Compared to classic COX inhibition strategy in cancer treatment, our novel D5D-*KD* strategy will result in dual inhibitory effects on cancer by not only limiting PGE2 (cancer promoter) formation from arachidonic acid (the common objective as COX inhibitor), but also improving formation of 8-HOA *via* capitalizing on the high COX-2 expression in cancers and the abundance of ω-6s in the daily diet. Thus, D5D represents a novel drug target for cancer treatment and investigation on D5D inhibition will be a promising direction for cancer research.

Our strategy could also be expected to kill low or deficient COX-2 cancer cells in a paracrine-like manner as they surrounded by many other cancer cells (overexpressing COX-2) that can continuously produce sufficient 8-HOA. Our theory is supported by several studies showing that increased levels of COX-2 can be found in the cancer associated fibroblasts that make up the bulk of cancer stroma [174-175].

In sum, my research has led to the following (1) establishment of a new dogma of COX-2 biology in cancer treatment by taking advantage of overexpression of COX-2 in cancer; (2) improvement of DGLA's anti-cancer effects by promoting 8-HOA formation *via* D5D-*KD*; (3) enhancement of chemotherapy drugs' efficacy for pancreatic cancer treatment. Our research strategy will lead to a better therapeutic outcome with less side effect for cancer treatment and a novel ω-6s-based diet care strategy for treating cancer as cancer cells have higher COX-2 expression, fatty acid intake, and HDAC expression compared to normal cells.

6.3. Future direction

6.3.1. Assessment of the effect of our strategy on gene levels in cancer cells and tumors *via* RT-PCR

RT-PCR is a common technique to test the alternation of levels of gene expression in cancer cells and tumors. Studies have shown that HDAC inhibitors relax the structure of chromatin, allowing transcriptional activators or repressors to bind with DNA and alter the levels of gene expression involved in cancer growth and metastasis [152-154]. In order to illustrate the mechanism of 8-HOA inhibiting cancer cell growth and migration, we will use RT-PCR to test the effects of our strategy (i.e. D5D-*KD* and DGLA treatment) on the gene expression for key genes that play an important role in cancer growth and metastasis.

6.3.2. Study of the effect of our strategy on pancreatic cancer associated fibroblasts and tumor hypoxia

Cancer associated fibroblasts make up the majority of stroma which infiltrates and enwraps the cancer cells and promote tumor growth as well as metastasis. Although some pancreatic cancer cells are deficient in COX-2, they can still take advantage of prostaglandins formed from stromal cells with high levels of COX-2 to promote their own proliferation [176-

177]. However, in our study, high COX-2 expression in pancreatic cancer associated fibroblasts will not be seen as a problem but a solution to pancreatic cancer cells lacking COX-2. High COX-2 in cancer associated fibroblasts can be used to promote formation of 8-HOA which can inhibit pancreatic cancer growth and metastasis in a paracrine-like manner. We propose that our strategy can also work on pancreatic cancer cells that lack COX-2 as the pancreatic cancer associated fibroblasts possess high COX-2 expression.

Tumor hypoxia is caused by insufficient oxygen supply to tumor cells as sometime tumor cells grow rapidly, leaving parts of the tumors in the region with less oxygen concentration [178]. Tumor hypoxia is closely associated with increased metastasis potential and resistance to therapy [178]. Studies have shown that hypoxia can induce the expression of COX-2 in tumors *via* hypoxia-inducible factor-1α binding a hypoxia-responsive element on the COX-2 promoter [179-180]. In our study, we can exploit the induction of COX-2 in hypoxic cancer cells and tumors to promote the formation of 8-HOA (cancer inhibitor) from COX-2-catalyzed DGLA peroxidation. We propose that our strategy can also be used on cancer cells and tumors undergoing hypoxia.

6.3.3. Investigation of the effect of our strategy on inhibition of pancreatic tumor growth and metastasis in orthotopic mouse model

Human xenograft mouse models are mainly categorized into: heterotopic and orthotopic based on the locations of transferred cancer cells or tumors. Although the subcutaneous mouse model requires less techniques to operate and is of lower cost, its ability to reveal the real effect of therapeutic regiments on human patients is limited. The orthotopic pancreatic tumor model is more preferred for pancreatic cancer study as cancer cells or tumors can be transplanted into the pancreas from which the cancer originated so that the tumors can simulate the actual pancreatic

tumors in clinical patients [181-183]. The orthotopic xenograft models have similar tumor microenvironment as the original pancreatic tumor and are therefore considered to be more associated with the natural tumorigenesis in humans. In addition, the orthotopic model is fitting to study pancreatic cancer metastasis as metastatic cancer cells develop spontaneously from the primary tumor, and progressively spread to other organs including lymph nodes, liver and lung [184]. We will establish orthotopic models by injecting pancreatic cancer cells into the pancreas of the mice to determine the effect of D5D-*KD* and DGLA supplementation on pancreatic tumor growth and metastasis as well as tumor microenvironment.

We selected female mice in our subcutaneous tumor xenografts study is due to their less aggressive nature. Although there is no indication that gender has a significant impact on pancreatic cancer development or progression, in order to achieve a more comprehensive and convincing outcome, we will use both male and female mice in future animal studies.

6.3.4. Study of delivery of D5D siRNA to cancer cells and tumors using RNA nanoparticle

RNA nanoparticles have arisen recently as a new platform for targeted drug, siRNA, miRNA, anti-miRNA and immunomodulator delivery for cancer therapy. The RNA nanoparticles can specifically target cancer with little to no accumulation in healthy tissues, highlighting the benefits of translating RNA nanoparticles for cancer therapy with enhanced targeting efficiency and reduced side effects [185-187]. In addition, the modular design of RNA nanoparticles with different shape, size, stoichiometry, targeting ligand, and functionalities with their flexibility, versatility, and ample design space provides opportunities for future optimization [188-189]. We are now can working on construction of stable RNA nanoparticles harboring D5D siRNA to allow specific delivery of D5D siRNA to cancer cells or tumors which

could be a more practical approach to downregulate D5D. We will deliver nanoparticles containing D5D siRNA to downregulate D5D in pancreatic cancer cells and tumors.

REFERENCES

1. Ibarguren M, López DJ, Escribá PV. The effect of natural and synthetic fatty acids on membrane structure, microdomain organization, cellular functions and human health. *Biochim Biophys Acta*. 2014, **1838:** 1518-1528.
2. Calder PC. Functional Roles of Fatty Acids and Their Effects on Human Health. *JPEN J Parenter Enteral Nutr*. 2015, **39:** 18S-32S.
3. Lapshina EA, Zavodnik IB, Bryszewska M. Effect of free fatty acids on the structure and properties of erythrocyte membrane. *Scand. J. Clin. Lab. Invest*. 1995, **55:** 391-397.
4. Calder, P. C. Polyunsaturated fatty acids and inflammation. *Biochem Soc Trans*. 2005, **33:** 423-7.
5. Schmitz, G, Ecker, J. The opposing effects of n-3 and n-6 fatty acids. *Prog Lipid Res*. 2008, **47:** 147-55.
6. Calder PC, Grimble RF. Polyunsaturated fatty acids, inflammation and immunity. *Eur J Clin Nutr*. 2002, **56:** S14-9.
7. Das, U. N. Essential Fatty acids - a review. *Curr Pharm Biotechnol*. 2006, **7:** 467-482.
8. Das, U. N. Biological significance of essential fatty acids. *J Assoc Physicians India*. 2006, **54:** 309-19.
9. Das, U. N. Essential fatty acids: biochemistry, physiology and pathology. *Biotechnol J*. 2006, **1:** 420-39.
10. Bézard J, Blond JP, Bernard A, Clouet P. The metabolism and availability of essential fatty acids in animal and human tissues. *Reprod Nutr Dev*. 1994, **34:** 539-68.
11. Sprecher H, Metabolism of highly unsaturated n-3 and n-6 fatty acids. *Biochim. Biophys. Acta*. 2000, **1486:** 219-231.

12. Melin T, Nilsson A. Delta-6-desaturase and delta-5-desaturase in human Hep G2 cells are both fatty acid interconversion rate limiting and are unregulated under essential fatty acid deficient conditions. *Prostag Leukotr Ess*. 1997, **56:** 437-442.
13. Calder PC. Mechanisms of action of (n-3) fatty acids. *J Nutr*. 2012, **142:** 592S-599S.
14. Sargent, J. R. Fish oils and human diet. *Br J Nutr*. 1997, **78 Suppl 1:** S5-13.
15. Gebauer SK, Psota TL, Harris WS, Kris-Etherton PM. n-3 fatty acid dietary recommendations and food sources to achieve essentiality and cardiovascular benefits. *Am J Clin Nutr*. 2006, **83:** 1526S-1535S.
16. Robinson, JG, Ijioma N, Harris W. Omega-3 fatty acids and cognitive function in women. *Womens Health (Lond)*. 2010, **6:** 119-134.
17. Calder PC, Yaqoob P. Omega-3 polyunsaturated fatty acids and human health outcomes. *Biofactors*. 2009, **35:** 266-272.
18. Simopoulos, A. P. Omega-3 fatty acids in inflammation and autoimmune diseases. *J Am Coll Nutr*. 2002, **21:** 495-505.
19. Kelly, F. J. The metabolic role of n-3 polyunsaturated fatty acids: relationship to human disease. *Comp Biochem Physiol A Comp Physiol*. 1991, **98:** 581-5.
20. Swanson D, Block R, Mousa SA. Omega-3 fatty acids EPA and DHA: health benefits throughout life. *Adv Nutr*. 2012, **3:** 1-7.
21. Walz CP, Barry AR, Koshman SL. Omega-3 polyunsaturated fatty acid supplementation in the prevention of cardiovascular disease. *Can Pharm J (Ott)*. 2016, **149:** 166-73.
22. Werner K, Küllenberg de Gaudry D, Taylor LA, Keck T, Unger C, Hopt UT, Massing U. Dietary supplementation with n-3-fatty acids in patients with pancreatic cancer and

cachexia: marine phospholipids versus fish oil - a randomized controlled double-blind trial. *Lipids Health Dis*. 2017, **16:** 104.

23. Swamy MV, Citineni B, Patlolla JM, Mohammed A, Zhang Y, Rao CV. Prevention and treatment of pancreatic cancer by curcumin in combination with omega-3 fatty acids. *Nutr Cancer*. 2008, **60 Suppl 1:** 81-9.
24. Larsson SC, Kumlin M, Ingelman-Sundberg M, Wolk A. Dietary long-chain n-3 fatty acids for the prevention of cancer: a review of potential mechanisms. *Am J Clin Nutr*. 2004, **79:** 935-45.
25. Berquin IM, Edwards IJ, Chen YQ. Multi-targeted therapy of cancer by omega-3 fatty acids. *Cancer Lett*. 2008, **269:** 363-77.
26. Woutersen RA, Appel MJ, van Garderen-Hoetmer A, Wijnands MV. Dietary fat and carcinogenesis. *Mutat Res*. 1999, **443:** 111-27.
27. Eltweri AM, Thomas AL, Metcalfe M, Calder PC, Dennison AR, Bowrey DJ. Potential applications of fish oils rich in omega-3 polyunsaturated fatty acids in the management of gastrointestinal cancer. *Clin Nutr*. 2017, **36:** 65-78.
28. Park KS, Lim JW, Kim H. Inhibitory mechanism of omega-3 fatty acids in pancreatic inflammation and apoptosis. *Ann N Y Acad Sci*. 2009, **1171:** 421-7.
29. Shirota T, Haji S, Yamasaki M, Iwasaki T, Hidaka T, Takeyama Y, Shiozaki H, Ohyanagi H. Apoptosis in human pancreatic cancer cells induced by eicosapentaenoic acid. *Nutrition*. 2005, **21:** 1010-7.
30. Merendino N, Loppi B, D'Aquino M, Molinari R, Pessina G, Romano C, Velotti F. Docosahexaenoic acid induces apoptosis in the human PaCa-44 pancreatic cancer cell line

by active reduced glutathione extrusion and lipid peroxidation. *Nutr Cancer*. 2005; **52:** 225-33.

31. D'Eliseo D, Manzi L, Merendino N, Velotti F. Docosahexaenoic acid inhibits invasion of human RT112 urinary bladder and PT45 pancreatic carcinoma cells via down-modulation of granzyme B expression. *J Nutr Biochem*. 2012, **23:** 452-7.
32. Merendino N, Molinari R, Loppi B, Pessina G, D' Aquino M, Tomassi G, Velotti F. Induction of apoptosis in human pancreatic cancer cells by docosahexaenoic acid. *Ann N Y Acad Sci*. 2003, **1010:** 361-4.
33. Fukui M, Kang KS, Okada K, Zhu BT. EPA, an omega-3 fatty acid, induces apoptosis in human pancreatic cancer cells: role of ROS accumulation, caspase-8 activation, and autophagy induction. *J Cell Biochem*. 2013, **114:** 192-203.
34. Haqq J, Howells LM, Garcea G, Dennison AR. Targeting pancreatic cancer using a combination of gemcitabine with the omega-3 polyunsaturated fatty acid emulsion, Lipidem™. *Mol Nutr Food Res*. 2016, **60:** 1437-47.
35. Hering J, Garrean S, Dekoj TR, Razzak A, Saied A, Trevino J, Babcock TA, Espat NJ. Inhibition of proliferation by omega-3 fatty acids in chemoresistant pancreatic cancer cells. *Annals of Surgical Oncology*. 2007, **14:** 3620–3628.
36. Song KS, Jing K, Kim JS, Yun EJ, Shin S, Seo KS, Park JH, Heo JY, Kang JX, Suh KS, Wu T, Park JI, Kweon GR, Yoon WH, Hwang BD, Lim K. Omega-3-polyunsaturated fatty acids suppress pancreatic cancer cell growth in vitro and in vivo via downregulation of Wnt/Beta-catenin signaling. *Pancreatology*. 2011, **11:** 574-84.
37. Mohammed A, Janakiram NB, Brewer M, Duff A, Lightfoot S, Brush RS, Anderson RE, Rao CV. Endogenous n-3 polyunsaturated fatty acids delay progression of pancreatic ductal

adenocarcinoma in Fat-1-p48 (Cre/+)-LSL-Kras (G12D/+) mice. *Neoplasia*. 2012, **14:** 1249-59.

38. Kris-Etherton PM, Taylor DS, Yu-Poth S, Huth P, Moriarty K, Fishell V, Hargrove RL, Zhao G, Etherton TD. Polyunsaturated fatty acids in the food chain in the United States. Am *J Clin Nutr*. 2000, **71:** 179S-88S.
39. Blasbalg TL, Hibbeln JR, Ramsden CE, Majchrzak SF, Rawlings RR. Changes in consumption of omega-3 and omega-6 fatty acids in the United States during the 20th century. *Am J Clin Nutr*. 2011, **93:** 950-62.
40. Hibbeln JR, Nieminen LR, Blasbalg TL, Riggs JA, Lands WE. Healthy intakes of n-3 and n-6 fatty acids: Estimations considering worldwide diversity. Am J Clin Nutr. 2006, **83:** 1483S-1493S.
41. Simopoulos AP, Leaf A, Salem N Jr. Essentiality of and recommended dietary intakes for omega-6 and omega-3 fatty acids. Ann Nutr Metab. 1999;43(2):127-30.
42. Simopoulos AP, Leaf A, Salem N Jr. Workshop on the essentiality of and recommended dietary intakes for omega-6 and omega-3 fatty acids. *J Am Coll Nutr*. 1999, **18:** 487-9.
43. Simopoulos, AP. Evolutionary aspects of diet, the omega-6/omega-3 ratio and genetic variation: nutritional implications for chronic diseases. *Biomed Pharmacother*. 2006, **60:** 502-7.
44. Lewis JD, Abreu MT. Diet as a trigger or therapy for inflammatory bowel diseases. *Gastroenterology*. 2017, **152:** 398-414.
45. Simopoulos AP. An increase in the omega-6/omega-3 fatty acid ratio increases the risk for obesity. *Nutrients*. 2016, **8:** 128.

46. Blasbalg TL, Hibbeln JR, Ramsden CE, Majchrzak SF, Rawlings RR. Changes in consumption of omega-3 and omega-6 fatty acids in the United States during the 20th century. *Am J Clin Nutr*. 2011, **93:** 950-62.
47. de Lorgeril M, Salen P. New insights into the health effects of dietary saturated and omega-6 and omega-3 polyunsaturated fatty acids. *BMC Med*. 2012, **10:** 50.
48. Simopoulos AP. The importance of the ratio of omega-6/omega-3 essential fatty acids. *Biomed Pharmacother*. 2002, **56:** 365-79.
49. Freitas HR, Isaac AR, Malcher-Lopes R, Diaz BL, Trevenzoli IH, De Melo Reis RA. Polyunsaturated fatty acids and endocannabinoids in health and disease. *Nutr Neurosci*. 2017, **7:** 1-20.
50. Buczynski MW, Dumlao DS, Dennis EA. thematic review series: proteomics. an integrated omics analysis of eicosanoid biology. *J Lipid Res*. 2009, **50:** 1015-38.
51. Fantone JC, Marasco WA, Elgas LJ, Ward PA. Anti-inflammatory effects of prostaglandin E1: in vivo modulation of the formyl peptide chemotactic receptor on the rat neutrophil. *J Immunol*. 1983, **130:** 1495-1497.
52. Ellis LM, Copeland EM, Bland KI, Sitren HS. Inhibition of tumor growth and metastasis by chronic intravenous infusion of prostaglandin E1. *Annals of Surgery*. 1990, **212:** 45-50.
53. Ikeguchi M, Maeta M, Kaibara N. Cisplatin combined with prostaglandin E1 chemotherapy in rat peritoneal carcinomatosis. *Int J Cancer*. 2000, **88:** 474-478.
54. Kornberg A, Witt U, Kornberg J, Friess H, Thrum K. Treating ischaemia-reperfusion injury with prostaglandin E1 reduces the risk of early hepatocellular carcinoma recurrence following liver transplantation. *Aliment Pharmacol Ther*. 2015, **42:** 1101-1110.

55. Vigor C, Bertrand-Michel J, Pinot E, Oger C, Vercauteren J, Le Faouder P, Galano JM, Lee JC, Durand T. Non-enzymatic lipid oxidation products in biological systems: assessment of the metabolites from polyunsaturated fatty acids. *J Chromatogr B Analyt Technol Biomed Life Sci*. 2014, **964:** 65-78.
56. Valérie Bultel-Poncé, Thierry Durand, Alexandre Guy, Camille Oger and Jean-Marie Galano. Non enzymatic metabolites of polyunsaturated fatty acids: friend or foe. *Oilseeds& fats Crops and Lipids*. 2016, **23:** D118.
57. Rouzer CA, Marnett LJ. Endocannabinoid oxygenation by cyclooxygenases, lipoxygenases, and cytochromes P450: cross-talk between the eicosanoid and endocannabinoid signaling pathways. *Chem Rev*. 2011, **111:** 5899-921.
58. Smith WL, Song I. The enzymology of prostaglandin endoperoxide H synthases-1 and -2. *Prostaglandins Other Lipid Mediat*. 2002, **68-69:** 115-28.
59. Kim JB, Han AR, Park EY, Kim JY, Cho W, Lee J, Seo EK, Lee KT. Inhibition of LPS-induced iNOS, COX-2 and cytokines expression by poncirin through the NF-kappaB inactivation in RAW 264.7 macrophage cells. *Biol Pharm Bull.* 2007, **30:** 2345-2351.
60. Eliopoulos AG, Dumitru CD, Wang CC, Cho J, Tsichlis PN. Induction of COX-2 by LPS in macrophages is regulated by Tpl2-dependent CREB activation signals. *EMBO J.* 2002, **21:** 4831-4840.
61. Mitchell JA, Belvisi MG, Akarasereenont P, Robbins RA, Kwon OJ, Croxtall J, Barnes PJ, Vane JR. Induction of cyclo-oxygenase-2 by cytokines in human pulmonary epithelial cells: regulation by dexamethasone. *Br J Pharmacol.* 1994, **113:** 1008-1014.

62. Akarasereenont P, Bakhle YS, Thiemermann C, Vane JR. Cytokine-mediated induction of cyclo-oxygenase-2 by activation of tyrosine kinase in bovine endothelial cells stimulated by bacterial lipopolysaccharide. *Br J Pharmacol.* 1995, **115:** 401-408.
63. Yip-Schneider MT, Barnard DS, Billings SD, Cheng L, Heilman DK, Lin A, Marshall SJ, Crowell PL, Marshall MS, Sweeney CJ. Cyclooxygenase-2 expression in human pancreatic adenocarcinomas. *Carcinogenesis*. 2000, **21:** 139-46.
64. Hasan S, Satake M, Dawson DW, Funahashi H, Angst E, Go VL, Reber HA, Hines OJ, Eibl G. Expression analysis of the prostaglandin E2 production pathway in human pancreatic cancers. *Pancreas*. 2008, **37:** 121-7.
65. Takahashi H, Li A, Dawson DW, Hines OJ, Reber HA, Eibl G. Cyclooxygenase-2 confers growth advantage to syngeneic pancreatic cancer cells. *Pancreas*. 2011, **40:** 453-9.
66. Schuller HM. Regulatory role of G protein-coupled receptors in pancreatic cancer development and progression. *Curr Med Chem*. 2017 Mar 3.
67. Ito H, Duxbury M, Benoit E, Clancy TE, Zinner MJ, Ashley SW, Whang EE. Prostaglandin E2 enhances pancreatic cancer invasiveness through an Ets-1-dependent induction of matrix metalloproteinase-2. *Cancer Res*. 2004, **64:** 7439-46.
68. Bu X, Zhao C, Dai X. Involvement of COX-2/PGE (2) Pathway in the Upregulation of MMP-9 Expression in Pancreatic Cancer. *Gastroenterol Res Pract*. 2011, **2011:** 214269.
69. Eibl G, Bruemmer D, Okada Y, Duffy JP, Law RE, Reber HA, Hines OJ. PGE (2) is generated by specific COX-2 activity and increases VEGF production in COX-2-expressing human pancreatic cancer cells. *Biochem Biophys Res Commun*. 2003, **306:** 887-97.
70. Wang D, DuBois RN. Cyclooxygenase 2-derived prostaglandin E2 regulates the angiogenic switch. *Proc Natl Acad Sci U S A*. 2004, **101:** 415-6.

71. Charo C, Holla V, Arumugam T, Hwang R, Yang P, Dubois RN, Menter DG, Logsdon CD, Ramachandran V. Prostaglandin E2 regulates pancreatic stellate cell activity via the EP4 receptor. *Pancreas*. 2013, **42:** 467-74.

72. Pomianowska E, Sandnes D, Grzyb K, Schjølberg AR, Aasrum M, Tveteraas IH, Tjomsland V, Christoffersen T, Gladhaug IP. Inhibitory effects of prostaglandin E2 on collagen synthesis and cell proliferation in human stellate cells from pancreatic head adenocarcinoma. *BMC Cancer*. 2014, **14:** 413.

73. Pinho AV, Chantrill L, Rooman I. Chronic pancreatitis: a path to pancreatic cancer. *Cancer Lett*. 2014, **345:** 203-9.

74. Yadav D, Lowenfels AB. The epidemiology of pancreatitis and pancreatic cancer. *Gastroenterology*. 2013, **144:** 1252-61.

75. Hausmann S, Kong B, Michalski C, Erkan M, Friess H. The role of inflammation in pancreatic cancer. *Adv Exp Med Biol*. 2014, **816:** 129-51.

76. Abu Dayyeh BK, Conwell D, Buttar NS, Kadilaya V, Hart PA, Baumann NA, Bick BL, Chari ST, Chowdhary S, Clain JE, Gleeson FC, Lee LS, Levy MJ, Pearson RK, Petersen BT, Rajan E, Steen H, Suleiman S, Banks PA, Vege SS, Topazian M. Pancreatic juice prostaglandin e2 concentrations are elevated in chronic pancreatitis and improve detection of early disease. *Clin Transl Gastroenterol*. 2015,**6:** e72.

77. Raimondi S, Lowenfels AB, Morselli-Labate AM, Maisonneuve P, Pezzilli R. Pancreatic cancer in chronic pancreatitis; aetiology, incidence, and early detection. *Best Pract Res Clin Gastroenterol*. 2010, **24:** 349-58.

78. Kirane A, Toombs JE, Ostapoff K, Carbon JG, Zaknoen S, Braunfeld J, Schwarz RE, Burrows FJ, Brekken RA. Apricoxib, a novel inhibitor of COX-2, markedly improves

standard therapy response in molecularly defined models of pancreatic cancer. *Clin Cancer Res*. 2012, **18:** 5031-42.

79. Yip-Schneider MT, Wu H, Hruban RH, Lowy AM, Crooks PA, Schmidt CM. Efficacy of dimethylaminoparthenolide and sulindac in combination with gemcitabine in a genetically engineered mouse model of pancreatic cancer. *Pancreas*. 2013, **42:** 160-7.
80. Rosendahl AH, Gundewar C, Said K, Karnevi E, Andersson R. Celecoxib synergizes human pancreatic ductal adenocarcinoma cells to sorafenib-induced growth inhibition. *Pancreatology*. 2012, **12:** 219-26.
81. Al-Wadei HA, Al-Wadei MH, Ullah MF, Schuller HM. Celecoxib and GABA cooperatively prevent the progression of pancreatic cancer in vitro and in xenograft models of stress-free and stress-exposed mice. *PLoS One*. 2012; **7:** e43376.
82. Lipton A, Campbell-Baird C, Witters L, Harvey H, Ali S. Phase II trial of gemcitabine, irinotecan, and celecoxib in patients with advanced pancreatic cancer. *J Clin Gastroenterol*. 2010, **44:** 286-8.
83. Ding N, Cui XX, Gao Z, Huang H, Wei X, Du Z, Lin Y, Shih WJ, Rabson AB, Conney AH, Hu C, Zheng X. A triple combination of atorvastatin, celecoxib and tipifarnib strongly inhibits pancreatic cancer cells and xenograft pancreatic tumors. *Int J Oncol*. 2014, **44:** 2139-45.
84. Molina MA, Sitja-Arnau M, Lemoine MG, Frazier ML, Sinicrope FA. Increased cyclooxygenase-2 expression in human pancreatic carcinomas and cell lines: growth inhibition by nonsteroidal anti-inflammatory drugs. *Cancer Res*. 1999, **59:** 4356-62.

85. Yip-Schneider MT, Wu H, Hruban RH, Lowy AM, Crooks PA, Schmidt CM. Efficacy of dimethylaminoparthenolide and sulindac in combination with gemcitabine in a genetically engineered mouse model of pancreatic cancer. *Pancreas*. 2013, **42:** 160-7.
86. Rao PN, Grover RK. Apricoxib, a COX-2 inhibitor for the potential treatment of pain and cancer. *IDrugs*. 2009, **12:** 711-22.
87. Zhou YY, Hu ZG, Zeng FJ, Han J. Clinical profile of cyclooxygenase-2 cnhibitors in treating non-small cell lung cancer: a meta-analysis of nine randomized clinical trials. *PLoS One*. 2016, **11:** e0151939.
88. Edelman MJ, Wang X, Hodgson L, Cheney RT, Baggstrom MQ, Thomas SP, Gajra A, Bertino E, Reckamp KL, Molina J, Schiller JH, Mitchell-Richards K, Friedman PN, Ritter J, Milne G, Hahn OM, Stinchcombe TE, Vokes EE; Alliance for Clinical Trials in Oncology. Phase iii randomized, placebo-controlled, double-blind trial of celecoxib in addition to standard chemotherapy for advanced non-small-cell lung cancer with cyclooxygenase-2 overexpression: CALGB 30801 (Alliance). *J Clin Oncol*. 2017, **35:** 2184-2192.
89. Hawkey CJ, Langman MJS. Non-steroidal anti-inflammatory drugs: overall risks and management. Complementary roles for COX-2 inhibitors and proton pump inhibitors. *Gut*. 2003; **52:** 600-608.
90. Greenberg JD, Fisher MC, Kremer J, Chang H, Rosenstein ED, Kishimoto M, Lee S, Yazici Y, Kavanaugh A, Abramson SB, CORRONA Investigators. The COX-2 inhibitor market withdrawals and prescribing patterns by rheumatologists in patients with gastrointestinal and cardiovascular risk. *Clin Exp Rheumatol*. 2009, **27:** 395-401.
91. Moss JWE, Ramji DP. Nutraceutical therapies for atherosclerosis. *Nat. Rev. Cardiol*. 2016, **13:** 513-532.

92. Takai S, Jin D, Kawashima H, Kimura M, Shiraishi-Tateishi A, Tanaka T, Kakutani S, Tanaka K, Kiso Y, Miyazaki M. Anti-atherosclerotic effects of dihomo-gamma-linolenic acid in ApoE-deficient mice. *J Atheroscler Thromb*. 2009, **16:** 480-9.
93. Amagai Y, Oida K, Matsuda A, Jung K, Kakutani S, Tanaka T, Matsuda K, Jang H, Ahn G, Xia Y, Kawashima H, Shibata H, Matsuda H, Tanaka A. Dihomo-γ-linolenic acid prevents the development of atopic dermatitis through prostaglandin D1 production in NC/Tnd mice. *J Dermatol Sci*. 2015, **79:** 30-7.
94. Kawashima H, Tateishi N, Shiraishi A, Teraoka N, Tanaka T, Tanaka A, Matsuda H, Kiso Y. Oral administration of dihomo-gamma-linolenic acid prevents development of atopic dermatitis in NC/Nga mice. *Lipids*. 2008, **43:** 37-43.
95. Umeda-Sawada R, Fujiwara Y, Ushiyama I, Sagawa S, Morimitsu Y, Kawashima H, Ono Y, Kiso Y, Matsumoto A, Seyama Y. Distribution and metabolism of dihomo-gamma-linolenic acid (DGLA, 20:3n-6) by oral supplementation in rats. *Biosci Biotechnol Biochem*. 2006, **70:** 2121-30.
96. Ramchurren N, Karmali R. Effects of gamma-linolenic and dihomo-gamma-linolenic acids on 7,12-dimethylbenz(alpha)anthracene-induced mammary tumors in rats. *Prostaglandins Leukot Essent Fatty Acids*. 1995, **53:** 95-101.
97. Sravan Kumar G, Das UN. Cytotoxic action of alpha-linolenic and eicosapentaenoic acids on myeloma cells in vitro. *Prostaglandins Leukot Essent Fatty Acids*. 1997, **56:** 285-93.
98. Sagar PS, Das UN. Cytotoxic action of cis-unsaturated fatty acids on human cervical carcinoma (HeLa) cells in vitro. *Prostaglandins Leukot Essent Fatty Acids*. 1995, **53:** 287-99.

99. Girotti, A. W. Mechanisms of lipid peroxidation. *Journal of free radicals in biology & medicine*. 1985, **1:** 87-95.

100. Gardner H.W. Oxygen radical chemistry of polyunsaturated fatty acids. *Free radic. Biol. Med*. 1989, **7:** 65-86.

101. Wagner BA, Buettner GR, Burns CP. Free radical-mediated lipid peroxidation in cells: oxidizability is a function of cell lipid bis-allylic hydrogen content. *Biochemistry*. 1994, **33:** 4449-53.

102. Qian SY, Wang HP, Schafer FQ, Buettner GR. EPR detection of lipid-derived free radicals from PUFA, LDL, and cell oxidations. *Free Radic Biol Med*. 2000, **29:** 568-79.

103. Yu Q, Purwaha P, Ni K, Sun C, Mallik S, Qian SY. Characterization of novel radicals from COX-catalyzed arachidonic acid peroxidation. *Free Radic Biol Med*. 2009, **47:** 568-76.

104. Xiao Y, Gu Y, Purwaha P, Ni K, Law B, Mallik S, Qian SY. Characterization of free radicals formed from COX-catalyzed DGLA peroxidation. *Free Radic Biol Med*. 2011, **50:** 1163-70.

105. Gu Y, Xu Y, Law B, Qian SY The first characterization of free radicals formed from cellular COX-catalyzed peroxidation. *Free Radic Biol Med*. 2013, **57:** 49-60.

106. Yang X, Xu Y, Brooks A, Guo B, Miskimins KW, Qian SY. Knockdown delta-5-desaturase promotes the formation of a novel free radical byproduct from COX-catalyzed ω-6 peroxidation to induce apoptosis and sensitize pancreatic cancer cells to chemotherapy drugs. *Free Radic Biol Med*. 2016, **97:** 342-350.

107. Yang X, Xu Y, Wang T, Shu D, Guo P, Miskimins K, Qian SY. Inhibition of cancer migration and invasion by knocking down delta-5-desaturase in COX-2 overexpressed cancer cells. *Redox Biol*. 2017, **11:** 653-662.

108. Cho HP, Nakamura M, Clarke SD. Cloning, expression, and fatty acid regulation of the human delta-5 desaturase. *J Biol Chem*. 1999, **274:** 37335-9.

109. Warensjö E, Rosell M, Hellenius ML, Vessby B, De Faire U, Risérus U. Associations between estimated fatty acid desaturase activities in serum lipids and adipose tissue in humans: links to obesity and insulin resistance. *Lipids Health Dis*. 2009, **8:** 37.

110. Saito E, Okada T, Abe Y. Abdominal adiposity is associated with fatty acid desaturase activity in boys: implications for C-reactive protein and insulin resistance. *Prostaglandins Leukot Essent Fatty Acids*. 2013, **88:** 307-11.

111. Obukowicz MG, Welsch DJ, Salsgiver WJ. Novel, selective delta6 or delta5 fatty acid desaturase inhibitors as antiinflammatory agents in mice. *J Pharmacol Exp Ther*. 1998, **287:** 157-66.

112. Obukowicz MG, Raz A, Pyla PD, Rico JG, Wendling JM, Needleman P. Identification and characterization of a novel delta6/delta5 fatty acid desaturase inhibitor as a potential anti-inflammatory agent. *Biochem Pharmacol*. 1998, **55:** 1045-58.

113. Chavali SR, Forse RA. Decreased production of interleukin-6 and prostaglandin E2 associated with inhibition of delta-5 desaturation of omega6 fatty acids in mice fed safflower oil diets supplemented with sesamol. *Prostaglandins Leukot Essent Fatty Acids*. 1999, **61:** 347-52.

114. Chavali SR, Zhong WW, Forse RA. Dietary alpha-linolenic acid increases TNF-alpha, and decreases IL-6, IL-10 in response to LPS: effects of sesamin on the delta-5 desaturation of omega6 and omega3 fatty acids in mice. *Prostaglandins Leukot Essent Fatty Acids*. 1998, **58:** 185-91.

115. Fan YY, Monk JM, Hou TY, Callway E, Vincent L, Weeks B, Yang P, Chapkin RS. Characterization of an arachidonic acid-deficient (Fads1 knockout) mouse model. *J Lipid Res*. 2012, **53:** 1287-95.
116. Fan YY, Callaway E, M Monk J, S Goldsby J, Yang P, Vincent L, S Chapkin R. A new model to study the role of arachidonic acid in colon cancer pathophysiology. *Cancer Prev Res (Phila)*. 2016, **9:** 750-7.
117. Powell DR, Gay JP, Smith M, Wilganowski N, Harris A, Holland A, Reyes M, Kirkham L, Kirkpatrick LL, Zambrowicz B, Hansen G, Platt KA, van Sligtenhorst I, Ding ZM, Desai U. Fatty acid desaturase 1 knockout mice are lean with improved glycemic control and decreased development of atheromatous plaque. *Diabetes Metab Syndr Obes*. 2016, **9:** 185-99.
118. Gresham GK, Wells GA, Gill S, Cameron C, Jonker DJ. Chemotherapy regimens for advanced pancreatic cancer: a systematic review and network meta-analysis. *BMC Cancer*. 2014, **14:** 471.
119. Haller DG. Chemotherapy for advanced pancreatic cancer. *Int J Radiat Oncol Biol Phys*. 2003, **56:** 16-23.
120. Seicean A, Petrusel L, Seicean R. New targeted therapies in pancreatic cancer. *World J Gastroenterol*. 2015, **21:** 6127-6145.
121. Renouf DJ, Tang PA, Hedley D. A phase II study of erlotinib in gemcitabine refractory advanced pancreatic cancer. *Eur J Cancer*. 2014, **50:** 1909-15.
122. Lu YY, Jing DD, Xu M, Wu K, Wang XP. Anti-tumor activity of erlotinib in the BxPC-3 pancreatic cancer cell line. *World J Gastroenterol*. 2008, **14:** 5403-11.

123. Diep CH, Munoz RM, Choudhary A, Von Hoff DD, Han H. Synergistic effect between erlotinib and MEK inhibitors in KRAS wild-type human pancreatic cancer cells. *Clin Cancer Res*. 2011, **17:** 2744-56.

124. Iwai T, Moriya Y, Shirane M, Fujimoto-Ouchi K, Mori K. Continuous inhibition of epidermal growth factor receptor phosphorylation by erlotinib enhances antitumor activity of chemotherapy in erlotinib-resistant tumor xenografts. *Oncol Rep*. 2012, **27:** 923-8.

125. Ali S, Banerjee S, Ahmad A, El-Rayes BF, Philip PA, Sarkar FH. Apoptosis-inducing effect of erlotinib is potentiated by 3, 3'-diindolylmethane in vitro and in vivo using an orthotopic model of pancreatic cancer. *Mol Cancer Ther*. 2008, **7:** 1708-19.

126. Xiong HQ, Varadhachary GR, Blais JC, Hess KR, Abbruzzese JL, Wolff R.A. Phase 2 trial of oxaliplatin plus capecitabine (XELOX) as second-line therapy for patients with advanced pancreatic cancer. *Cancer*. 2008, **113:** 2046-52.

127. Safran H, Miner T, Resnick M, Dipetrillo T, McNulty B, Evans D, Joseph P, Plette A, Millis R, Sears D, Gutman N, Kennedy T. Lapatinib/gemcitabine and lapatinib/ gemcitabine /oxaliplatin: a phase I study for advanced pancreaticobiliary cancer. *Am J Clin Oncol*. 2008, **31:** 140-4.

128. de Sousa Cavalcante L, Monteiro G. Gemcitabine: metabolism and molecular mechanisms of action, sensitivity and chemoresistance in pancreatic cancer. *Eur J Pharmacol*. 2014, **741:** 8-16.

129. Andersson R, Aho U, Nilsson BI, Peters GJ, Pastor-Anglada M, Rasch W, Sandvold ML. Gemcitabine chemoresistance in pancreatic cancer: molecular mechanisms and potential solutions. *Scand J Gastroenterol*. 2009, **44:** 782-6.

130. Shi, X, Liu, S, Kleeff, J, Friess H, Büchler MW. Acquired resistance of pancreatic cancer cells towards 5-Fluorouracil and gemcitabine is associated with altered expression of apoptosis regulating genes. *Oncology*. 2002, **62:** 354-362.

131. Zheng C, Jiao X, Jiang Y, Sun S. ERK1/2 activity contributes to gemcitabine resistance in pancreatic cancer cells. *J Int Med Res*. 2013, **41:** 300-6.

132. Horiguchi S, Shiraha H, Nagahara T, Kataoka J, Iwamuro M, Matsubara M, Nishina S, Kato H, Takaki A, Nouso K, Tanaka T, Ichimura K, Yagi T, Yamamoto K. Loss of runt-related transcription factor 3 induces gemcitabine resistance in pancreatic cancer. *Mol Oncol*. 2013, **7:** 840-9.

133. Chen Q, Wang Z, Zhang K, Liu X, Cao W, Zhang L, Zhang S, Yan B, Wang Y, Xia C. Clusterin confers gemcitabine resistance in pancreatic cancer. *World J Surg Oncol*. 2011, **9:** 59.

134. Franken NA, Rodermond HM, Stap J, Haveman J, van Bree C. Clonogenic assay of cells in vitro. *Nat Protoc*. 2006, **1:** 2315-9.

135. Quehenberger O, Armando A, Dumlao D, Stephens DL, Dennis EA. Lipidomics analysis of essential fatty acids in macrophages. *Prostaglandins Leukot Essent Fatty Acids*. 2008, **79:** 123-9.

136. Padi SK, Zhang Q, Rustum YM, Morrison C, Guo B. MicroRNA-627 mediates the epigenetic mechanisms of vitamin D to suppress proliferation of human colorectal cancer cells and growth of xenograft tumors in mice. *Gastroenterology*. 2013, **145:** 437-46.

137. Wang Y, Zhou Y, Jia G, Han B, Liu J, Teng Y, Lv J, Song Z, Li Y, Ji L, Pan S, Jiang H, Sun B. Shikonin suppresses tumor growth and synergizes with gemcitabine in a pancreatic

cancer xenograft model: Involvement of NF-κB signaling pathway. *Biochem Pharmacol*. 2014, **88:** 322-33.

138. Charan J, Kantharia ND. How to calculate sample size in animal studies? *J Pharmacol Pharmacother*. 2013, **4:** 303-6.
139. Siegel RL, Miller KD, Jemal A. Cancer statistics, 2016. *CA Cancer J Clin*. 2016, **66:** 7-30.
140. Tabolacci C, Lentini A, Provenzano B, Gismondi A, Rossi S, Beninati S. Similar antineoplastic effects of nimesulide, a selective COX-2 inhibitor, and prostaglandin E1 on B16-F10 murine melanoma cells. *Melanoma Res*. 2010, **20:** 273-9.
141. Glozak MA, Seto E. Histone deacetylases and cancer. *Oncogene*. 2007, **26:** 5420-32.
142. Schneider G, Krämer OH, Fritsche P, Schüler S, Schmid RM, Saur D. Targeting histone deacetylases in pancreatic ductal adenocarcinoma. *J Cell Mol Med*. 2010, **14:** 1255-63.
143. Mariadason JM. HDACs and HDAC inhibitors in colon cancer. *Epigenetics*. 2008, **3:** 28-37.
144. Bi G, Jiang G. The molecular mechanism of HDAC inhibitors in anticancer effects. *Cell Mol Immunol*. 2006, **3:** 285-90.
145. Koutsounas I, Giaginis C, Theocharis S. Histone deacetylase inhibitors and pancreatic cancer: are there any promising clinical trials? *World J Gastroenterol*. 2013, **19:** 1173-81.
146. De U, Kundu S, Patra N, Ahn MY, Ahn JH, Son JY, Yoon JH, Moon HR, Lee BM, Kim HS. A New Histone Deacetylase Inhibitor, MHY219, Inhibits the Migration of Human Prostate Cancer Cells via HDAC1. *Biomol Ther (Seoul)*. 2015, **23:** 434-41.
147. Chen, J.S.; Faller, D.V.; Spanjaard, R.A. Short-chain fatty acid inhibitors of histone deacetylases: promising anticancer therapeutics? *Curr Cancer Drug Targets*. 2003, **3:**219-236.

148. Zeng H, Briske-Anderson M. Prolonged butyrate treatment inhibits the migration and invasion potential of HT1080 tumor cells. *J Nutr*. 2005, **135:** 291-5.

149. Rodríguez-Salvador J, Armas-Pineda C, Perezpeña-Diazconti M, Chico-Ponce de León F, Sosa-Sáinz G, Lezama P, Recillas-Targa F, Arenas-Huertero F. Effect of sodium butyrate on pro-matrix metalloproteinase-9 and -2 differential secretion in pediatric tumors and cell lines. *J Exp Clin Cancer Res*. 2005, **24:** 463-73.

150. Wang HG, Huang XD, Shen P, Li LR, Xue HT, Ji GZ. Anticancer effects of sodium butyrate on hepatocellular carcinoma cells in vitro. *Int J Mol Med*. 2013, **31:** 967-74.

151. Wang Y, Kuramitsu Y, Kitagawa T, Tokuda K, Baron B, Akada J, Nakamura K. The histone deacetylase inhibitor valproic acid sensitizes gemcitabine-induced cytotoxicity in gemcitabine-resistant pancreatic cancer cells possibly through inhibition of the DNA repair protein gamma-H2AX. *Target Oncol*. 2015, **10:** 575-81.

152. Zhang L, Wang G, Wang L, Song C, Wang X, Kang J. Valproic acid inhibits prostate cancer cell migration by up-regulating E-cadherin expression. *Pharmazie*. 2011, **66:** 614-8.

153. Bhaskara S, Chyla BJ, Amann JM, Knutson SK, Cortez D, Sun ZW, Hiebert SW. Deletion of histone deacetylase 3 reveals critical roles in S phase progression and DNA damage control. *Mol Cell*. 2008, **30:** 61-72.

154. Norbury CJ, Zhivotovsky B. DNA damage-induced apoptosis. *Oncogene*. 2004, **23:** 2797-808.

155. Bolden JE, Peart MJ, Johnstone RW. Anticancer activities of histone deacetylase inhibitors. *Nat Rev Drug Discov*. 2006, **5:** 769-84.

156. Li, Y.; Li, X.; Guo, B. Chemopreventive agent 3,3'-diindolylmethane selectively induces proteasomal degradation of class I histone deacetylases. *Cancer Res.* 2010, **70:** 646-654.

157. Keleg S, Büchler P, Ludwig R, Büchler MW, Friess H. Invasion and metastasis in pancreatic cancer. *Mol Cancer*. 2003, **2:** 14.

158. Deer EL, González-Hernández J, Coursen JD, Shea JE, Ngatia J, Scaife CL, Firpo MA, Mulvihill SJ. Phenotype and genotype of pancreatic cancer cell lines. *Pancreas*. 2010, **39:** 425-35.

159. Chang GC, Hsu SL, Tsai JR, Wu WJ, Chen CY, Sheu GT. Extracellular signal-regulated kinase activation and Bcl-2 downregulation mediate apoptosis after gemcitabine treatment partly via a p53-independent pathway. *Eur J Pharmacol*. 2004, **502:** 169-83.

160. Elnaggar M, Giovannetti E, Peters GJ. Molecular targets of gemcitabine action: rationale for development of novel drugs and drug combinations. *Curr Pharm Des*. 2012, **18:** 2811-29.

161. Ploquin A, Truant S, Piessen G, Vuagnat P, Baldini C, Cattan S, Hebbar M. Locally advanced or metastatic pancreatic adenocarcinoma: easily available factors of predictive prolonged survival under gemcitabine. *In Vivo*. 2017, **31:** 731-735.

162. Haq M, Shafii A, Zervos EE, Rosemurgy AS. Addition of matrix metalloproteinase inhibition to conventional cytotoxic therapy reduces tumor implantation and prolongs survival in a murine model of human pancreatic cancer. *Cancer Res*. 2000, **60:** 3207-11.

163. Banerjee J, Al-Wadei HA, Al-Wadei MH, Dagnon K, Schuller HM. Differential modulation of nicotine-induced gemcitabine resistance by GABA receptor agonists in pancreatic cancer cell xenografts and in vitro. *BMC Cancer*. 2014, **14:** 725.

164. Liao ZJ, Guo YH, Zhao Z, Yao JT, Xu R, Nan KJ. Gemcitabine inhibits the micrometastasis of non-small cell lung cancer by targeting the EpCAM-positive circulating tumor cells via the HGF/cMET pathway. *Int J Oncol*. **45:** 651-8.

165. Quint K, Tonigold M, Di Fazio P, Montalbano R, Lingelbach S, Rückert F, Alinger B, Ocker M, Neureiter D. Pancreatic cancer cells surviving gemcitabine treatment express markers of stem cell differentiation and epithelial-mesenchymal transition. *Int J Oncol*. 2012, **41:** 2093-102.

166. Yu Y, Wang J, Xia N, Li B, Jiang X. Maslinic acid potentiates the antitumor activities of gemcitabine in vitro and in vivo by inhibiting NF-κB-mediated survival signaling pathways in human gallbladder cancer cells. *Oncol Rep*. 2015, **33:** 1683-90.

167. Mach CM, Mathew L, Mosley SA, Kurzrock R, Smith JA. Determination of minimum effective dose and optimal dosing schedule for liposomal curcumin in a xenograft human pancreatic cancer model. *Anticancer Res*. 2009, **29:** 1895-9.

168. Sun JD, Liu Q, Ahluwalia D, Li W, Meng F, Wang Y, Bhupathi D, Ruprell AS, Hart CP. Efficacy and safety of the hypoxia-activated prodrug TH-302 in combination with gemcitabine and nab-paclitaxel in human tumor xenograft models of pancreatic cancer. *Cancer Biol Ther*. 2015, **16:** 438-49.

169. José E. Belizário. Immunodeficient Mouse Models: An Overview. *Open Immunol J*, 2009, **2:** 79-85.

170. Scholzen T, Gerdes J. The Ki-67 protein: from the known and the unknown. *J Cell Physiol*. 2000, **182:** 311-22.

171. Chang SL, Chou RH, Zeng HJ, Lin YH, Chiu TY, Yang DM, Hung SC, Lai CH, Hsieh JT, Shyu WC, Yu YL. Downregulation of DAB2IP promotes mesenchymal-to-neuroepithelial transition and neuronal differentiation of human mesenchymal stem cells. *PLoS One*. 2013, **8:** e75884.

172. Rossdeutscher L, Li J, Luco AL, Fadhil I, Ochietti B, Camirand A, Huang DC, Reinhardt TA, Muller W, Kremer R. Chemoprevention activity of 25-hydroxyvitamin D in the MMTV-PyMT mouse model of breast cancer. *Cancer Prev Res (Phila)*. 2015, **8:** 120-8.
173. Sena P, Roncucci L, Marzona L, Mariani F, Maffei S, Manenti A, De Pol A. Altered expression of apoptosis biomarkers in human colorectal microadenomas. *Cancer Epidemiol Biomarkers Prev*. 2010, **19:** 351-7.
174. Bressenot A, Marchal S, Bezdetnaya L, Garrier J, Guillemin F, Plénat F. Assessment of apoptosis by immunohistochemistry to active caspase-3, active caspase-7, or cleaved PARP in monolayer cells and spheroid and subcutaneous xenografts of human carcinoma. *J Histochem Cytochem*. 2009, **57:** 289-300.
175. Mustafi R, Dougherty U, Shah H, Dehghan H, Gliksberg A, Wu J, Zhu H, Joseph L, Hart J, Dive C, Fichera A, Threadgill D, Bissonnette M. Both stromal cell and colonocyte epidermal growth factor receptors control HCT116 colon cancer cell growth in tumor xenografts. *Carcinogenesis*. 2012, **33:** 1930-1939.
176. Mao Y, Keller ET, Garfield DH, Shen K, Wang J. Stromal cells in tumor microenvironment and breast cancer. *Cancer Metastasis Rev*. 2013, **32:** 303-15.
177. Omura N, Griffith M, Vincent A, Li A, Hong SM, Walter K, Borges M, Goggins M. Cyclooxygenase-deficient pancreatic cancer cells use exogenous sources of prostaglandins. *Mol Cancer Res*. 2010, **8:** 821-32.
178. Höckel M, Vaupel P. Tumor hypoxia: definitions and current clinical, biologic, and molecular aspects. *J Natl Cancer Inst*. 2001, **93:** 266-76.
179. Kaidi A, Qualtrough D, Williams AC, Paraskeva C. Direct transcriptional up-regulation of cyclooxygenase-2 by hypoxia-inducible factor (HIF)-1 promotes colorectal tumor cell

survival and enhances HIF-1 transcriptional activity during hypoxia. *Cancer Res*. 2006, **66:** 6683-91.

180. Lee JJ, Natsuizaka M, Ohashi S, Wong GS, Takaoka M, Michaylira CZ, Budo D, Tobias JW, Kanai M, Shirakawa Y, Naomoto Y, Klein-Szanto AJ, Haase VH, Nakagawa H. Hypoxia activates the cyclooxygenase-2-prostaglandin E synthase axis. *Carcinogenesis*. 2010, **31:** 427-34.
181. Killion JJ, Radinsky R, Fidler IJ. Orthotopic models are necessary to predict therapy of transplantable tumors in mice. *Cancer Metastasis Rev*. 1998-1999, **17:** 279-84.
182. Fu X, Guadagni F, Hoffman RM. A metastatic nude-mouse model of human pancreatic cancer constructed orthotopically with histologically intact patient specimens. *Proc Natl Acad Sci U S A*. 1992, **89:** 5645-9.
183. Qiu W, Su GH. Development of orthotopic pancreatic tumor mouse models. *Methods Mol Biol*. 2013, **980:** 215-23.
184. Kim MP, Evans DB, Wang H, Abbruzzese JL, Fleming JB, Gallick GE. Generation of orthotopic and heterotopic human pancreatic cancer xenografts in immunodeficient mice. *Nat Protoc*. 2009, **4:** 1670-80.
185. Shu D, Shu Y, Haque F, Abdelmawla S, Guo P. Thermodynamically stable RNA three-way junction for constructing multifunctional nanoparticles for delivery of therapeutics. *Nat Nanotechnol*. 2011, **6:** 658-67.
186. Cui D, Zhang C, Liu B, Shu Y, Du T, Shu D, Wang K, Dai F, Liu Y, Li C, Pan F, Yang Y, Ni J, Li H, Brand-Saberi B, Guo P. Regression of gastric cancer by systemic injection of RNA nanoparticles carrying both ligand and siRNA. *Sci Rep*. 2015, **5:** 10726.

187. Shu D, Li H, Shu Y, Xiong G, Carson WE 3rd, Haque F, Xu R, Guo P. Systemic delivery of anti-miRNA for suppression of triple negative breast cancer utilizing RNA nanotechnology. *ACS Nano*. 2015, **9:** 9731-40.

188. Binzel DW, Shu Y, Li H, Sun M, Zhang Q, Shu D, Guo B, Guo P. Specific delivery of miRNA for high efficient inhibition of prostate cancer by RNA nanotechnology. *Mol Ther*. 2016, **24:** 1267-77.

189. Khaled A, Guo S, Li F, Guo P. Controllable self-assembly of nanoparticles for specific delivery of multiple therapeutic molecules to cancer cells using RNA nanotechnology. *Nano Lett*. 2005, **5:** 1797-808.